Editors' Suggestion

Landau-Pomeranchuk-Migdal effect in sequential bremsstrahlung: Gluon shower development

Peter Arnold and Omar Elgedawy
Department of Physics, University of Virginia, Charlottesville, Virginia 22904-4714, USA

Shahin Iqbal
National Centre for Physics, Quaid-i-Azam University Campus, Islamabad, 45320, Pakistan

(Received 28 February 2023; accepted 21 July 2023; published 19 October 2023)

We give details of our study as to whether high-energy gluon showers inside a QCD medium can be treated as a sequence of individual splitting processes $g \to gg$, or whether there is significant quantum overlap between where one splitting ends and the next begins (neglecting effects that can be absorbed into an effective value of the jet-quenching parameter $\hat{q}$ that characterizes the medium). The study is carried out by imagining in-medium gluon-shower development in the simplest theoretical situation, which includes imagining a very large, static, homogeneous medium and taking the large N_c limit. Along the way, we also show how in-medium shower evolution can be written in terms of a "net" splitting rate $[d\Gamma/dx]_{\rm net}$, and we provide a moderately simple analytic fit to our numerical results for the overlap effects included in that rate, which we hope may be of use to others wishing to study possible consequences of overlapping splittings.

DOI: 10.1103/PhysRevD.108.074015

I. INTRODUCTION

When passing through matter, high energy particles lose energy by showering, via the splitting processes of hard bremsstrahlung and pair production. At very high energy, the quantum mechanical duration of each splitting process, known as the formation time, exceeds the mean free time for collisions with the medium, leading to a significant reduction in the splitting rate known as the Landau-Pomeranchuk-Migdal (LPM) effect [1–3].[1] A long-standing problem in field theory has been to understand how to implement this effect in cases where the formation times of two consecutive splittings overlap. Several authors [5–7] previously analyzed this issue for QCD at leading-log order, which arises from the limit where one bremsstrahlung gluon is soft compared to the other very high-energy partons. They found large effects at high energy, but those effects could be absorbed into an effective value $\hat{q}_{\rm eff}$ of the medium parameter $\hat{q}$ that encodes the rate of transverse momentum kicks to a high-energy particle by the medium. In a short companion Letter [8], which should be read first, we motivated and outlined a method for investigating the size of overlapping formation time effects that cannot be absorbed into $\hat{q}$, and we presented selected results. The purpose of the current paper is to provide details of the methods and derivations used in Ref. [8], and to provide a more complete exposition of results.

As described in Ref. [8], our focus will be on computing the statistically averaged distribution $\epsilon(z)$ of energy deposited in the medium by a gluon shower initiated by a very high-energy gluon with energy E_0 that starts at the origin traveling in the z direction. We will be particularly focused on overlapping formation time corrections to the shape of that distribution,

$$S(Z) \equiv \frac{\langle z\rangle}{E_0}\epsilon(\langle z\rangle Z), \tag{1.1}$$

where

$$\langle z\rangle \equiv \frac{1}{E_0}\int_0^\infty dz\, z\, \epsilon(z) \tag{1.2}$$

is the characteristic length of the shower (of parametric order $\alpha_s^{-1}\sqrt{E_0/\hat{q}}$), and $Z \equiv z/\langle z\rangle$.

Our results will all be derived in terms of what we call the net rate $[d\Gamma/dx]_{\rm net}$ for splitting [9], defined as the rate for splittings (including the case of two overlapping splittings) to produce one daughter of energy xE plus any other daughters from a parent of energy E. Formulas for overlapping formation time effects appearing in the net rate, developed in Refs. [9–15], are extremely long and

[1]The papers of Landau and Pomeranchuk [1,2] are also available in English translation [4].

complicated. They are also time consuming to evaluate numerically. In this paper, we will present a relatively simple function that fits our numerical results well (at first order in overlap effects) for $[d\Gamma/dx]_{\rm net}$. We need this quick-to-evaluate fit function to make our analysis of the shape function $S(Z)$ numerically practical, but perhaps others may find the fit function useful as well.

A. Assumptions

For the sake of theoretical simplicity, we make the assumptions outlined in Ref. [8], which mostly follow those of the underlying rate calculations developed in Refs. [9–15]. We assume a homogeneous, static medium large enough to stop the shower[2]; a nearly on shell initial gluon[3]; transverse momentum transfer from the medium described by the multiple-scattering ($\hat{q}$) approximation; the large-N_c limit, and so purely gluonic showers.

We also focus on $p_\perp$-insensitive quantities such as the energy deposition distribution $\epsilon(z)$ and its shape (1.1) so that we only need to track $p_\perp$-integrated distributions of energy in gluon showers.[4]

There was another simplifying assumption, made implicitly in Ref. [8], which we should be explicit about here. To first order in high-energy radiative corrections, write the effective value of $\hat{q}$ as $\hat{q}_{\rm eff} = \hat{q}_{(0)} + \delta q$. Here, $\hat{q}_{(0)}$ is what we might call the bare value of $\hat{q}$—the value from scatterings of a high-energy parton with the medium that are not accompanied by high-energy splitting. In our analysis, we will treat $\hat{q}_{(0)}$ as a constant, independent of energy. There are caveats and countercaveats concerning logarithmic dependence of that approximation, which we will simply ignore in this paper.[5]

In principle, the analysis of this paper can be applied to any sufficiently thick QCD medium where the $\hat{q}$ approximation is appropriate. However, our own interest is ultimately motivated by quark-gluon plasmas (QGPs), and so we will sometimes use that language. In that context, we are making no assumption about whether the coupling $\alpha_s(T)$ of the QGP is large or small—all of the details of the QGP are hidden away in the value of $\hat{q}_{(0)}$. We will, however, work perturbatively in the size of the $\alpha_s(\mu)$ associated with a high-energy splitting vertex, for which the transverse momentum scale is parametrically $\mu \sim (\hat{q}\omega)^{1/4}$, where ω is the energy of the softest daughter.

Throughout this paper, we will only focus on the high-energy particles ($E \gg T$) in showers. We ignore thermal gluon masses for the high-energy gluons in our (purely gluonic) showers.

B. Outline

The next section briefly summarizes the calculation of overlapping splitting rates, previously worked out in Refs. [9–15], and explains how the results of that work are packaged into results for different types of rates (2.2).

Section III describes, and presents results for, the net rate $[d\Gamma/dx]_{\rm net}$ that will be used throughout the rest of the paper. We first review how rates can be combined into the net rate. The net rate is split into leading-order (BDMPS-Z) and next-to-leading-order (overlap) pieces. We review logarithmic infrared divergences of the net rate, due to soft radiative corrections to hard splittings $g \to gg$, and then factorize out those soft radiative corrections as described in Ref. [8]. Numerical results, and an analytic fit, are presented for overlap corrections to $[d\Gamma/dx]_{\rm net}$. The section concludes with discussion of how to convert $[d\Gamma/dx]_{\rm net}$ between different choices of factorization scale.

In principle, the factorized soft radiative corrections should be resummed and absorbed into an effective value $\hat{q}_{\rm eff}$ of $\hat{q}$, and that change will affect the effective "leading-order" development of the shower. Section IV argues that this complication can be ignored in our calculation. This point is somewhat nontrivial and requires partial discussion of resumming soft radiative corrections to $\hat{q}$ at next-to-leading-log order (NLLO); the current state of the art is leading-log order.

[2]The underlying rate calculations of Refs. [9–15] only assumed that the medium was approximately static and homogeneous over the formation time and corresponding formation length. The analysis in this paper is made simpler by assuming that it is static and homogeneous over the entire development of the shower.

[3]For some discussion, in various approximations, of how to marry an initial vacuumlike cascade of virtuality after a relativistic heavy-ion collision with later nearly on shell showering in a finite medium (but not attempting to analyze the overlap effects that are the subject of this paper), see e.g. Refs. [16–18].

[4]This allows us to use existing calculations of $p_\perp$-integrated rates [9] for in-medium double splitting with overlapping formation times. For a discussion of generalizing BDMPS-Z rate calculations to $p_\perp$ dependence of nonoverlapping splitting rates in various situations, see e.g. Refs. [19–23]. More recently, Ref. [24] investigated $p_\perp$ dependence for soft emissions overlapping harder splittings with the latter treated in antenna approximations such as in Refs. [25,26]. Our $p_\perp$-integrated calculations avoid soft-emission approximations (or more general energy and/or $p_\perp$ ordering assumptions about sequential emissions), within the context of our other assumptions. By avoiding antenna approximations in particular, our calculations capture the (important for us) full backreaction of an overlapping second emission on the probability for the original splitting to occur in the first place. This is just like Refs. [5–7] except that we avoid all soft-emission approximations. (See also footnote 34.)

[5]For example, for fixed-coupling calculations for a weakly-coupled medium, the large-$q_\perp$ Rutherford tail $d\Gamma_{\rm el}/d(q_\perp^2) \propto \alpha_s^2 n/q_\perp^4$ of the elastic scattering cross section causes logarithmic dependence of $\langle q_\perp^2 \rangle$ on the upper scale of $q_\perp$ relevant to the process under consideration. On the other hand, including running of α_s as $d\Gamma_{\rm el}/d(q_\perp^2) \propto \alpha_s^2(q_\perp) n/q_\perp^4$ is enough to eventually tame that dependence if the relevant upper scale $Q_\perp$ for $q_\perp$ is large enough that $\alpha_s(Q_\perp)$ is small compared to the strength of α_s at the scale of the medium. (See, for example, Sec. VI B of Ref. [27], which combined earlier observations of Refs. [28,29].)

Section V provides the starting point for our analysis of shower energy deposition by showing that the deposited energy distribution $\epsilon(z)$ satisfies an integrodifferential equation (5.15) in terms of the net splitting rate $[d\Gamma/dx]_{\rm net}$. Since our goal is to study aspects of showers that are as insensitive as possible to physics that can be absorbed into the effective value of $\hat{q}$, our ultimate interest will be to follow Ref. [8] and study the shape $S(Z)$ of $\epsilon(z)$ given by (1.1).

Numerically, the features of $\epsilon(z)$ that are easiest to calculate are its moments $\langle z^n\rangle$. Section VI presents a recursion relation (6.2a) for those moments in terms of integrals of $[d\Gamma/dx]_{\rm net}$. These are then converted to various moments $\langle Z^n\rangle$ of the shape function $S(Z)$. Our interest lies in the relative size of overlap corrections to those moments, which will be presented in Table III. We will find that most overlap corrections are very small, but the fourth cumulant of $S(Z)$ turns out to be very sensitive to overlap effects.

In order to convince ourselves that overlap effects on the shape function are very small, regardless of the sensitivity of the fourth cumulant, Sec. VII turns away from moments and takes on the more numerically complicated task of directly calculating the size of overlap corrections to the full $S(Z)$ as a function of Z, summarized in Fig. 14. As prequel to this next-to-leading-order calculation, we also provide what, as far as we know, are the first full leading-order (BDMPS-Z) numerical calculations of $\epsilon(z)$ and $S(Z)$, and we compare those to what they would be in the instructive Blaizot/Iancu/Mehtar-Tani analytic model for (leading-order) showers [30,31].

Section VIII demonstrates that the ability to analyze showers in terms of $[d\Gamma/dx]_{\rm net}$ is not restricted to just energy deposition but also applies more generally to the time development of the gluon distribution of the shower. This generalizes leading-order versions of shower evolution equations used by others [30,31], but we have not made any attempt to simulate our evolution equation.

The results we find are that overlap effects on $S(Z)$ are very small—much smaller than related effects previously computed for large-$N_{\rm f}$ QED [32]. Section IX attempts to give some crude, incomplete, after-the-fact analysis of why the results of the two calculations are so qualitatively different, which generates questions for future work.

In Sec. X, we discuss what cross-checks are available for our calculation of overlap effects. Then we offer short concluding remarks in Sec. XI.

II. REVIEW OF THE BUILDING BLOCKS: SPLITTING RATES

A. Diagrams

The calculation of the LPM effect was generalized from QED to QCD by Baier *et al.* [28,33,34] and Zakharov [35,36] (BDMPS-Z). When specialized to an infinite medium in the $\hat{q}$ approximation, their formalism gives the in-medium $g \to gg$ splitting rate[6]

$$\left[\frac{d\Gamma}{dx}\right]^{\rm LO} = \frac{\alpha_{\rm s} P_{g\to gg}(x)}{2\pi}\sqrt{\frac{(1-x+x^2)\hat{q}_{\rm A}}{x(1-x)E}} \tag{2.1}$$

for energies $E \to xE + (1-x)E$. The subscript on $\hat{q}_{\rm A}$ indicates the $\hat{q}$ appropriate for the adjoint color representation, i.e. for gluons, and $C_{\rm A} = N_{\rm c}$ is the adjoint-representation quadratic Casimir. $P_{g\to gg}(x)$ is the Dokshitzer-Gribov-Lipatov-Altarelli-Parisi (DGLAP) splitting function.[7] We refer to (2.1) as the "leading-order" (LO) result for $g \to gg$. For us, leading order means the leading order in the number of high-energy splitting vertices and includes the effects of an arbitrary number of interactions with the medium. In the following discussion, we will adopt Zakharov's picture [35,36] of LPM rate calculations, which is to think of the rate for $g \to gg$ as time-ordered diagrams, such as Fig. 1,

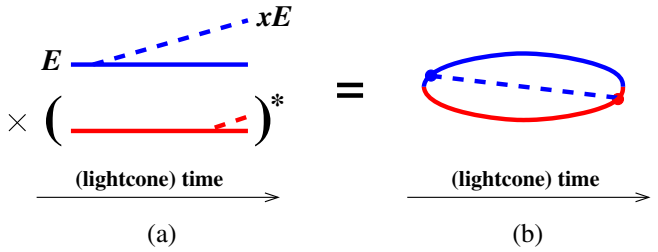

FIG. 1. (a) A time-ordered contribution to the LO rate for single splitting $g \to gg$, with amplitude in blue and conjugate amplitude in red. (b) A single diagram representing this contribution to the rate. In both cases, all lines implicitly interact with the medium. We need not follow particles after the emission has occurred in both the amplitude and conjugate amplitude because we will consider only the $p_\perp$-integrated rate. (See, for example, Sec. 4.1 of Ref. [10] for a more explicit argument, although applied there to a more complicated diagram.) Nor need we follow them before the first emission because we approximate the initial particle as on shell. Only one of the two time orderings that contribute to the LO rate is shown above.

[6]It is difficult to figure out whom to reference for the first appearance of (2.1). BDMS [37] give the $q \to qg$ formula in their Eq. (42b) [with the relevant limit here being the infinite volume limit $\tau_0 \to \infty$ for their time τ_0]. They then discuss elements of the $g \to gg$ case after that but do not quite give an explicit formula for the entire rate. (They are not explicit about the formula for ω_0.) Zakharov makes a few general statements about the $g \to gg$ case after Eq. (75) of Ref. [38]. As an example from ten years later, the explicit formula is given by Eqs. (2.26) and (4.6) of Ref. [39] in the case where s represents a gluon.

[7]Our $P_{g\to gg}(x) = 2C_{\rm A}(1-x+x^2)^2/x(1-x)$ does *not* contain the pieces of the usual DGLAP splitting function used to include the effect of virtual diagrams. In particular, the $1/(1-x)$ in our formula for $P_{g\to gg}$ is just the ordinary function $1/(1-x)$ and not the distribution $1/(1-x)_+$, and our $P_{g\to gg}$ does not contain a δ-function term $\delta(1-x)$. When we need to deal with virtual diagrams in this paper, we will do so explicitly.

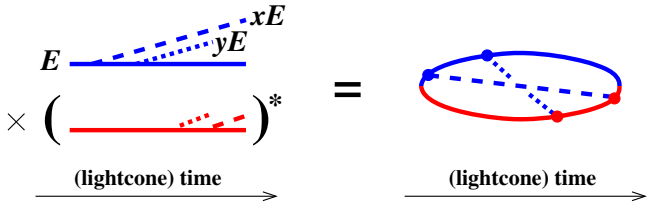

FIG. 2. A particular example of two overlapping splittings.

combining the amplitude for $g \to gg$ (blue) with the conjugate amplitude (red). Zakharov then thought of Fig. 1(b) as three particles propagating forward in time which, in the high-energy limit, could be described (between the splitting vertices) as a 3-particle, two-dimensional quantum mechanics problem in the transverse plane. The medium-averaged effect of interactions with the medium can be described by a non-Hermitian, effective "potential energy" between the three particles in the quantum mechanics problem. In this language, the $\hat{q}$ approximation corresponds to a harmonic oscillator problem (with imaginary-valued spring constants). For a discussion and review in the particular context of our problem with our notation, see, for example, Refs. [10,40].

We refer to the effects of two overlapping $g \to gg$ splittings, such as Fig. 2, as one type of next-to-leading-order (NLO) effect. Since there are four high-energy splitting vertices in this rate diagram, it is suppressed by one power of high-energy $\alpha_s(\mu)$ compared to the leading-order splitting of Fig. 1. Figure 3 shows examples of diagrams contributing to the rate, drawn in the style of Fig. 1(b). The subtraction in Fig. 3 means that our rates represent the difference between (i) a full calculation of (potentially overlapping) $g \to gg \to ggg$, and (ii) approximating a double splitting as two independent, consecutive single splittings $g \to gg$ that each occur with the LO single splitting rate (2.1).[8] At the same order in $\alpha_s(\mu)$, there are also NLO virtual corrections to single splitting $g \to gg$, for which we show a few examples in Fig. 4. Figure 5 shows examples of some more direct $g \to ggg$ processes that also contribute at the same order in $\alpha_s(\mu)$. A complete list of all diagrams contained in our calculation may be found in Refs. [9,15].

Throughout this paper, α_s will refer to high-energy $\alpha_s(\mu)$ unless stated otherwise.

B. Notation for rates

Following Ref. [9], we will refer to the leading-order $g \to gg$ rate, its NLO correction, and the $g \to ggg$ rate as

$$\left[\frac{d\Gamma}{dx}\right]^{\rm LO}, \qquad \left[\Delta\frac{d\Gamma}{dx}\right]^{\rm NLO}_{g\to gg}, \qquad \left[\Delta\frac{d\Gamma}{dxdy}\right]_{g\to ggg}. \tag{2.2}$$

The last one, $[\Delta d\Gamma/dxdy]_{g\to ggg}$, represents both (i) overlap corrections to two consecutive splittings, such as in Fig. 3, and (ii) processes involving direct $g \to ggg$, such as Figs. 5(a) and 5(b). In both cases, energy is being split as $E \to xE + yE + (1-x-y)E$. The symbol "Δ" in front of that rate is a reminder that it represents a correction to an LO-based calculation of double splitting as two, consecutive, independent $g \to gg$ splitting events. $[\Delta d\Gamma/dx]^{\rm NLO}_{g\to gg}$ similarly represents the corresponding virtual corrections to single splitting, such as in Figs. 4 and 5(c). In this case, energy is being split as $E \to xE + (1-x)E$.

Formulas for the rates (2.2) are presented in Refs. [9,15],[9] which carried out the calculation in light cone perturbation theory (LCPT). We will be slightly sloppy with our terminology in this paper. Technically, we should define x and y by the splitting of light cone longitudinal momentum; $P^+ \to xP^+ + yP^+ + (1-x-y)P^+$ for $g \to ggg$ and $P^+ \to xP^+ + (1-x)P^+$ for $g \to gg$. But the splittings relevant to shower development are high energy and nearly collinear, and so we may also refer to x and y simply as "energy fractions" in our applications.[10]

In the case of the virtual diagrams, the rate calculation involves integration over the light cone longitudinal momentum fraction y of one of the loop lines, as labeled in Figs. 4 and 5(c). One consequence of LCPT is that the p^+ of every (transverse-polarized) gluon must be non-negative, which imposes constraints on the allowed range of y in the virtual diagrams. References [9,15] divide virtual diagrams into two classes. Class I (such as the top line of Fig. 4) means that (i) y should be integrated over $0 < y < 1-x$ and (ii) the substitution $x \to 1-x$ generates a distinct set of diagrams that must also be included. Class II (such as the bottom line of Fig. 4) means that (i) y should be integrated over $0 < y < 1$ and (ii) the substitution $x \to 1-x$ does not generate any new diagrams. With this nomenclature,

$$\begin{aligned}\left[\Delta\frac{d\Gamma}{dx}\right]^{\rm NLO}_{g\to gg} &= \left(\left[\Delta\frac{d\Gamma}{dx}\right]^{\rm NLO}_{\rm class\ I}\right) + (x\to 1-x) + \left[\Delta\frac{d\Gamma}{dx}\right]^{\rm NLO}_{\rm class\ II} \\ &= \left(\int_0^{1-x} dy \left[\Delta\frac{d\Gamma}{dxdy}\right]^{\rm NLO}_{\rm class\ I}\right) + (x\to 1-x) \\ &\quad + \int_0^1 dy \left[\Delta\frac{d\Gamma}{dxdy}\right]^{\rm NLO}_{\rm class\ II},\end{aligned} \tag{2.3}$$

[8]The key importance of this subtraction is explained in Sec. 1.1 of Ref. [11].

[9]More specifically, see Appendix A of Ref. [9], but supplement the formulas there as explained in Appendix A of Ref. [15] in order to include diagrams like Fig. 5. Various pieces of these formulas are taken from earlier papers [10–14].

[10]More specifically, the difference between p^+/P^+ and p^0/E is suppressed by $p_\perp^2/E^2 \sim \hat{q}t_{\rm form}/E^2 \sim \hat{q}^{1/2}/E^{3/2}$, and in all of our analysis we ignore effects that are suppressed by powers of E.

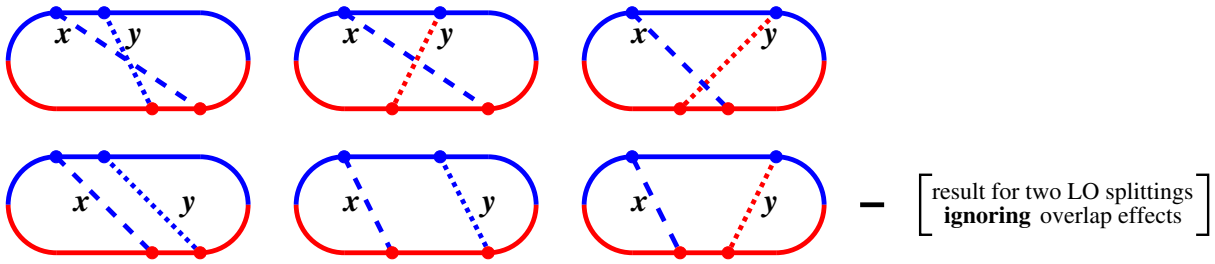

FIG. 3. Examples of diagrams contributing to the effects of overlapping formation times for two splittings $g \to gg \to ggg$. The first and second rows (when combined with their conjugates and appropriate permutations of the daughters) were analyzed in Refs. [10,11], respectively.

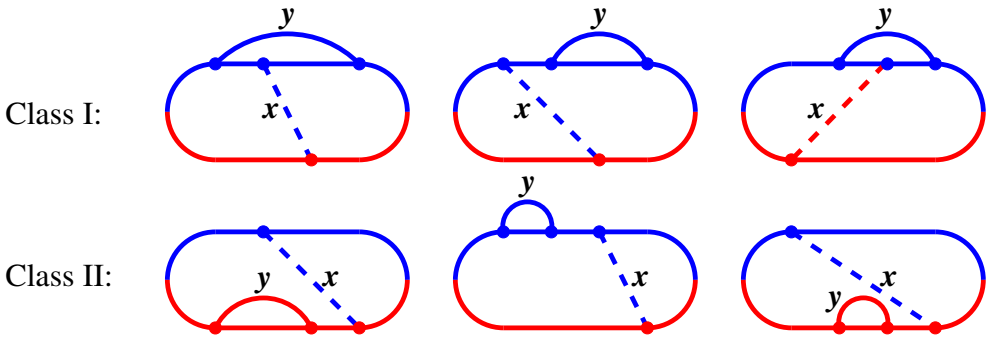

FIG. 4. Some examples from Ref. [9] of NLO virtual corrections to single splitting $g \to gg$.

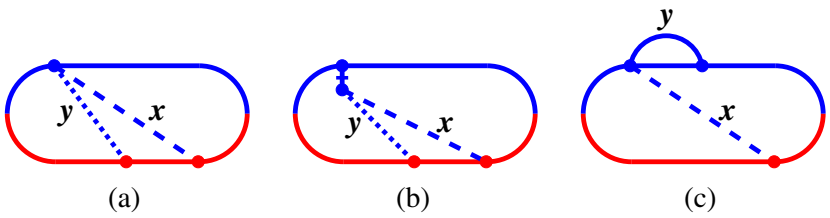

FIG. 5. Some examples from Ref. [15] that involve (a) and (c) a 4-gluon vertex or (b) exchange of a longitudinally polarized gluon (denoted by the vertical line crossed by a bar) in light cone perturbation theory (LCPT).

where the subscripts refer to Class I and Class II virtual diagrams.[11] The virtual diagrams were computed with $\overline{\text{MS}}$ ultraviolet renormalization, and so $\alpha_s(\mu)$ will refer to the $\overline{\text{MS}}$ coupling in our work.

In this paper, we will need to do y integrals numerically. Reference [9] found it convenient to separate out a piece containing the renormalization scale μ dependence from the integrals in (2.3) and to integrate that piece analytically. That is a choice, and a detail, that we leave to Appendix A, where the reader may find the exact connection with the rate formulas as they are presented in Refs. [9,15].[12]

In what follows, we will consider the shower as being made up of $1 \to 2$ splittings and effective $1 \to 3$ splittings. In that context, we find it convenient to use the notation

$$\left[\frac{d\Gamma}{dx}\right]_{1\to 2} \equiv \left[\frac{d\Gamma}{dx}\right]^{\text{LO}} + \left[\Delta\frac{d\Gamma}{dx}\right]^{\text{NLO}}_{g\to gg}, \tag{2.4a}$$

[11]Following Ref. [9], our convention is that, when there is a loop in the amplitude (or a loop in the conjugate amplitude), the loop-symmetry factor (if any) is already accounted for in the formulas for $[\Delta d\Gamma/dxdy]^{\text{NLO}}_{\text{class I}}$ and $[\Delta d\Gamma/dxdy]^{\text{NLO}}_{\text{class II}}$.

[12]We have intentionally used subscript names "class I" and "class II" in (2.3) that are different from those used in Ref. [9] to avoid confusing the formulas given there, where some pieces have been separated out, with the integrands in (2.3), where they have not. See Appendix A.

$$\left[\frac{d\Gamma}{dxdy}\right]_{1\to3} \equiv \left[\Delta\frac{d\Gamma}{dxdy}\right]_{g\to ggg}. \tag{2.4b}$$

Remember that, for simplicity, we are only considering purely gluonic showers, and so the daughters of every splitting are identical particles. Our convention is to not include final-state identical particle factors in differential rates. So, formally, the total rate for any sort of $1\to2$ or $1\to3$ splittings would be

$$\Gamma = \frac{1}{2!}\int_0^1 dx\left[\frac{d\Gamma}{dx}\right]_{1\to2} + \frac{1}{3!}\int_0^1 dx\int_0^{1-x} dy\left[\frac{d\Gamma}{dxdy}\right]_{1\to3}, \tag{2.5}$$

or, equivalently,

$$\Gamma = \int_{x<1-x} dx\left[\frac{d\Gamma}{dx}\right]_{1\to2} + \int_{y<x<1-x-y} dxdy\left[\frac{d\Gamma}{dxdy}\right]_{1\to3}. \tag{2.6}$$

(We say "formally" because the total rate is infrared divergent.)

We should note that the "$1\to3$" rate (2.4b) can have either sign [11] because, as mentioned earlier, part of it represents an overlap correction to a shower of LO $1\to2$ splittings, and corrections may have either sign.

III. $[d\Gamma/dx]_{\rm net}$ AND ITS FACTORIZATION

A. Definition and properties

As mentioned earlier, we define the "net" rate $[d\Gamma/dx]_{\rm net}$ as the probability per unit time that splittings of a parent with energy E create a daughter with energy xE (along with any other daughters). For a shower made up of $1\to2$ and $1\to3$ splittings,

$$\left[\frac{d\Gamma}{dx}\right]_{\rm net} = \left[\frac{d\Gamma}{dx}\right]_{1\to2} + \frac{1}{2!}\int_0^{1-x} dy\left[\frac{d\Gamma}{dxdy}\right]_{1\to3} \tag{3.1}$$

if all the particles are identical (i.e. gluons in our case). The reason for the $1/2!$ factor on the $1\to3$ terms is that one of the three daughters has been distinguished as having energy xE, but we do not want to double count the integration over the energies of the other two (identical) daughters.

Note that the total rate (2.5) is not equal to $\int dx[d\Gamma/dx]_{\rm net}$. But one may show that

$$\Gamma = \int_0^1 dx\, x\left[\frac{d\Gamma}{dx}\right]_{\rm net}. \tag{3.2}$$

To see this, use (3.1) to write the right-hand side as

$$\int_0^1 dx\, x\left[\frac{d\Gamma}{dx}\right]_{\rm net} = \int_0^1 dx\, x\left[\frac{d\Gamma}{dx}\right]_{1\to2} + \frac{1}{2!}\int_0^1 dx\, x\int_0^{1-x} dy\left[\frac{d\Gamma}{dxdy}\right]_{1\to3}. \tag{3.3}$$

For the $1\to2$ integral in (3.3), average (i) the integral with (ii) itself after the change of integration variable $x\to1-x$. Since the daughters $(x,1-x)$ of the splitting are identical particles, $[d\Gamma/dx]_{1\to2}$ does not change under $x\to1-x$, and so

$$\int_0^1 dx\, x\left[\frac{d\Gamma}{dx}\right]_{1\to2} = \int_0^1 dx\frac{x+(1-x)}{2}\left[\frac{d\Gamma}{dx}\right]_{1\to2} = \frac{1}{2}\int_0^1 dx\left[\frac{d\Gamma}{dx}\right]_{1\to2}. \tag{3.4}$$

Do the same for the $1\to3$ integral in (3.3) except average over (i) the original integral, (ii) $x\leftrightarrow y$, and (iii) $x\leftrightarrow1-x-y$. These are just certain permutations of the three identical daughters $(x,y,1-x-y)$, and so $[d\Gamma/dxdy]_{1\to3}$ does not change. Comparing the resulting rewriting of (3.3) to (2.5) gives (3.2).

B. IR divergences and factorization

As written, the definition (3.1) of $[d\Gamma/dx]_{\rm net}$, when applied to the $1\to2$ and $1\to3$ processes (2.4), is plagued with infrared divergences. First, there are power-law infrared divergences associated with the different boundaries (0, $1-x$, and 1) of the y integrations in (3.1) and (2.3), but these divergences cancel each other when all added together. It is possible to re-arrange the y integrals so that (i) the IR divergences (for fixed x) all become associated with $y\to0$ and (ii) the terms which generate power-law IR divergences all cancel in the integrand. Specifically, Ref. [9] showed that (3.1) could be rewritten as

$$\left[\frac{d\Gamma}{dx}\right]_{\rm net} = \left[\frac{d\Gamma}{dx}\right]^{\rm LO} + \left[\frac{d\Gamma}{dx}\right]^{\rm NLO}_{\rm net} \tag{3.5}$$

with[13]

[13]See Sec. 1.2 of Ref. [9]. Here we use a capital letter for the function V to distinguish it from the lower-case function v of Ref. [9]. This is a technical point arising from our use of the full NLO virtual rates $[\Delta d\Gamma/dxdy]^{\rm NLO}_{\rm class\ I}$ and $[\Delta d\Gamma/dxdy]^{\rm NLO}_{\rm class\ II}$ in our discussion here, instead of their $\overline{\rm NLO}$ counterparts in Ref. [9] (where a piece including the renormalization scale dependence has been separated out). See footnote 12 and Appendix A. We have also capitalized the function name R for consistency of notation, but it is identical to the function r in Ref. [9].

$$\left[\frac{d\Gamma}{dx}\right]^{\rm NLO}_{\rm net} = \int_0^{1/2} dy \Bigg\{ V(x,y)\theta\left(y < \frac{1-x}{2}\right) + V(1-x,y)\theta\left(y < \frac{x}{2}\right) + R(x,y)\theta\left(y < \frac{1-x}{2}\right)\Bigg\}, \tag{3.6}$$

where

$$V(x,y) \equiv \left(\left[\Delta\frac{d\Gamma}{dxdy}\right]^{\rm NLO}_{\rm class\ I} + \left[\Delta\frac{d\Gamma}{dxdy}\right]^{\rm NLO}_{\rm class\ II}\right) + (y \leftrightarrow 1-x-y), \tag{3.7a}$$

$$R(x,y) \equiv \left[\Delta\frac{d\Gamma}{dxdy}\right]_{g\to ggg}. \tag{3.7b}$$

The $\theta(\cdots)$ in (3.6) represent unit step functions [$\theta(\text{true}) = 1$ and $\theta(\text{false}) = 0$], and they just implement upper limits on the y integration. The advantage of using the θ functions is so that all the integrals can be combined: the integrals for the separate terms each have power-law IR divergences, but their sum does not.

The explicit upper limit $1/2$ on the y integral sign $\int dy$ in (3.6) could just as well be replaced by ∞ because the actual limits on various terms in the integrand are implemented by the θ functions. $1/2$ is simply the largest any of those limits on y could ever be.

Though IR power-law divergences cancel, there remains an uncanceled IR double-log divergence associated with $y \to 0$ in (3.6). This is a double logarithm [5–7] associated with soft radiative corrections to an underlying, hard single-splitting process $[d\Gamma/dx]^{\rm LO}$. It is essentially the same double logarithm that was originally discovered by considering radiative corrections to $\hat{q}$ [41]. Physically, this double logarithm is cut off in the infrared where the $\hat{q}$ approximation breaks down. If one works exclusively in the $\hat{q}$ approximation, however, the double log manifests as an infrared divergence that must be regularized and/or subtracted. Equation (3.6) also generates a subleading, single logarithm IR divergence that was extracted analytically in Ref. [42] and alternatively derived from the known radiative corrections to $\hat{q}$ in Ref. [40]. The small-y behavior of the integral in (3.6) was found to be

$$-\frac{C_{\rm A}\alpha_{\rm s}}{4\pi}\left[\frac{d\Gamma}{dx}\right]^{\rm LO}\int_{y\ll\min(x,1-x)}\frac{dy}{y}\left[\ln y + \bar{s}(x)\right] \tag{3.8}$$

for fixed x, where

$$\bar{s}(x) = -\ln(16x(1-x)(1-x+x^2)) + 2\frac{[x^2(\ln x - \frac{\pi}{8}) + (1-x)^2(\ln(1-x) - \frac{\pi}{8})]}{(1-x+x^2)}. \tag{3.9}$$

For us, "soft" radiation means soft compared to both high-energy daughters of the underlying LO splitting $E \to xE + (1-x)E$, and so the small-y approximation used in (3.8) is only valid for $y \ll \min(x, 1-x)$, which is parametrically equivalent to $y \ll x(1-x)$.

$\bar{s}(x)$ diverges proportional to $\ln(x(1-x))$ for $x \to 0$ or $x \to 1$. It is natural to rewrite the $\ln y + \bar{s}(x)$ in a way that combines the $\ln y$ and $\ln(x(1-x))$ behavior,

$$\ln y + \bar{s}(x) = \ln\left(\frac{y}{x(1-x)}\right) + \hat{s}(x) \tag{3.10}$$

with

$$\hat{s}(x) = -\ln(16(1-x+x^2)) + 2\frac{[x^2(\ln x - \frac{\pi}{8}) + (1-x)^2(\ln(1-x) - \frac{\pi}{8})]}{(1-x+x^2)}. \tag{3.11}$$

[$\hat{s}(x)$ remains finite for $x \to 0$ and $x \to 1$.] It will also sometimes be useful to think of the integral (3.8) in terms of energy and so rewrite it as

$$-\frac{C_{\rm A}\alpha_{\rm s}}{4\pi}\left[\frac{d\Gamma}{dx}\right]^{\rm LO}\int_{\omega_y\ll\min(x,1-x)E}\frac{d\omega_y}{\omega_y}\left[\ln\left(\frac{\omega_y}{x(1-x)E}\right) + \hat{s}(x)\right], \tag{3.12}$$

where $\omega_y \equiv yE$ is the energy of the soft y daughter.

By itself, the integral in (3.12) is IR divergent and so ultimately depends on the IR physics or IR regulator that cuts off those divergences. We will not be sensitive to the IR details because we intend to study infrared-safe characteristics of the shower, namely the shape (1.1) of the energy deposition distribution $\epsilon(z)$. To this end, we will introduce an energy factorization scale $\Lambda_{\rm fac}$ and separate the NLO contribution to the net rate into

$$\left[\frac{d\Gamma}{dx}\right]^{\rm NLO}_{\rm net} = \left[\frac{d\Gamma}{dx}\right]^{\rm NLO,fac}_{\rm net} - \frac{C_{\rm A}\alpha_{\rm s}}{4\pi}\left[\frac{d\Gamma}{dx}\right]^{\rm LO}\int_0^{\Lambda_{\rm fac}}\frac{d\omega_y}{\omega_y} \times\left[\ln\left(\frac{\omega_y}{x(1-x)E}\right) + \hat{s}(x)\right], \tag{3.13}$$

where the superscript "fac" above stands for "factorized." The IR-subtracted net rate

$$\left[\frac{d\Gamma}{dx}\right]^{\rm NLO,fac}_{\rm net} \equiv \int_0^\infty dy\Bigg\{V(x,y)\theta\left(y < \frac{1-x}{2}\right) + V(1-x,y)\theta\left(y < \frac{x}{2}\right) + R(x,y)\theta\left(y < \frac{1-x}{2}\right) + \frac{C_{\rm A}\alpha_{\rm s}}{4\pi}\left[\frac{d\Gamma}{dx}\right]^{\rm LO}\frac{\ln y + \bar{s}(x)}{y}\theta(yE < \Lambda_{\rm fac})\Bigg\} \tag{3.14}$$

is then finite, and it can be computed numerically.

Our program is to absorb the last (IR-sensitive) term of (3.13) into an effective value $\hat{q}_{\rm eff}$ of $\hat{q}$ and so into an effective value $[d\Gamma/dx]^{\rm LO}_{\rm eff}$ of the leading-order $g \to gg$ splitting rate. In principle, this simply shuffles the problem of IR-sensitive physics to $[d\Gamma/dx]^{\rm LO}_{\rm eff}$. Moreover, in principle, the large double and single IR logarithms in $[d\Gamma/dx]^{\rm LO}_{\rm eff}$ would then have to be tamed by a next-to-leading-log order (NLLO) resummation of IR logarithms to all orders in $\alpha_{\rm s}(\mu)$. In practice, we will find that we can ignore the replacement of $[d\Gamma/dx]^{\rm LO}$ by $[d\Gamma/dx]^{\rm LO}_{\rm eff}$ in evaluating whether those overlap effects that cannot be absorbed into $\hat{q}$ are large or small. In part, this is because constant shifts $\delta\hat{q}$ to the value of $\hat{q}$ will, by design, have no effect on the shape function (1.1)—that is precisely why we choose to study the shape function. Additionally, it is because we will later show that changes that could affect the leading-order shape function do not affect the relative sizes NLO/LO of overlap effects at the order of our calculation. For now, the upshot is that we will focus on the IR-subtracted version (3.14) of the net splitting rate.

Note that we have written the integral as $\int_0^\infty dy$ in (3.14). However, the largest y for which the integrand is nonzero is $\max(x/2, (1-x)/2, \Lambda_{\rm fac}/E)$.

C. Choice of factorization and renormalization scales

1. Our usual choice

As previously noted, IR logarithms result from soft radiation with energies ω_y up to the parametric scale $\min(x, 1-x)E$. The choice of factorization scale that subtracts as much of the IR logarithms as possible is then $\Lambda_{\rm fac} \sim \min(x, 1-x)E$, and our usual choice will be

$$\Lambda_{\rm fac} = \kappa x(1-x)E, \tag{3.15}$$

where κ is an $O(1)$ constant that we will canonically choose to be 1, but which we will vary later.

Our UV renormalization scale μ should be chosen so that the explicit $\alpha_{\rm s}(\mu)$ in the leading-order splitting rate $[d\Gamma/dx]^{\rm LO}$ (the $\alpha_{\rm s}$ associated with the high-energy splitting vertex) is evaluated at an appropriate physics scale to account for anti-screening from virtual particle pairs present in the vacuum. During a formation time, the transverse separation b of the daughters of a $g \to gg$ splitting is of order $(\hat{q}\omega)^{-1/4}$, where $\omega = \min(x, 1-x)E$. (Note that this is parametrically small compared to medium scales in the high-energy limit.) So we want $\alpha_{\rm s}(1/b)$, which is $\alpha_{\rm s}(\mu)$ with $\mu \sim (\hat{q}\omega)^{1/4}$. In terms of our choice (3.15), this is $\mu \sim (\hat{q}\Lambda_{\rm fac})^{1/4}$. Rather than varying the exact choices of μ and $\Lambda_{\rm fac}$ separately, we will simply combine the two by choosing

$$\Lambda_{\rm fac} = \kappa x(1-x)E, \qquad \mu = (\hat{q}_{\rm A}\Lambda_{\rm fac})^{1/4}. \tag{3.16}$$

2. An alternate choice

We will also consider another choice for comparison. In our theorist's limit of arbitrarily high energy showers (and an infinite-size medium), an underlying LO single splitting process $g \to gg$, with $E \to xE + (1-x)E$, should not affect where energy is deposited in the z direction in the limit that the radiated energy fraction x (or $1-x$) is extremely small, since that soft x gluon deposits negligible energy. So it will not matter if we make a poor estimate of the size of the IR logarithms for the even softer radiative corrections to such an already very soft process. Parametrically, we only need do a reasonable job with choosing the factorization scale for the case where $\min(x, 1-x) \sim 1$. So, though (3.16) is a more physically sensible choice, one should in principle, for the purpose of calculating $\epsilon(z)$ and then its shape $S(Z)$, be able to get away with choosing

$$\Lambda_{\rm fac} = rE, \qquad \mu = (\hat{q}_{\rm A}\Lambda_{\rm fac})^{1/4} \tag{3.17}$$

instead, where r is an $O(1)$ constant.

We will later compare results using (3.16) and (3.17) to check the robustness of our conclusions about the impact of overlap corrections that cannot be absorbed into $\hat{q}$. Note that, for a perfectly democratic splitting with $x = \frac{1}{2}$, our two different choices (3.16) and (3.17) match up when $r = \kappa/4$.

D. Numerical results and fits for $\Lambda_{\rm fac} = x(1-x)E$

Using (3.14), with the rate formulas of Refs. [9,15] as described in Appendix A of this paper, and choosing $\Lambda_{\rm fac} = x(1-x)E$, we have numerically computed[14] the values of $[d\Gamma/dx]^{\rm NLO,fac}_{\rm net}$ represented by the data points in Fig. 6 and in the last column of Table I.[15] More specifically, the figure and table show the values of

$$f(x) \equiv \frac{\left[\frac{d\Gamma}{dx}\right]^{\rm NLO,fac}_{\rm net}}{C_{\rm A}\alpha_{\rm s}\left[\frac{d\Gamma}{dx}\right]^{\rm LO}}, \tag{3.18}$$

where $[d\Gamma/dx]^{\rm LO}$ is given by (2.1). It is convenient to plot this ratio not only to see the relative size (in units of $C_{\rm A}\alpha_{\rm s}$) of the NLO correction compared to the leading-order rate, but also because both the numerator and denominator blow up proportional to $[x(1-x)]^{-3/2}$ (up to logarithms) as $x \to 0$ or $x \to 1$, and so $f(x)$ is a smoother function than $[d\Gamma/dx]^{\rm NLO,fac}_{\rm net}$.

[14] See Appendix B 1 for some information on our numerical methods.

[15] The data points in Table I and Fig. 8 that have extremely tiny x or $1-x$ are not intended to be relevant to any actual phenomenological situation, since our high-energy approximations fail when xE or $(1-x)E$ are $\lesssim T$. They are included just for the purpose of understanding the asymptotic behavior of our formulas.

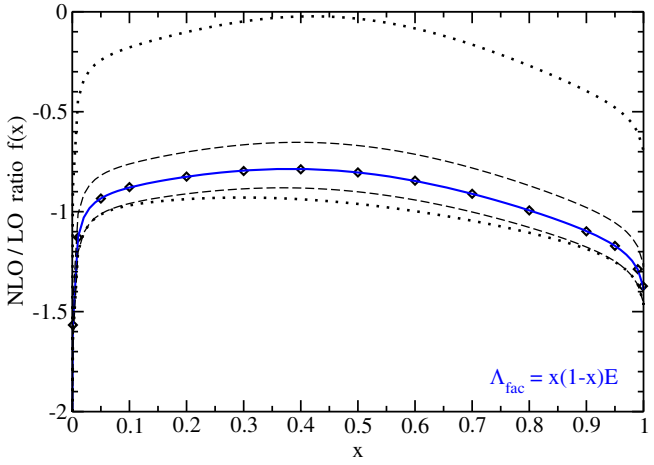

FIG. 6. Plot of the ratio (3.18) vs x for $\Lambda_{\rm fac} = \kappa x(1-x)E$ and $\mu = (\hat{q}_{\rm A}\Lambda_{\rm fac})^{1/4}$. The diamonds are numerically computed data points for $\kappa = 1$, and the solid curve is a fit (3.19) to those points. For the sake of later discussion, the dashed lines show the results for $\kappa = \frac{1}{2}$ (upper) and $\kappa = 2$ (lower), and the dotted lines for $\kappa = \frac{1}{16}$ (upper) and $\kappa = 16$ (lower).

TABLE I. Our numerical results for $f(x)$ for $\Lambda_{\rm fac} = x(1-x)E$ and $\mu = (\hat{q}_{\rm A}\Lambda_{\rm fac})^{1/4}$. The last column shows values for the ratio (3.18), as plotted by the diamonds in Fig. 6. The second column breaks out the contribution from only diagrams [9] without $F = 4 + I$ vertices. The third column is the contribution from diagrams [15] with $F = 4 + I$ vertices, which are shown by diamonds in Fig. 7. We estimate our numerical error in these results to be roughly ± 1 in the last digit for all entries except the entries for $x = 0.0001$ and 0.9999 [where we estimate $\pm$(a few) in the last digit]. We expended computational effort to get the second-column entries for $x = 0.0001$ and 0.9999 in order to capture and fit the log behavior of (3.19b), but we did not see a need to expend similar effort for corresponding entries in the third column, which have been left blank.

	$f(x)$		
x	Non-F	F diagrams	Total
0.0001	−2.087		
0.001	−1.525	−0.0425	−1.568
0.01	−1.081	−0.0470	−1.128
0.05	−0.8787	−0.0551	−0.9339
0.1	−0.8178	−0.0586	−0.8764
0.2	−0.7673	−0.0571	−0.8245
0.3	−0.7455	−0.0509	−0.7965
0.4	−0.7422	−0.0459	−0.7881
0.5	−0.7573	−0.0463	−0.8037
0.6	−0.7924	−0.0530	−0.8453
0.7	−0.8477	−0.0625	−0.9102
0.8	−0.9237	−0.0697	−0.9935
0.9	−1.0276	−0.0697	−1.0974
0.95	−1.1057	−0.0653	−1.1710
0.99	−1.228	−0.0577	−1.286
0.999	−1.319	−0.0542	−1.374
0.9999	−1.361		

The first thing to note about these results is that the relative size of the (factorized) NLO contribution to $[d\Gamma/dx]_{\rm net}$ is a roughly $C_{\rm A}\alpha_{\rm s} \times 100\%$ correction to $[d\Gamma/dx]^{\rm LO}$. One would need $C_{\rm A}\alpha_{\rm s} = N_{\rm c}\alpha_{\rm s}$ to be small for this to be a small correction. But remember that our motivation is to study overlap effects that cannot be absorbed into $\hat{q}$. If $f(x)$ were independent of x, then, no matter how large f was, the NLO corrections would simply rescale the size of $[d\Gamma/dx]^{\rm LO}$, which could be absorbed by rescaling the size of $\hat{q}$, which would have no effect on, for example, the shape $S(Z)$ of the energy deposition distribution. So what will be important about Fig. 6 is how it varies with x, not its overall value. We must wait until we compute the NLO effect on the shape before we can draw conclusions.

The leading-order rate $[d\Gamma/dx]^{\rm LO}$ for $g \to gg$ is symmetric under swapping the two daughters via $x \leftrightarrow 1-x$. The second thing to note about Fig. 6 is that $f(x)$ and so $[d\Gamma/dx]^{\rm NLO}_{\rm fac}$ are not symmetric in $x \leftrightarrow 1-x$. In general, $[d\Gamma/dx]_{\rm net}$ is not symmetric because $1 \to 3$ processes are not. Those processes (such as overlapping $g \to gg \to ggg$) have three daughters; they are symmetric under permutations of $(x, y, 1-x-y)$ but not under $x \leftrightarrow 1-x$.

We will be curious later to understand the relative importance or unimportance of processes involving fundamental or effective 4-gluon interactions such as Fig. 5 on the shape properties that we will calculate. Following Ref. [15], we refer to such interactions as "F = 4 + I" interactions, where "F" is meant to be evocative of the word "four"; "4" stands for fundamental 4-gluon vertices and "I" stands for interactions via longitudinally polarized gluon exchange, which are "instantaneous" in LCPT. Figure 7

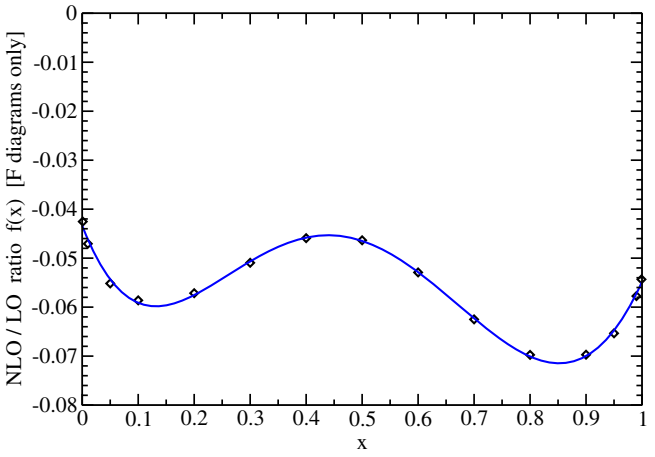

FIG. 7. Like Fig. 6 but here showing only the contribution from diagrams that contain at least one F = 4 + I interaction [15], like the examples in Fig. 5. These diagrams do not have IR divergences and so do not require factorization, and so they do not affect the infrared subtraction in (3.14) and are not sensitive to the choice of $\Lambda_{\rm fac}$. These diagrams are also UV convergent and are not sensitive to the choice of renormalization scale μ. The solid curve corresponds to the fit (3.19c).

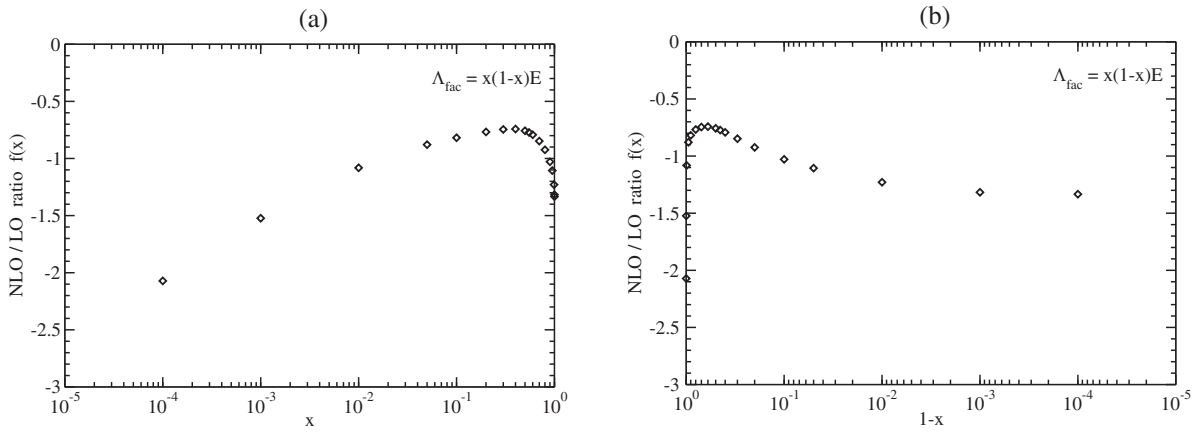

FIG. 8. (a) A log-linear plot of the non-F contributions to the ratio $f(x)$ of (3.18). (b) The same data plotted vs $1-x$ instead of x. Note that we have arranged both plots so that $x \to 0$ is on the left and $x \to 1$ is on the right.

shows our result for the piece of Fig. 6 that comes from processes involving F interactions [15].

Since data points like those of Table I are slow to compute numerically, and since we will later need to use $[d\Gamma/dx]_{\rm net}$ both in integrals and in integrodifferential equations, we need a reasonable alternative that is quick to evaluate. We have therefore fit the data of Table I to a fairly accurate functional form. We will continue to distinguish the contribution of the F diagrams, and so we write

$$f(x) = f_{\text{non-F}}(x) + f_{\rm F}(x). \tag{3.19a}$$

We have found a good fit to the non-F contributions (the second column of Table I) by the function

$$\begin{aligned} f_{\text{non-F}}(x) = {} & 0.26873 \ln x + 0.00745 \ln(1-x) - 3.92750 \\ & + 8.96222x - 1.69021x^2 - 2.93372x^{1/2} \\ & - 1.71625x^{3/2} + 1.26448(1-x)^{1/2} \\ & + 3.08068(1-x)^{3/2}. \end{aligned} \tag{3.19b}$$

This fits all the non-F data of the table with at most 0.003 absolute error and better than 0.3% relative error. The presence of $\ln x$ behavior as $x \to 0$ is clear from the log-linear plot of the non-F data in Fig. 8(a). In contrast, Fig. 8(b) does not convincingly demonstrate $\ln(1-x)$ behavior as $x \to 1$, and so for now the nonzero coefficient of the $\ln(1-x)$ term in our fit (3.19b) should not be taken too seriously. (We have not made the numerical effort to push our calculations to even smaller values of $1-x$.) For the rest of (3.19b), we found the use of half powers of x and $1-x$ necessary to fit the data well with a relatively few number of terms. This is a possibility that might have been anticipated; the somewhat-related experience of Ref. [42] was that small-y expansions of overlapping real splittings (and their virtual counterparts) were expansions in powers of $y^{1/2}$ rather than integer powers of y (where y was the softest gluon).

For the F diagram contributions of Fig. 7 (the third column of Table I), we found that a simple polynomial fit worked well enough,

$$\begin{aligned} f_{\rm F}(x) = {} & -0.04338 - 0.29586x + 1.69249x^2 - 3.29499x^3 \\ & + 2.38669x^4 - 0.49977x^5, \end{aligned} \tag{3.19c}$$

which is the solid curve plotted in Fig. 7. This fits the data points with at most 0.001 absolute error, which is small when combined with the non-F diagrams. The solid curve plotted in Fig. 6 is the total ratio (3.19a).

E. Converting between different choices of $\Lambda_{\rm fac}$

1. Overview

To understand how our results for $[d\Gamma/dx]^{\rm NLO,fac}_{\rm net}$ will change if one changes the factorization scale $\Lambda_{\rm fac}$ and renormalization scale μ, we just need to know how our results depend on those two scales. We can read the $\Lambda_{\rm fac}$ dependence from the last term of (3.14),[16]

$$\begin{aligned} \left[\frac{d\Gamma}{dx}\right]^{\rm NLO,fac}_{\rm net} & = (\Lambda_{\rm fac}\,\text{independent}) + \frac{C_{\rm A}\alpha_{\rm s}}{4\pi}\left[\frac{d\Gamma}{dx}\right]^{\rm LO} \\ & \quad \times \int_0^\infty dy \frac{\ln y + \bar{s}(x)}{y} \theta(yE < \Lambda_{\rm fac}) \\ & = (\Lambda_{\rm fac}\,\text{independent}) + \frac{C_{\rm A}\alpha_{\rm s}}{4\pi}\left[\frac{d\Gamma}{dx}\right]^{\rm LO} \\ & \quad \times \left\{ \frac{1}{2}\ln^2\left(\frac{\Lambda_{\rm fac}}{E}\right) + \bar{s}(x)\ln\left(\frac{\Lambda_{\rm fac}}{E}\right) \right\}. \end{aligned} \tag{3.20}$$

[16]The fact that the explicit integral shown in the first line of (3.20) is infrared divergent does not matter, since (i) that divergence does not depend on $\Lambda_{\rm fac}$ and (ii) the divergence cancels, by construction, against the other $\Lambda_{\rm fac}$-independent terms in (3.14).

The renormalization scale μ dependence is even easier to isolate. The explicit $\ln\mu$ dependence of the NLO result must cancel the implicit dependence in the coupling $\alpha_s(\mu)$ in the leading-order rate (2.1), and so

$$\left[\frac{d\Gamma}{dx}\right]^{\text{NLO,fac}}_{\text{net}} = (\mu\,\text{independent}) - \beta_0\alpha_s\left[\frac{d\Gamma}{dx}\right]^{\text{LO}}\ln\mu, \quad (3.21)$$

where β_0 is the leading-order coefficient of the renormalization group β function for α_s. Since we are investigating purely gluonic showers in the large-N_c limit, only the gluonic contribution matters,

$$\beta_0 = -\frac{11C_A}{6\pi}. \quad (3.22)$$

Putting together (3.20) and (3.21), the change $\delta[d\Gamma/dx]$ in the net rate due to changing Λ_{fac} and/or μ is

$$\delta\left[\frac{d\Gamma}{dx}\right]^{\text{NLO,fac}}_{\text{net}} = \frac{C_A\alpha_s}{4\pi}\left[\frac{d\Gamma}{dx}\right]^{\text{LO}}\times\delta\left\{\frac{1}{2}\ln^2\left(\frac{\Lambda_{\text{fac}}}{E}\right) + \bar{s}(x)\ln\left(\frac{\Lambda_{\text{fac}}}{E}\right) - \frac{4\pi\beta_0}{C_A}\ln\mu\right\}. \quad (3.23)$$

A change from $\Lambda_{\text{fac}} = x(1-x)E$ to $\Lambda_{\text{fac}} = \kappa x(1-x)E$, with $\mu = (\hat{q}_A\Lambda_{\text{fac}})^{1/4}$ in both cases, then gives

$$\left[\frac{d\Gamma}{dx}\right]^{\text{NLO,fac}}_{\text{net}}\Bigg|_{\substack{\Lambda_{\text{fac}}=\kappa x(1-x)E\\ \mu=(\hat{q}_A\Lambda_{\text{fac}})^{1/4}}} = \left[\frac{d\Gamma}{dx}\right]^{\text{NLO,fac}}_{\text{net}}\Bigg|_{\kappa=1} + \frac{C_A\alpha_s}{4\pi}\left[\frac{d\Gamma}{dx}\right]^{\text{LO}}\times\left\{\frac{1}{2}\ln^2\kappa + \left(\hat{s}(x) - \frac{\pi\beta_0}{C_A}\right)\ln\kappa\right\}. \quad (3.24)$$

The dashed curves in Fig. 6 show the variation in the ratio $f(x)$ of (3.18) from increasing the choice of κ up or down by a factor of 2. In estimating factorization scale dependence, one may reasonably wonder whether it is more physically relevant to vary the energy scale Λ_{fac} by a factor of 2 or so, or to vary the associated transverse momentum scale $(\hat{q}\Lambda_{\text{fac}})^{1/4}$ by a factor of 2 or so. The latter corresponds to varying Λ_{fac} up or down by a factor of 16, shown by the dotted curves in Fig. 6. The conservative conclusion is that $f(x)$ and so $[d\Gamma/dx]^{\text{NLOfac}}_{\text{net}}$ are potentially very sensitive to the choice of factorization scale. Fortunately, our final results concerning overlap corrections to the shape function $S(Z)$ will be dramatically less sensitive.

Note that the x-independent terms in the factor $\{\cdots\}$ in the rescaling (3.24) could be absorbed into a constant shift in $\hat{q}$ and so will not affect the shape function $S(Z)$. Only the x-dependent pieces will change the shape function. Note also that in this case the change in renormalization scale μ has no explicit effect on the size of the NLO correction to $S(Z)$.

2. An alternate choice

As mentioned earlier, we will eventually also examine how our results turn out if one chooses (more simply but more unphysically) an x-independent factorization scale $\Lambda_{\text{fac}} = rE$ as in (3.17). In that case, the relation to our numerical results for $\Lambda_{\text{fac}} = x(1-x)E$ is just (3.24) with κ replaced by $r/x(1-x)$,

$$\left[\frac{d\Gamma}{dx}\right]^{\text{NLO,fac}}_{\text{net}}\Bigg|_{\substack{\Lambda_{\text{fac}}=rE\\ \mu=(\hat{q}_A\Lambda_{\text{fac}})^{1/4}}} = \left[\frac{d\Gamma}{dx}\right]^{\text{NLO,fac}}_{\text{net}}\Bigg|_{\substack{\Lambda_{\text{fac}}=x(1-x)E\\ \mu=(\hat{q}_A\Lambda_{\text{fac}})^{1/4}}} + \frac{C_A\alpha_s}{4\pi}\left[\frac{d\Gamma}{dx}\right]^{\text{LO}}\left\{\frac{1}{2}\ln^2\left(\frac{r}{x(1-x)}\right) + \left(\hat{s}(x) - \frac{\pi\beta_0}{C_A}\right)\ln\left(\frac{r}{x(1-x)}\right)\right\}. \quad (3.25)$$

We note that, because of the double log in (3.25), the NLO/LO ratio $f(x)$ will diverge like $\ln^2(x(1-x))$ for $\Lambda_{\text{fac}} = rE$ as $x \to 0$ or $x \to 1$, instead of the milder $\ln x$ divergence as $x \to 0$ (and perhaps no divergence for $x \to 1$) that we found numerically for $\Lambda_{\text{fac}} = x(1-x)$. The worse divergence of $\Lambda_{\text{fac}} = rE$ is an indication that $\Lambda_{\text{fac}} = x(1-x)$ better captures the physics of $x \to 0$ and $x \to 1$, as we supposed.

3. Yet another choice

Though we will not use it for numerics, it will be convenient in some of our later discussion to also consider the choice

$$\Lambda_{\text{fac}} = rE_0, \qquad \mu = (\hat{q}_A\Lambda_{\text{fac}})^{1/4}, \quad (3.26)$$

where E_0 is the energy of the original particle that initiates the shower, and r is again a fixed, $O(1)$ constant. At first sight, a seeming failure of this choice is that it is the wrong scale late in the development of the shower (or any part of the shower), when particle energies have dropped to $E \ll E_0$. In that case, however, those particles are already effectively stopped, since their remaining stopping distance $\ell_{\text{stop}}(E) \sim \alpha_s^{-1}\sqrt{E/\hat{q}}$ is then parametrically small compared to the overall stopping distance $\ell_{\text{stop}}(E_0) \sim \alpha_s^{-1}\sqrt{E_0/\hat{q}}$. Having chosen Λ_{fac} poorly for those $E \ll E_0$ splittings will not have a significant effect on the energy deposition distribution $\epsilon(z)$. As to the lack of x dependence in (3.26), the argument that was made in the case of (3.17) applies here as well.

For later reference, the conversion is

$$\left[\frac{d\Gamma}{dx}\right]^{\text{NLO,fac}}_{\text{net}}\Bigg|_{\substack{\Lambda_{\text{fac}}=rE_0\\ \mu=(\hat{q}_{\text{A}}\Lambda_{\text{fac}})^{1/4}}} = \left[\frac{d\Gamma}{dx}\right]^{\text{NLO,fac}}_{\text{net}}\Bigg|_{\substack{\Lambda_{\text{fac}}=x(1-x)E\\ \mu=(\hat{q}_{\text{A}}\Lambda_{\text{fac}})^{1/4}}} + \frac{C_{\text{A}}\alpha_{\text{s}}}{4\pi}\left[\frac{d\Gamma}{dx}\right]^{\text{LO}}\left\{\frac{1}{2}\ln^2\left(\frac{rE_0}{x(1-x)E}\right) + \left(\hat{s}(x)-\frac{\pi\beta_0}{C_{\text{A}}}\right)\ln\left(\frac{rE_0}{x(1-x)E}\right)\right\}. \tag{3.27}$$

F. Scaling of $[d\Gamma/dx]^{\text{fac}}_{\text{net}}$ with energy E

The only dimensionful scales in the original NLO differential rates $\Delta d\Gamma/dxdy$ are $\hat{q}$ and the parent energy E. Like the leading-order rate (2.1), those differential rates are proportional to $\sqrt{\hat{q}/E}$ and so scale like $E^{-1/2}$ for fixed x and y. However, the integration over y in (3.6) to get $[d\Gamma/dx]^{\text{NLO}}_{\text{net}}$ produced IR log divergences. To factorize out those divergences, we introduced a new energy scale Λ_{fac} to define $[d\Gamma/dx]^{\text{NLO,fac}}_{\text{net}}$ in (3.14). If we take our canonical choice $\Lambda_{\text{fac}}=\kappa x(1-x)E$ or the alternate choice $\Lambda_{\text{fac}}=rE$, then we are not introducing a new dimensionful parameter, and $[d\Gamma/dx]^{\text{NLO,fac}}_{\text{net}}$ will scale as $E^{-1/2}$. But this is not the case if we instead choose $\Lambda_{\text{fac}}=rE_0$ as in (3.26). Specifically, (3.27) shows that this choice would introduce a term into $[d\Gamma/dx]^{\text{NLO,fac}}_{\text{net}}$ that scales as $E^{-1/2}\ln^2(E_0/E)$. Later, in Sec. V and beyond, we make use of simplifications that occur when $[d\Gamma/dx]^{\text{fac}}_{\text{net}}$ scales exactly as $E^{-1/2}$. At that time, we will only consider choices where $\Lambda_{\text{fac}}\propto E$, like $\Lambda_{\text{fac}}=x(1-x)E$ or $\Lambda_{\text{fac}}=rE$, and not $\Lambda_{\text{fac}}\propto E_0$.

IV. LO VS EFFECTIVE LO RATES

In defining the factorized net rate (3.14), we subtracted the IR log divergences from the net rate and imagined absorbing those divergences into an effective leading-order $g\to gg$ splitting rate $[d\Gamma/dx]^{\text{LO}}_{\text{eff}}$. Formally, within our approximations so far,[17]

$$\left[\frac{d\Gamma}{dx}\right]^{\text{LO}}_{\text{eff}} = \left[\frac{d\Gamma}{dx}\right]^{\text{LO}}\left\{1-\frac{C_{\text{A}}\alpha_{\text{s}}}{4\pi}\int_0^{\Lambda_{\text{fac}}}\frac{d\omega_y}{\omega_y}\times\left[\ln\left(\frac{\omega_y}{x(1-x)E}\right)+\hat{s}(x)\right]\right\}. \tag{4.1}$$

However, to really compute $[d\Gamma/dx]^{\text{LO}}_{\text{eff}}$, one would have to correctly account for the infrared physics that cuts off the IR divergence of the integral above. Parametrically, the result at leading-log order is

$$\left[\frac{d\Gamma}{dx}\right]^{\text{LO}}_{\text{eff}} \approx \left[\frac{d\Gamma}{dx}\right]^{\text{LO}}\left\{1-\frac{C_{\text{A}}\alpha_{\text{s}}}{8\pi}\ln^2\left(\frac{\Lambda_{\text{fac}}}{T}\right)\right\}. \tag{4.2}$$

In the high-energy limit, the double logarithm becomes large since we choose $\Lambda_{\text{fac}}\propto E$. That means that $\alpha_{\text{s}}\ln^2(\Lambda_{\text{fac}}/T)$ is not small at high energy, and one must resum logarithms to all orders in α_{s} to get a usable result for $[d\Gamma/dx]^{\text{LO}}_{\text{eff}}$.

Let us ignore that complication for just a moment to give a very crude preview of the type of argument we will eventually make. Imagine, just for a moment, that the logarithms were not large and that $\alpha_{\text{s}}\ln^2(\Lambda_{\text{fac}}/T)$ had size $O(\alpha_{\text{s}})$. In this paper, we want to explore the relative size of NLO corrections that cannot be absorbed into $\hat{q}$, as measured by the shape function $S(Z)$. That means that we will look at the ratio of the factorized NLO correction to the effective LO result for $S(Z)$. But (if logarithms were not large), this ratio would be

$$\frac{\text{NLO}_{\text{fac}}}{\text{LO}_{\text{eff}}} = \frac{\text{NLO}_{\text{fac}}}{\text{LO}\times[1+O(\alpha_{\text{s}})]} = \frac{\text{NLO}_{\text{fac}}}{\text{LO}}\times[1+O(\alpha_{\text{s}})]. \tag{4.3}$$

The desired ratio $\text{NLO}_{\text{fac}}/\text{LO}_{\text{eff}}$ is itself $O(\alpha_{\text{s}})$, but (4.3) means that the difference between using LO and LO_{eff} in the denominator is an even higher-order correction to the ratio and so can be ignored. At the order of our calculation, we can simply calculate $\text{NLO}_{\text{fac}}/\text{LO}$ instead of $\text{NLO}_{\text{fac}}/\text{LO}_{\text{eff}}$. Unfortunately, the logic of (4.3) fails because the accompanying logarithms are large.[18]

So think schematically about resumming the large logarithms in $[d\Gamma/dx]^{\text{LO}}_{\text{eff}}$ to all orders in α_{s}. At first order in α_{s}, (4.1) absorbs not only a leading, double log but also a subleading, single log. To be consistent, we must then consider NLLO resummation of large logarithms. We do not know how to do the full NLLO resummation. Fortunately, we do not need it because the shape function $S(Z)$ and its moments are completely insensitive to any constant shift in $\hat{q}$, which corresponds to any constant (i.e. x and E independent) contributions to the braces $\{\cdots\}$ in (4.1). Understanding the x and E dependence of the NLLO resummation is much easier than understanding the full NLLO resummation. To preview the result of this section we will argue that, for large logarithms, the resummed version of (4.3) is

$$\frac{\text{NLO}_{\text{fac}}}{\text{LO}_{\text{eff}}} = \frac{\text{NLO}_{\text{fac}}}{\text{LO}\times[1+O(\sqrt{\alpha_{\text{s}}})]} = \frac{\text{NLO}_{\text{fac}}}{\text{LO}}\times[1+O(\sqrt{\alpha_{\text{s}}})] \tag{4.4}$$

[17] In (4.1), we are using the version of the integral from (3.13).

[18] In fact, such logarithms have to be large if we wish to treat our high-energy $\alpha_{\text{s}}(\mu)$ as smaller than the $\alpha_{\text{s}}(T)$ of the medium.

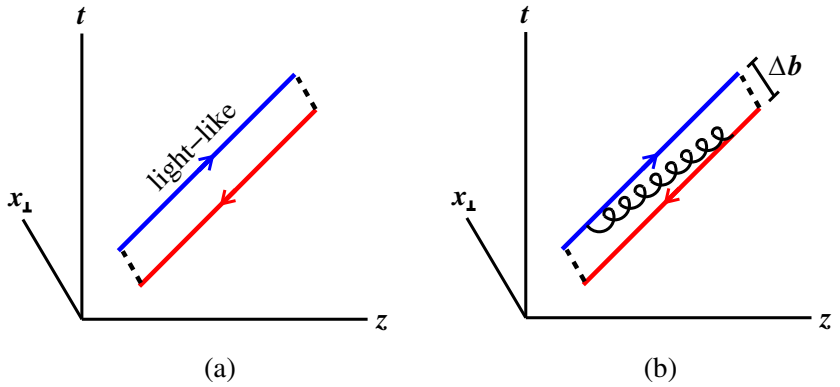

FIG. 9. (a) A Wilson loop with long, lightlike sides and transverse spatial width Δb, whose expectation gives $\exp(-\frac{1}{4}\hat{q}(\Delta b)\mathbb{T}(\Delta b)^2)$ for small Δb and large extent $\mathbb{T}$ in time t. (b) An example of a high-energy nearly-collinear radiative contribution to the Wilson loop.

provided the LO quantity is (like the shape function) insensitive to constant shifts of $\hat{q}$.

The following discussion may be a little clearer if we first remove any x and E dependence from our choice of factorization scale, taking $\Lambda_{\rm fac} = rE_0$ as in (3.26) for the purpose of this argument. The conversion (3.27) between this scale and our usual choice $\Lambda_{\rm fac} = x(1-x)E$ is finite and is free of large logarithms unless $x(1-x) \ll 1$ or $E \ll E_0$. As discussed in Secs. III C 2 and III E 3, those limiting cases will not significantly affect the calculation of the shower energy deposition distribution $\epsilon(z)$ and its shape, and so the conversion (3.27) does not need to be resummed.

A. Origin of the IR double and single logs in (4.1)

We need to review the origin of the remaining, explicit x and E dependence in (4.1) so that we can discuss how to resum it. We will use the combined analysis of IR double and single logarithms presented in Ref. [40]. There, the usual, leading-order BDMPS-Z rate calculation (in $\hat{q}$ approximation) was modified by replacing $\hat{q}$ by the effective transverse momentum broadening parameter $\hat{q}_{\rm eff}(\Delta b)$ originally calculated by Liou, Mueller and Wu (LMW) [41], which incorporates the effect of soft radiation carrying away transverse momentum. The Δb in $\hat{q}_{\rm eff}(\Delta b)$ represents transverse separation. Formally, $\hat{q}_{\rm eff}(\Delta b)$ is extracted from the thermal expectation of a Wilson loop with long, lightlike sides separated by transverse distance Δb, as depicted in Fig. 9(a). The bare $\hat{q}_{(0)}$ corresponds to the contribution from thermal-scale correlations in the medium; the double and single logarithms come from the exchange of a nearly collinear, high-energy gluon ($\omega \gg T$) as in Fig. 9(b). In our application, those logarithms are cut off at high energy by the factorization scale $\Lambda_{\rm fac}$, so that $T \ll \omega \le \Lambda_{\rm fac}$. We should really write $\hat{q}_{\rm eff}(\Delta b; \Lambda_{\rm fac})$ instead of just $\hat{q}_{\rm eff}(\Delta b)$, but we will stick with the shorter notation $\hat{q}_{\rm eff}(\Delta b)$ for now, with the $\Lambda_{\rm fac}$ dependence implicit.[19]

As reviewed in our notation in Ref. [40], the Zakharov picture of the usual BDMPS-Z calculation for $g \to gg$ involves solving for the propagator of 3-particle quantum mechanics in the two-dimensional transverse plane with Hamiltonian

$$H = \frac{p_{\perp 1}^2}{2|p_{z_1}|} + \frac{p_{\perp 2}^2}{2|p_{z_2}|} - \frac{p_{\perp 3}^2}{2|p_{z_3}|} - \frac{i\hat{q}_{\rm A}}{8}(b_{12}^2 + b_{23}^2 + b_{31}^2), \quad (4.5)$$

where $\boldsymbol{b}_{ij} \equiv \boldsymbol{b}_i - \boldsymbol{b}_j$ are the transverse separations between the three "particles" in Fig. 10 and $(p_{z1}, p_{z2}, p_{z3}) = (1-x, x, -1)E$ are the corresponding longitudinal momenta of those particles. Symmetries are used to reduce this to a 1-particle quantum mechanics problem in a single transverse position variable $\boldsymbol{B}$ related by

$$\boldsymbol{b}_{12} = \boldsymbol{B}, \qquad \boldsymbol{b}_{23} = -(1-x)\boldsymbol{B}, \qquad \boldsymbol{b}_{31} = -x\boldsymbol{B}, \quad (4.6)$$

which reduces (4.5) to

$$H = \frac{P^2}{2x(1-x)E} - \frac{i\hat{q}_{\rm A}}{8}(1 + (1-x)^2 + x^2)B^2, \quad (4.7)$$

where $\boldsymbol{P}$ is conjugate to $\boldsymbol{B}$. In the LO splitting process of Fig. 10, transverse separations vary with time, but the typical value $\bar{\mathcal{B}}$ of B during the splitting is parametrically

[19] In the original work of LMW [41] on momentum broadening, the role of our "$\Lambda_{\rm fac}$" is played by the largest "soft" bremsstrahlung energy ω that has a formation time that fits inside the length L of the medium, which corresponds to $\Lambda_{\rm fac} \sim \hat{q}L^2$. Our canonical choice (3.16) of $\Lambda_{\rm fac}$ in this paper corresponds to replacing that L by the formation time of the underlying hard single-splitting process $E \to xE + (1-x)E$ that one is computing soft radiative corrections too.

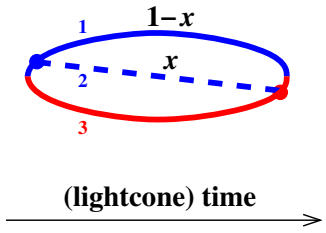

FIG. 10. This is Fig. 1(b) for LO splitting $g \to gg$, but here with the three lines labeled (1,2,3).

$$\bar{\mathcal{B}} \sim [x(1-x)E\hat{q}]^{-1/4}. \tag{4.8}$$

Reference [40] argued that, in the large-N_c limit, the modification of (4.5) that would correctly reproduce the IR double and single logs from soft radiative corrections to the hard, underlying $g \to gg$ process was, with one caveat,

$$H = \frac{p_{\perp 1}^2}{2|p_{z_1}|} + \frac{p_{\perp 2}^2}{2|p_{z_2}|} - \frac{p_{\perp 3}^2}{2|p_{z_3}|} - \frac{i}{8}[\hat{q}_{\rm A}^{\rm eff}(b_{12})b_{12}^2 + \hat{q}_{\rm A}^{\rm eff}(b_{23})b_{23}^2 + \hat{q}_{\rm A}^{\rm eff}(b_{31})b_{31}^2]. \tag{4.9}$$

The caveat is that the momentum broadening analysis of LMW [41] gives the $\hat{q}_{\rm eff}$ between an amplitude (blue) line and a conjugate amplitude (red) line in Fig. 10. The $\hat{q}_{\rm eff}$ between two amplitude (blue) lines is slightly different. In the analysis of Ref. [40], this difference was equivalent to replacing

$$\hat{q}_{\rm A}^{\rm eff}(b_{12}) \to \hat{q}_{\rm A}^{\rm eff}(e^{-i\pi/8}b_{12}), \tag{4.10}$$

in (4.9). The modified (4.9) then reduces to

$$H = \frac{P^2}{2x(1-x)E} - \frac{i}{8}[\hat{q}_{\rm A}^{\rm eff}(e^{-i\pi/8}B) + (1-x)^2\hat{q}_{\rm A}^{\rm eff}((1-x)B) + x^2\hat{q}_{\rm A}^{\rm eff}(xB)]B^2. \tag{4.11}$$

Reference [40] used this Hamiltonian instead of (4.7) for the BDMPS-Z calculation and reproduced the soft radiative corrections (3.8) to the usual leading-order BDMPS-Z rate (2.1). The result may be summarized in the form[20]

$$\left[\frac{d\Gamma}{dx}\right]_{\rm eff}^{\rm LO} = \left[\frac{d\Gamma}{dx}\right]^{\rm LO} {\rm Re}\left\{\sqrt{2}e^{-i\pi/4}\left[w_{12}\sqrt{\frac{\hat{q}_{\rm A}^{\rm eff}(\bar{\mathcal{B}})}{\hat{q}_{\rm A(0)}}} + w_{23}\sqrt{\frac{\hat{q}_{\rm A}^{\rm eff}(e^{-i\pi/8}(1-x)\bar{\mathcal{B}})}{\hat{q}_{\rm A(0)}}} + w_{31}\sqrt{\frac{\hat{q}_{\rm A}^{\rm eff}(e^{-i\pi/8}x\bar{\mathcal{B}})}{\hat{q}_{\rm A(0)}}}\right]\right\}, \tag{4.12}$$

where here[21]

$$\bar{\mathcal{B}} \equiv e^{-\gamma_E/2}\left[\frac{1}{2}x(1-x)(1-x+x^2)\hat{q}_{\rm A}E\right]^{-1/4}, \tag{4.13}$$

and the weights (w_{12}, w_{23}, w_{31}) are defined by

$$w_{12} = \frac{1}{1+(1-x)^2+x^2}, \qquad w_{23} = \frac{(1-x)^2}{1+(1-x)^2+x^2}, \qquad w_{31} = \frac{x^2}{1+(1-x)^2+x^2}, \tag{4.14}$$

with

$$w_{12} + w_{23} + w_{31} = 1. \tag{4.15}$$

The intricate details of these formulas will not matter for our argument, but we thought it useful to have something concrete to reference. There are two aspects of (4.12) that will matter.

The first is that, for our application, the arguments Δb of the three $\hat{q}_{\rm A}^{\rm eff}(\Delta b)$'s in (4.12) are all of order

$$\Delta b \sim \mathcal{B}_0 \equiv (\hat{q}_{\rm A}E_0)^{-1/4}. \tag{4.16}$$

That is because, as previously discussed, processes with parametrically (i) $E \ll E_0$ or (ii) $x \ll 1$ or $1-x \ll 1$ are not important to determining the shape function $S(Z)$.

The second important aspect is that, if one were to replace all three of the different $\hat{q}_{\rm A}^{\rm eff}(\Delta b)$'s in (4.12) by the fixed (x and E independent)[22] value $\hat{q}_{\rm A}^{\rm eff}(\mathcal{B}_0)$, then the effective LO rate $[d\Gamma/dx]_{\rm eff}^{\rm LO}$ would be a fixed multiple of the original $[d\Gamma/dx]^{\rm LO}$ (i.e. something that could be

[20]Though some broader claims were made at the end, Ref. [40] only did explicit calculations for the part of the double-log region to the right of the corner marked β in our Fig. 11. However, that region contains all of the Δb dependence of the logarithms, which is our ultimate interest here.

[21]Our $\bar{\mathcal{B}}$ defined in (4.13) differs from the $\bar{B}$ defined in Ref. [40] by a factor of $i^{1/4} = e^{i\pi/8}$.

[22]$\hat{q}_{\rm A}^{\rm eff}(\Delta b) = \hat{q}_{\rm A}^{\rm eff}(\Delta b; \Lambda_{\rm fac})$ also depends on $\Lambda_{\rm fac}$. Remember the earlier argument that the difference between using $\Lambda_{\rm fac} = rE_0$ and $\Lambda_{\rm fac} = rE$ or $\Lambda_{\rm fac} = \kappa x(1-x)E$ does not involve large logarithms in our application, and so, for simplicity, we would carry out our discussion of resumming large logarithms using the fixed scale choice $\Lambda_{\rm fac} = rE_0$. That simplifies the discussion here because the only x and E dependence inside the braces $\{\cdots\}$ in (4.12) is that of the arguments Δb of $\hat{q}_{\rm A}^{\rm eff}(\Delta b; \Lambda_{\rm fac})$; we need not be distracted by the possibility of x or E dependence of $\Lambda_{\rm fac}$ in this analysis.

absorbed by a constant shift of $\hat{q}$), and so the shape of the energy deposition distribution would be unchanged; $S^{\rm LO}_{\rm eff}(Z) = S^{\rm LO}(Z)$. That means that the actual difference between $S^{\rm LO}_{\rm eff}(Z)$ and $S^{\rm LO}(Z)$ depends specifically on how $\hat{q}^{\rm eff}_{\rm A}(\Delta b)$ varies when one varies Δb.

B. The dependence of resummed $\hat{q}^{\rm eff}_{\rm A}(\Delta b)$ on Δb

The dependence of the original LMW $\hat{q}_{\rm eff}(\Delta b)$ on Δb is easy to extract from parametric arguments for the double log in Ref. [41], provided we rewrite their parametric formulas in terms of variables more relevant here. Figure 11 shows the double-log region, where τ_0 is the scale of the mean free path for elastic scattering of high-energy particles from the medium. The difference with similar discussion in LMW is that they were interested specifically in the problem of transverse-momentum broadening after passing through a large length L of medium, and in that context they eventually set the transverse separation to be $\Delta b \sim (\hat{q}L)^{-1/2}$. We want to keep everything in terms of Δb, which can be achieved by substituting back $L \sim 1/\hat{q}(\Delta b)^2$ in their general discussion. With this translation, they found

$$\begin{aligned}\hat{q}_{\rm eff}(\Delta b) &= \hat{q}_{(0)} + \delta\hat{q}(\Delta b)\\ &\approx \hat{q}_{(0)}\left[1 + \frac{C_{\rm A}\alpha_{\rm s}}{2\pi}\ln^2\left(\frac{1}{\hat{q}\tau_0(\Delta b)^2}\right)\right]\end{aligned} \tag{4.17}$$

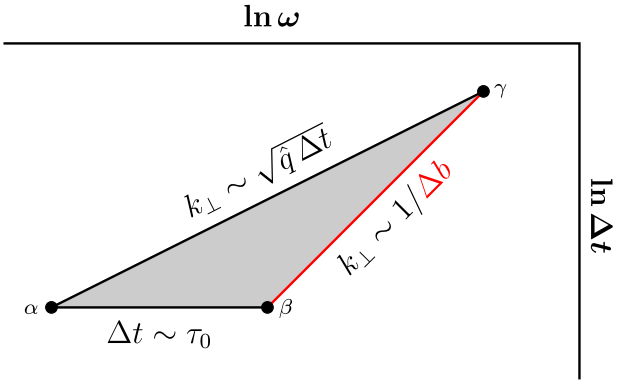

FIG. 11. The integration region giving rise to the double logs of LMW [41]. Here ω is the energy of the soft-radiated gluon (which we called yE earlier), and Δt is the time over which it is radiated (the difference of the emission time in the amplitude and the emission time in the conjugate amplitude). The transverse momentum of the soft-radiated gluon is $k_\perp \sim \sqrt{\omega/\Delta t}$. The only boundary that is sensitive to Δb is the red one. For a quark-gluon plasma, the three vertices (α, β, γ) above respectively correspond to $(\omega, \Delta t)$ of order (T, τ_0), $(\tau_0/(\Delta b)^2, \tau_0)$, and $(1/\hat{q}(\Delta b)^4, 1/\hat{q}(\Delta b)^2)$. The last one is also parametrically $\sim(\Lambda_{\rm fac}, t_{\rm form}(\Lambda_{\rm fac}))$ for our application. We have not shown any vertical snip off the γ corner corresponding to constraining $\omega \le \Lambda_{\rm fac}$ because it is unimportant as far as large logarithms are concerned and so, for this purpose, is a detail hidden inside the circle marking that corner.

at leading-log order, to first order in $\alpha_{\rm s}(\mu)$. In fact, the Δb dependence of the double log above contains all of the Δb dependence including the single log as well [41]. We can therefore use LMW's results for leading-log order resummation to all orders in $\alpha_{\rm s}(\mu)$ to also obtain the results for the Δb dependence of a NLLO resummation. (We outline a more detailed argument of this claim in Appendix C.)

Equation (4.17) was derived by LMW for the case where one ignores running of $\alpha_{\rm s}(k_\perp)$. In that case, they obtained an analytic result for the leading-log resummation. We will continue with their fixed-coupling analysis, but later argue that a running coupling will not change our conclusion that $\mathrm{NLO/LO_{eff}} \simeq \mathrm{NLO/LO}$ as in (4.4). Their resummed result, when translated from their L back to Δb, is

$$\hat{q}_{\rm eff}(\Delta b) \approx \hat{q}_{(0)}\frac{I_1\left(2\left(\frac{C_{\rm A}\alpha_{\rm s}}{\pi}\right)^{1/2}\ln\left(\frac{1}{\hat{q}\tau_0(\Delta b)^2}\right)\right)}{\left(\frac{C_{\rm A}\alpha_{\rm s}}{\pi}\right)^{1/2}\ln\left(\frac{1}{\hat{q}\tau_0(\Delta b)^2}\right)}, \tag{4.18}$$

where I_1 is the modified Bessel function. Remember that in our problem $\Delta b \sim \mathcal{B}_0 = (\hat{q}_{\rm A}E_0)^{-1/4}$, and so[23]

$$\frac{1}{\hat{q}\tau_0(\Delta b)^2} \sim \sqrt{\frac{E_0}{T}}. \tag{4.19}$$

In the high-energy limit of large logarithms, (4.18) becomes

$$\hat{q}_{\rm eff}(\Delta b) \approx \hat{q}_{(0)}\left(\frac{1}{\hat{q}\tau_0(\Delta b)^2}\right)^{2\sqrt{C_{\rm A}\alpha_{\rm s}/\pi}}, \tag{4.20}$$

where we have suppressed a prefactor proportional to $1/(\sqrt{\alpha_{\rm s}}\log)^{3/2}$ that will not affect the argument (see Appendix C 4 for details). Since $\Delta b \sim \mathcal{B}_0$, this can be expanded as

$$\begin{aligned}\hat{q}_{\rm eff}(\Delta b) \approx \hat{q}_{(0)}&\left(\frac{1}{\hat{q}\tau_0\mathcal{B}_0^2}\right)^{2\sqrt{C_{\rm A}\alpha_{\rm s}/\pi}}\\ &\times\left[1 - 2\left(\frac{C_{\rm A}\alpha_{\rm s}}{\pi}\right)^{1/2}\ln\left(\frac{(\Delta b)^2}{\mathcal{B}_0^2}\right)\right]\end{aligned} \tag{4.21}$$

and so

[23]In the case of a weakly coupled QGP with gauge coupling coupling g, we have used $\hat{q}_{(0)} \sim g^4T^3$ and $\tau_0 \sim 1/g^2T$ and so $\hat{q}_{(0)}\tau_0^2 \sim T$ in (4.19). For a strongly coupled QGP, the only relevant scale here is T. One can worry that one should self-consistently use $\hat{q}_{\rm eff}$ instead of $\hat{q}_{(0)}$ for $\hat{q}$ in (4.19), but the difference would only generate a subleading $O(\alpha_{\rm s})$ correction to the $O(\sqrt{\alpha_{\rm s}})$ exponents in (4.20) and (4.21) and will not affect the conclusion (4.22).

$$\hat{q}_{\rm eff}(\Delta b) = \hat{q}_{\rm eff}(\mathcal{B}_0)[1 + O(\sqrt{\alpha_s})] = (\text{fixed constant}) \times [1 + O(\sqrt{\alpha_s})]. \quad (4.22)$$

The expansion in $\sqrt{\alpha_s}$ made here is valid because $\ln(\Delta b/\mathcal{B}_0)$ is not a large logarithm in our application. Equation (4.22) is the justification for our earlier claim (4.4) that we could ignore the difference between $S^{\rm LO}(Z)$ and $S^{\rm LO}_{\rm eff}(Z)$ when computing the relative size of NLO corrections to $S^{\rm LO}_{\rm eff}(Z)$.

C. Running of $\alpha_s(k_\perp)$

In the preceding, we used an explicit resummation formula (4.18) that ignored running of $\alpha_s(k_\perp)$. At leading-log order, one may find more sophisticated discussions in Refs. [43–45]. However, that analysis is not needed for our argument.

First note that the red boundary $k_\perp \sim 1/\Delta b$ in Fig. 11 is the part of the double-log region where $k_\perp$ is the largest and so $\alpha_s(k_\perp)$ is the smallest. In our previous argument, we were trying to show that

$$\left| \frac{\hat{q}_{\rm eff}(\Delta b) - \hat{q}_{\rm eff}(\mathcal{B}_0)}{\hat{q}_{\rm eff}(\mathcal{B}_0)} \right| \ll 1 \quad (4.23)$$

for $\Delta b \sim \mathcal{B}_0$, so that $\hat{q}_{\rm eff}(\Delta b)$ could be replace by $\hat{q}_{\rm eff}(\mathcal{B}_0)$. For fixed coupling, we argued that this ratio was $O(\sqrt{\alpha_s})$. Imagine that the fixed coupling we had taken was the coupling associated with the red boundary, $\alpha_s(1/\Delta b)$. Note that $1/\Delta b \sim 1/\mathcal{B}_0 \sim (\hat{q}E_0)^{1/4} \sim \mu$ in our application, and so, up to higher-order corrections, $\alpha_s(1/\Delta b)$ is just the $\alpha_s = \alpha_s(\mu)$ that we have been using throughout this entire paper. Now imagine replacing fixed $\alpha_s = \alpha_s(1/\Delta b)$ by a running $\alpha_s(k_\perp)$. The numerator in (4.23) does not change, because it only involves the physics of $k_\perp \sim 1/\Delta b$. But the denominator gets bigger because, in the rest of the double-log region, $\alpha_s(k_\perp)$ is bigger than before. So, the parametric inequality (4.23) remains valid for small $\alpha_s(\mu)$.

D. Notation: LO vs bare

Going forward, it will be helpful to somewhat streamline our notation. From now on, we will use "LO" to refer to calculations based on the leading-order splitting rates (2.1) with $\hat{q}$ taken to be $\hat{q}_{\rm eff}(\mathcal{B}_0)$, as opposed to the bare $\hat{q}_{(0)}$. With this nomenclature, we now formally have

$$\text{LO}_{\rm eff} = \text{LO} \times [1 + O(\sqrt{\alpha_s})] \quad (4.24)$$

for any quantity we will discuss in the context of energy deposition, including ones that are (unlike the shape function) sensitive to constant shifts in $\hat{q}$.

V. ENERGY DEPOSITION EQUATION

In this section, we derive the basic equation satisfied by the energy deposition distribution $\epsilon(z)$. We will build on the methods of Refs. [32,46].[24] One might be able to directly figure out the final formula in terms of the net rate $[d\Gamma/dx]_{\rm net}$, but we think it is clearer to first review earlier results written in terms of $[d\Gamma/dx]_{1\to2}$ and $[d\Gamma/dx]_{1\to3}$.

For simplicity, start by considering a shower composed of only $1 \to 2$ splittings. Let $\epsilon(E, z)$ represent the distribution of deposited energy as a function of position z for a shower initiated by a particle of energy E, with

$$\int_0^\infty dz\, \epsilon(E, z) = E. \quad (5.1)$$

The starting equation is

$$\epsilon(E, z + \Delta z) \simeq [1 - \Gamma(E)\Delta z]\epsilon(E, z) + \frac{1}{2}\int_0^1 dx \left[\frac{d\Gamma}{dx}(E, x)\right]_{1\to2} \times \Delta z\{\epsilon(xE, z) + \epsilon((1-x)E, z)\} \quad (5.2)$$

for small Δz. To see this, think of traveling the distance $z + \Delta z$ indicated on the left-hand side as first traveling Δz followed by traveling distance z. In the first Δz of distance, the particle has a chance $1 - \Gamma(E)\Delta z$ of not splitting at all, and then the energy density deposited after traveling the remaining distance z will just be $\epsilon(E, z)$. This possibility is represented by the first term on the right-hand side of (5.2). Alternatively, there is a chance that the particle does split in the first Δz. In this case, we will have two particles with energies xE and $(1-x)E$, which will deposit energy density $\epsilon(xE, z)$ and $\epsilon((1-x)E, z)$ respectively after traveling the remaining distance z. Both daughter's eventual contribution to the deposited energy are added together in the second term of (5.2). The factor of $\frac{1}{2}$ in the second term is the identical final-state particle factor for the two daughter gluons,

$$\Gamma(E) = \frac{1}{2}\int_0^1 dx \left[\frac{d\Gamma}{dx}(E, x)\right]_{1\to2}. \quad (5.3)$$

Rearranging the terms in (5.2) and taking the limit $\Delta z \to 0$ yields the integrodifferential equation

$$\frac{\partial\epsilon(E, z)}{\partial z} = -\Gamma(E)\epsilon(E, z) + \frac{1}{2}\int_0^1 dx \left[\frac{d\Gamma}{dx}(E, x)\right]_{1\to2} \times \{\epsilon(xE, z) + \epsilon((1-x)E, z)\}. \quad (5.4)$$

[24] See in particular Appendix A.1 of Ref. [32], but specialize throughout to the case of a single type of particle (namely gluons).

Now use the symmetry of $[d\Gamma/dx]_{1\to 2}$ under exchange of the final-state daughters x and $1-x$ to rewrite this as

$$\frac{\partial\epsilon(E,z)}{\partial z} = -\Gamma(E)\epsilon(E,z) + \int_0^1 dx \left[\frac{d\Gamma}{dx}(E,x)\right]_{1\to 2} \epsilon(xE,z). \tag{5.5}$$

$1\to 3$ splittings may be included by following the same steps. First, add a $1\to 3$ term

$$+\frac{1}{3!}\int_0^1 dx \int_0^{1-x} dy \left[\frac{d\Gamma}{dxdy}(E,x,y)\right]_{1\to 3} \times \{\epsilon(xE,z)+\epsilon(yE,z)+\epsilon((1-x-y)E,z)\} \tag{5.6}$$

to the right-hand side of (5.4). Using the symmetry of the three daughters, this generalizes (5.5) to

$$\begin{aligned}\frac{\partial\epsilon(E,z)}{\partial z} &= -\Gamma(E)\epsilon(E,z) + \int_0^1 dx \left[\frac{d\Gamma}{dx}(E,x)\right]_{1\to 2} \epsilon(xE,z) \\ &\quad + \frac{1}{2}\int_0^1 dx \int_0^{1-x} dy \left[\frac{d\Gamma}{dxdy}(E,x,y)\right]_{1\to 3} \epsilon(xE,z) \\ &= -\Gamma(E)\epsilon(E,z) + \int_0^1 dx \left[\frac{d\Gamma}{dx}(E,x)\right]_{\rm net} \epsilon(xE,z),\end{aligned} \tag{5.7}$$

where the last equality uses (3.1). We may now express everything in terms of $[d\Gamma/dx]_{\rm net}$ by (i) using (3.2) to rewrite Γ as $\int dx x[d\Gamma/dx]_{\rm net}$ and (ii) combining the x integrals,

$$\frac{\partial\epsilon(E,z)}{\partial z} = \int_0^1 dx \left[\frac{d\Gamma}{dx}(E,x)\right]_{\rm net} \{\epsilon(xE,z) - x\epsilon(E,z)\}. \tag{5.8}$$

Provided $[d\Gamma/dx]_{\rm net}$ scales with parent energy as $E^{-1/2}$, e.g. like the leading-order rate (2.1) does, we may define an energy-independent, rescaled rate $[d\tilde{\Gamma}/dx]_{\rm net}$ by[25]

$$\left[\frac{d\Gamma}{dx}(E,x)\right]_{\rm net} = E^{-1/2}\left[\frac{d\tilde{\Gamma}}{dx}(x)\right]_{\rm net}. \tag{5.9}$$

If rates scale like $E^{-1/2}$, then the distances z characteristic of shower development will scale like $E^{1/2}$, so the energy deposition distribution should scale as

$$\epsilon(E,z) \propto \tilde{\epsilon}(E^{-1/2}z). \tag{5.10}$$

[25]It might be more elegant to scale out a factor of $C_{\rm A}\alpha_{\rm s}\sqrt{\hat{q}_{\rm A}/E}$ in (5.9) instead of just $E^{-1/2}$, so that the rescaled rate $[d\tilde{\Gamma}/dx]_{\rm net}$ (and also eventually the coordinate $\tilde{z}$) would be dimensionless. We will find it convenient to do this later, in Sec. VII. We do not do it now because it would slightly clutter our equations and deemphasize the most essential point, the $E^{-1/2}$ dependence.

We want the rescaled function $\tilde{\epsilon}(s)$ to be independent of E and so have a normalization independent of E. We choose to normalize it so that

$$\int_0^\infty ds\, \tilde{\epsilon}(s) = 1, \tag{5.11}$$

which, together with (5.1), fixes the proportionality constant in (5.10),

$$\epsilon(E,z) = E^{1/2}\tilde{\epsilon}(E^{-1/2}z). \tag{5.12}$$

For a shower initiated by a particle of energy E_0, (5.8) becomes

$$\frac{\partial\tilde{\epsilon}(\tilde{z})}{\partial\tilde{z}} = \int_0^1 dx x \left[\frac{d\tilde{\Gamma}}{dx}(x)\right]_{\rm net} \{x^{-1/2}\tilde{\epsilon}(x^{-1/2}\tilde{z}) - \tilde{\epsilon}(\tilde{z})\}, \tag{5.13}$$

where

$$\tilde{z} \equiv E_0^{-1/2} z, \tag{5.14a}$$

and the original energy deposition distribution $\epsilon(z)$ that we were looking for is

$$\epsilon(z) \equiv \epsilon(E_0,z) = E_0^{1/2}\tilde{\epsilon}(\tilde{z}). \tag{5.14b}$$

Now that the variable $\tilde{z}$ has served its purpose, we may use (5.9) with $E=E_0$, along with (5.14), to rewrite (5.13) in terms of the original, unscaled variables as

$$\frac{\partial\epsilon(z)}{\partial z} = \int_0^1 dx\, x \left[\frac{d\Gamma}{dx}(E_0,x)\right]_{\rm net} \{x^{-1/2}\epsilon(x^{-1/2}z) - \epsilon(z)\}, \tag{5.15}$$

Just remember that this formula is only valid if $[d\Gamma/dx]_{\rm net}$ scales with energy as exactly $E^{-1/2}$.

Equation (5.15) will be the basic equation underlying the analysis in the rest of this paper. Like $[d\Gamma/dx]^{\rm LO}$ of (2.1), $[d\Gamma/dx]_{\rm net}$ diverges $\propto [x(1-x)]^{-3/2}$ for $x\to 0$ and $x\to 1$. It is useful to note that, nonetheless, the x integration in (5.15) is convergent as $x\to 1$ because the two terms inside the braces then cancel, and it is also convergent as $x\to 0$ because of (i) the overall factor of x in the integrand and (ii) the fact that the energy deposition distribution $\epsilon(z')$ must fall rapidly (at least exponentially) to zero as $z'\to\infty$.

VI. MOMENTS OF THE SHAPE $S(Z)$

The simplest aspects to calculate, of the energy deposition distribution $\epsilon(z)$ and its shape $S(Z)$, are their moments.

Before we start, we give a clarification about numerical accuracy. In this section, we give a variety of numerical results for moments in Tables II–V, where we will implicitly

TABLE II. Expansions (6.8) of the moments $\langle z^n\rangle$ of the energy deposition distribution $\epsilon(z)$ for $\Lambda_{\rm fac} = x(1-x)E$ [(3.16) with $\kappa = 1$]. The last two columns show similar expansions of $\langle z^n\rangle^{1/n}$, for which $\delta[\langle z^n\rangle^{1/n}] = \frac{1}{n}\langle z^n\rangle_{\rm LO}^{(1/n)-1}\delta\langle z^n\rangle$. The unit ℓ_0 is defined by (6.14).

	$\langle z^n\rangle_{\rm LO}$	$\delta\langle z^n\rangle$	$\langle z^n\rangle_{\rm LO}^{1/n}$	$\delta[\langle z^n\rangle^{1/n}]$
z^n	in units of ℓ_0^n		in units of ℓ_0	
z	2.1143	2.2338 $C_{\rm A}\alpha_{\rm s}$	2.1143	2.2338 $C_{\rm A}\alpha_{\rm s}$
z^2	5.7937	12.191 $C_{\rm A}\alpha_{\rm s}$	2.4070	2.5324 $C_{\rm A}\alpha_{\rm s}$
z^3	18.758	59.214 $C_{\rm A}\alpha_{\rm s}$	2.6570	2.7959 $C_{\rm A}\alpha_{\rm s}$
z^4	68.534	289.00 $C_{\rm A}\alpha_{\rm s}$	2.8772	3.0332 $C_{\rm A}\alpha_{\rm s}$

pretend that the fit (3.19) to our NLO/LO rate ratio $f(x)$ is exactly correct. In reality, though our fit is good, it is only an approximation to $f(x)$. We have not attempted to make systematic estimates of the error arising from this approximation. However, from our experience in (i) varying the number of terms in our fits and (ii) improvement over time of the accuracy of the values that culminated in our Table I, we estimate that the final results for the relative size of overlap effects on moments of $S(Z)$ should be accurate to roughly two significant figures.

A. Recursion formula for moments of $\epsilon(z)$

To find a formula for the moments, multiply both sides of (5.15) by z^n and integrate over z. After integrating by parts on the left-hand side of the equation, one finds the recursion relation

$$-n\langle z^{n-1}\rangle = \int_0^1 dx\, x\left[\frac{d\Gamma}{dx}(E_0,x)\right]_{\rm net}\{x^{n/2}\langle z^n\rangle - \langle z^n\rangle\}, \quad (6.1)$$

giving

$$\langle z^n\rangle = \frac{n\langle z^{n-1}\rangle}{{\rm Avg}[x(1-x^{n/2})]}, \quad (6.2a)$$

where we find it convenient to introduce the notation

$${\rm Avg}[g(x)] \equiv \int_0^1 dx\left[\frac{d\Gamma}{dx}(E_0,x)\right]_{\rm net} g(x). \quad (6.2b)$$

The moments $\langle Z^n\rangle$ of the shape $S(Z)$ [defined by (1.1)] are given in terms of the moments (6.2) as simply

$$\langle Z^n\rangle = \frac{\langle z^n\rangle}{\langle z\rangle^n}. \quad (6.3)$$

As examples, the stopping distance is

$$\ell_{\rm stop} \equiv \langle z\rangle = \frac{1}{{\rm Avg}[x(1-\sqrt{x})]}, \quad (6.4)$$

and the width of the energy deposition distribution is $\sigma = (\langle z^2\rangle - \langle z\rangle^2)^{1/2}$ with

$$\langle z^2\rangle = \frac{2\ell_{\rm stop}}{{\rm Avg}[x(1-x)]}. \quad (6.5)$$

The width of the shape $S(Z)$ is then

$$\sigma_S = \frac{\sigma}{\ell_{\rm stop}} = \left(\frac{2{\rm Avg}[x(1-\sqrt{x})]}{{\rm Avg}[x(1-x)]} - 1\right)^{1/2}. \quad (6.6)$$

B. Expansion in $\alpha_{\rm s}$ and results

We now want to expand results to NLO in $\alpha_{\rm s} = \alpha_{\rm s}(\mu)$ to compute the relative size of the changes to the moments due to overlapping formation times effects. We imagine splitting the rate into

$$\left[\frac{d\Gamma}{dx}\right]_{\rm net} = \left[\frac{d\Gamma}{dx}\right]_{\rm eff}^{\rm LO} + \left[\frac{d\Gamma}{dx}\right]_{\rm net}^{\rm NLO,fac} \quad (6.7)$$

as discussed in Sec. III B. We expand the moments as

$$\langle z^n\rangle \simeq \langle z^n\rangle_{\rm LO}^{\rm eff} + \delta\langle z^n\rangle, \quad (6.8a)$$

where $\langle z^n\rangle_{\rm LO}^{\rm eff}$ represents the result obtained using $[d\Gamma/dx]_{\rm eff}^{\rm LO}$ instead of $[d\Gamma/dx]_{\rm net}$ in (6.2), and $\delta\langle z^n\rangle$ represents the factorized NLO correction to $\langle z^n\rangle_{\rm LO}^{\rm eff}$ at first order in $[d\Gamma/dx]_{\rm net}^{\rm NLO,fac}$. Remember that, adopting the nomenclature of Sec. IV D,

$$\langle z^n\rangle_{\rm LO}^{\rm eff} = \langle z^n\rangle_{\rm LO}[1 + O(\sqrt{\alpha_{\rm s}})]. \quad (6.8b)$$

Expanding the recursion relation (6.2a) gives

$$\delta\langle z^n\rangle = \langle z^n\rangle_{\rm LO}\left[\frac{\delta\langle z^{n-1}\rangle}{\langle z^{n-1}\rangle_{\rm LO}} - \frac{\delta{\rm Avg}[x(1-x^{n/2})]}{{\rm Avg}[x(1-x^{n/2})]_{\rm LO}}\right], \quad (6.9)$$

where

$${\rm Avg}[g(x)]_{\rm LO} \equiv \int_0^1 dx\left[\frac{d\Gamma}{dx}(E_0,x)\right]^{\rm LO} g(x), \quad (6.10a)$$

$$\delta{\rm Avg}[g(x)] \equiv \int_0^1 dx\left[\frac{d\Gamma}{dx}(E_0,x)\right]_{\rm net}^{\rm NLO,fac} g(x), \quad (6.10b)$$

and $\delta\langle z^0\rangle \equiv 0$. The LO moments are determined recursively by the analog of (6.2a),

$$\langle z^n\rangle_{\rm LO} = \frac{n\langle z^{n-1}\rangle_{\rm LO}}{{\rm Avg}[x(1-x^{n/2})]_{\rm LO}}. \quad (6.11)$$

Though it is not our ultimate goal, we give results for the first few moments $\langle z^n\rangle$ in Table II. These were calculated using (2.1) for the LO rate and using

TABLE III. Expansions involving moments $\langle Z^n\rangle$, reduced moments $\mu_{n,S}$, and cumulants $k_{n,S}$ of the shape function $S(Z)$. Here we take $\Lambda_{\rm fac}=\kappa x(1-x)$ and show the κ dependence of the results. There are no NLO entries for $\langle Z\rangle$ because $\langle Z\rangle=1$ and $\langle Z\rangle_{\rm LO}=1$ by definition of $Z\equiv z/\langle z\rangle$. See the caveat about significant figures given at the beginning of Sec. VI; we estimate that our results for $\chi\alpha_{\rm s}$ are valid to roughly two significant digits, once one accounts for approximation error to the NLO/LO rate ratio $f(x)$.

Quantity Q	$Q_{\rm LO}$	δQ	$\chi\alpha_{\rm s}$
$\langle Z\rangle$	1		
$\langle Z^2\rangle^{1/2}$	1.1384	$(-0.0050+0.0004\ln\kappa)C_{\rm A}\alpha_{\rm s}$	$(-0.0044+0.0003\ln\kappa)C_{\rm A}\alpha_{\rm s}$
$\langle Z^3\rangle^{1/3}$	1.2567	$(-0.0053+0.0006\ln\kappa)C_{\rm A}\alpha_{\rm s}$	$(-0.0042+0.0005\ln\kappa)C_{\rm A}\alpha_{\rm s}$
$\langle Z^4\rangle^{1/4}$	1.3608	$(-0.0031+0.0007\ln\kappa)C_{\rm A}\alpha_{\rm s}$	$(-0.0023+0.0005\ln\kappa)C_{\rm A}\alpha_{\rm s}$
$\mu_{2,S}^{1/2}=k_{2,S}^{1/2}=\sigma_S$	0.5441	$(-0.0104+0.0008\ln\kappa)C_{\rm A}\alpha_{\rm s}$	$(-0.0191+0.0014\ln\kappa)C_{\rm A}\alpha_{\rm s}$
$\mu_{3,S}^{1/3}=k_{3,S}^{1/3}$	0.4587	$(0.0139+0.0004\ln\kappa)C_{\rm A}\alpha_{\rm s}$	$(0.0303+0.0010\ln\kappa)C_{\rm A}\alpha_{\rm s}$
$\mu_{4,S}^{1/4}$	0.7189	$(0.0011+0.0006\ln\kappa)C_{\rm A}\alpha_{\rm s}$	$(0.0016+0.0009\ln\kappa)C_{\rm A}\alpha_{\rm s}$
$k_{4,S}^{1/4}$	0.2561	$(0.3242-0.0086\ln\kappa)C_{\rm A}\alpha_{\rm s}$	$(1.2662-0.0338\ln\kappa)C_{\rm A}\alpha_{\rm s}$

$$\left[\frac{d\Gamma}{dx}\right]_{\rm net}^{\rm NLO,fac}=C_{\rm A}\alpha_{\rm s}\left[\frac{d\Gamma}{dx}\right]^{\rm LO}f(x) \tag{6.12}$$

with fit function (3.19) and $\Lambda_{\rm fac}=x(1-x)E$ for the NLO rate. The parametric scale for the stopping distance is

$$\ell_{\rm stop}\sim\frac{1}{C_{\rm A}\alpha_{\rm s}}\sqrt{\frac{E_0}{\hat q_{\rm A}}}, \tag{6.13}$$

and so we have expressed the moments in Table II in appropriate units of

$$\ell_0\equiv\frac{1}{C_{\rm A}\alpha_{\rm s}}\sqrt{\frac{E_0}{\hat q_{\rm A}}}. \tag{6.14}$$

Because different moments $\langle z^n\rangle$ have different dimensions, comparing those moments would be comparing apples and oranges. So we have also converted all the moments into lengths by presenting the expansions of $\langle z^n\rangle^{1/n}$ in the last two columns. In that comparison, the overlap corrections are roughly $O(100\%)\times C_{\rm A}\alpha_{\rm s}$ relative to the LO results. This is similar in size to the NLO corrections that we saw for $[d\Gamma/dx]_{\rm net}$ in Sec. III D.

Now look instead at the analog of $\langle z^n\rangle^{1/n}$ for moments of the shape function $S(Z)$,

$$\langle Z^n\rangle^{1/n}=\frac{\langle z^n\rangle^{1/n}}{\langle z\rangle}. \tag{6.15}$$

Their expansions to NLO are given in Table III, now using the adjustable factorization scale $\Lambda_{\rm fac}=\kappa x(1-x)$ and explicitly showing the κ dependence of the results.[26]

[26]If we had shown κ dependence for the moments of Table II, they would have double-log dependence on κ. For example, $\langle z\rangle=2.1143+(2.2338+0.3084\ln\kappa-0.0841\ln^2\kappa)$ in units of ℓ_0. We did not show this for everything since we are focused on the shape function, which is not affected by constant changes in $\hat q$.

In all these entries, $\chi\alpha_{\rm s}$ is our name for the relative size of NLO corrections:

$$\chi\alpha_{\rm s}\equiv\frac{\delta Q}{Q_{\rm LO}} \tag{6.16}$$

for any quantity Q.

Table III similarly show results for $(\mu_{n,S})^{1/n}$, where the reduced moment $\mu_{n,S}$ of the shape $S(Z)$ is

$$\mu_{n,S}\equiv\langle(Z-\langle Z\rangle)^n\rangle. \tag{6.17}$$

Our motivational example of such a moment [8] is

$$\sigma_S=\frac{\sigma}{\ell_{\rm stop}}=\mu_{2,S}^{1/2}, \tag{6.18}$$

for which the relative size $\chi\alpha_{\rm s}$ of NLO corrections is roughly $-2\%\times C_{\rm A}\alpha_{\rm s}$ for $\kappa=1$ and which remains small for κ varied over any reasonable range. All the other $\langle Z^n\rangle^{1/n}$ and $(\mu_{n,S})^{1/n}$ entries in Table III have similarly small NLO corrections.

Not content to leave well enough alone, we also considered similar expansions involving the cumulants $k_{n,S}$ of $S(Z)$ up through $n=4$. For $n<4$, cumulants are the same as reduced moments, but

$$k_{4,S}\equiv\mu_{4,S}-3\mu_{2,S}^2. \tag{6.19}$$

As can be seen in Table III, the NLO correction for $k_{4,S}^{1/4}$ is large—more than $100\%\times C_{\rm A}\alpha_{\rm s}$! This is because the LO values on the right-hand side of (6.19) cancel to within 2%, and so the relatively small NLO corrections to $\mu_{4,S}$ and $3\mu_{2,S}^2$ become a large relative correction to what's left over.

One can worry if the large correction to $k_{4,S}$ is an important effect, or whether something important may

happen for moments beyond $n = 4$. A simple way to settle this is to calculate the corrections to the shape function $S(Z)$ itself rather than merely its moments. It is trickier to get accurate numerics for $S(Z)$, but we will be able to see that the NLO corrections to $S(Z)$ are all very small, the fourth cumulant $k_{4,S}$ not withstanding.

C. A formula for later

We gave recursive expressions for $\delta\langle z^n\rangle$ and $\langle z^n\rangle_{\rm LO}$ in (6.9) and (6.11), but we have not bothered to explicitly write formulas for each δQ in Table II in terms of $\delta\langle z^n\rangle$ and $\langle z^n\rangle_{\rm LO}$ and thence in terms of integrals. For later reference, it will be helpful to have one explicit example: $\chi\alpha_{\rm s} = (\delta Q)/(Q_{\rm LO})$ in the case of $Q = \sigma_S = \sigma/\ell_{\rm stop}$. Starting from $\sigma = (\langle z^2\rangle - \langle z\rangle^2)^{1/2}$ and $\ell_{\rm stop} = \langle z\rangle$, we have

$$\begin{aligned}\delta\sigma_S &= \delta\left(\frac{\sigma}{\ell_{\rm stop}}\right) = \sigma_{S,\rm LO}\left(\frac{\delta(\sigma^2)}{2\sigma^2_{\rm LO}} - \frac{\delta\langle z\rangle}{\langle z\rangle_{\rm LO}}\right)\\ &= \sigma_{S,\rm LO}\left(\frac{\delta\langle z^2\rangle - 2\langle z\rangle_{\rm LO}\delta\langle z\rangle}{2(\langle z^2\rangle_{\rm LO} - \langle z\rangle^2_{\rm LO})} - \frac{\delta\langle z\rangle}{\langle z\rangle_{\rm LO}}\right),\end{aligned} \tag{6.20}$$

and so

$$[\chi\alpha_{\rm s}]_{\sigma_S} = \frac{\delta\langle z^2\rangle - 2\langle z\rangle_{\rm LO}\delta\langle z\rangle}{2(\langle z^2\rangle_{\rm LO} - \langle z\rangle^2_{\rm LO})} - \frac{\delta\langle z\rangle}{\langle z\rangle_{\rm LO}}. \tag{6.21}$$

Combined with (6.9) and (6.11), that's good enough for numerics. If desired, one may simplify this formula to[27]

$$[\chi\alpha_{\rm s}]_{\sigma_S} = \frac{\delta{\rm Avg}[x(1-\sqrt{x})^2]}{2{\rm Avg}[x(1-\sqrt{x})^2]_{\rm LO}} - \frac{\delta{\rm Avg}[x(1-x)]}{2{\rm Avg}[x(1-x)]_{\rm LO}}. \tag{6.22}$$

D. An alternate choice: $\Lambda_{\rm fac} = rE$

Before moving on, there is another check that can be made of the robustness of our qualitative conclusion that NLO corrections to moments (other than the fourth cumulant) are tiny relative to LO results. In Sec. III C 2, we argued that the choice $\Lambda_{\rm fac} = rE$, where r is an $O(1)$ constant, is a poor choice of factorization scale for small $x(1-x)$ but should be adequate for defining the factorization of the shower's energy deposition distribution $\epsilon(z)$, and hence shape $S(Z)$, into $\rm LO_{eff}$ and NLO pieces. Our $[d\Gamma/dx]^{\rm NLO,fac}_{\rm net}$ can be converted from our original choice $\Lambda_{\rm fac} = x(1-x)E$ to $\Lambda_{\rm fac} = rE$ using (3.25) and then used to compute moments. Table IV shows the result of converting the last column $\chi\alpha_{\rm s}$ of Table III to $\Lambda_{\rm fac} = rE$.[28]

TABLE IV. Like the last column of Table III (the relative size of NLO corrections) but computed here for factorization scale $\Lambda_{\rm fac} = rE$.

Quantity Q	$\chi\alpha_{\rm s}$ ($\Lambda_{\rm fac} = rE$)
$\langle Z\rangle$	
$\langle Z^2\rangle^{1/2}$	$(0.0023 + 0.0058\ln(4r))C_{\rm A}\alpha_{\rm s}$
$\langle Z^3\rangle^{1/3}$	$(0.0051 + 0.0082\ln(4r))C_{\rm A}\alpha_{\rm s}$
$\langle Z^4\rangle^{1/4}$	$(0.0081 + 0.0090\ln(4r))C_{\rm A}\alpha_{\rm s}$
$\mu^{1/2}_{2,S} = k^{1/2}_{2,S} = \sigma_S$	$(0.0102 + 0.0252\ln(4r))C_{\rm A}\alpha_{\rm s}$
$\mu^{1/3}_{3,S} = k^{1/3}_{3,S}$	$(0.0429 + 0.0140\ln(4r))C_{\rm A}\alpha_{\rm s}$
$\mu^{1/4}_{4,S}$	$(0.0236 + 0.0169\ln(4r))C_{\rm A}\alpha_{\rm s}$
$k^{1/4}_{4,S}$	$(0.8415 - 0.4878\ln(4r))C_{\rm A}\alpha_{\rm s}$

Like Table III, the relative sizes of NLO corrections remain small, except for $k^{1/4}_{4,S}$. Note that results for $\Lambda_{\rm fac} = rE$ are more sensitive to the exact choice of r than results for $\Lambda_{\rm fac} = \kappa x(1-x)E$ were to the choice of κ.

E. The relative importance of F diagrams

Table I, or a comparison of Figs. 6 and 7, shows that F = 4 + I diagrams (like those of Fig. 5) make a relatively small contribution to $[d\Gamma/dx]^{\rm NLO,fac}_{\rm net}$ for $\Lambda_{\rm fac} = x(1-x)E$. Was it (with hindsight) important to include them in our analysis? It is interesting to examine their contribution to the shape $S(Z)$ of energy deposition, which is insensitive to changes that can be absorbed into $\hat{q}$. How much do F diagrams affect the relative size $\chi\alpha_{\rm s}$ of NLO corrections, like those given in Table III? Table V shows the relative contribution of F diagrams to $\chi\alpha_{\rm s}$ compared to the total of all NLO diagrams. Their effect is small for our favorite characteristic $\mu^{1/2}_{2,S} = \sigma/\ell_{\rm stop}$ of the shape. However, their relative effect is larger for higher moments like $\mu^{1/4}_{4,S}$.

The takeaway is that calculation of the F diagrams [15] was important for getting good estimates of some of the shape moments in a particular factorization scheme, but their inclusion or exclusion did not affect the answer to the qualitative question of whether NLO corrections are large.

[27]The averages in the first term of (6.22) are related to the averages of $x(1-x^{n/2})$ that arise in an evaluation of (6.21) by the linearity of the definitions (6.10) of δAvg and $\rm Avg_{LO}$ in their argument, which gives $\delta{\rm Avg}[x(1-\sqrt{x})^2] = 2\delta{\rm Avg}[x(1-\sqrt{x})] - \delta{\rm Avg}[x(1-x)]$ and similarly for $\rm Avg_{LO}$.

[28]$\kappa = 1$ was our canonical choice for $\Lambda_{\rm fac} = \kappa x(1-x)E$. In Table IV, we implicitly made $r = \frac{1}{4}$ our "canonical" choice for $\Lambda_{\rm fac} = rE$, just because it matches $\Lambda_{\rm fac} = x(1-x)E$ for perfectly democratic splittings $x = 0.5$. This is the reason we write the logs in Table IV as $\ln(4r)$, so that the logs vanish for $r = \frac{1}{4}$.

TABLE V. The relative contribution of F = 4 + I diagrams to the $\chi\alpha_s$ values listed in Table III for $\kappa = 1$.

Quantity Q	$\frac{\chi\alpha_s(\text{F diags only})}{\chi\alpha_s(\text{total})}$
$\langle Z\rangle$	
$\langle Z^2\rangle^{1/2}$	−14%
$\langle Z^3\rangle^{1/3}$	−25%
$\langle Z^4\rangle^{1/4}$	−63%
$\mu_{2,S}^{1/2} = k_{2,S}^{1/2} = \sigma_S$	−14%
$\mu_{3,S}^{1/3} = k_{3,S}^{1/3}$	18%
$\mu_{4,S}^{1/4}$	225%
$k_{4,S}^{1/4}$	4%

VII. THE FULL SHAPE $S(Z)$

We now turn to finding the full shape function $S(Z)$ expanded to first order in $[d\Gamma/dx]^{\text{NLO,fac}}_{\text{net}}$.

A. Method

First, return to the basic Eq. (5.15) for $\epsilon(z)$. It will be useful for numerics and the following discussion to switch to dimensionless variables

$$\hat{z} \equiv \frac{z}{\ell_0}, \qquad \hat{\epsilon}(\hat{z}) \equiv \frac{\ell_0}{E_0}\epsilon(\ell_0\hat{z}), \qquad \frac{d\hat{\Gamma}}{dx} = \ell_0\frac{d\Gamma}{dx}, \tag{7.1}$$

with ℓ_0 defined by (6.14). Then

$$\frac{\partial\hat{\epsilon}(\hat{z})}{\partial\hat{z}} = \int_0^1 dx\, x\left[\frac{d\hat{\Gamma}}{dx}\right]_{\text{net}}\{x^{-1/2}\hat{\epsilon}(x^{-1/2}\hat{z}) - \hat{\epsilon}(\hat{z})\}. \tag{7.2}$$

The leading-order version is just

$$\frac{\partial\hat{\epsilon}_{\text{LO}}(\hat{z})}{\partial\hat{z}} = \int_0^1 dx\, x\left[\frac{d\hat{\Gamma}}{dx}\right]^{\text{LO}}\{x^{-1/2}\hat{\epsilon}_{\text{LO}}(x^{-1/2}\hat{z}) - \hat{\epsilon}_{\text{LO}}(\hat{z})\}. \tag{7.3}$$

To solve (7.3) numerically, we follow a procedure similar to Ref. [32].[29] First, we start with an approximate asymptotic solution for large $\hat{z}$,

$$\hat{\epsilon}_{\text{LO}}(\hat{z}) \sim e^{-\hat{z}^2/\pi}, \tag{7.4}$$

which is derived in Appendix D. [This leading exponential dependence is also the same as that for the Blaizot/Iancu/Mehtar-Tani (BIM) model for showers, discussed in Appendix E.] We choose a large value $\hat{z}_{\text{max}} \gg 1$ and use (7.4) for $\hat{z} > \hat{z}_{\text{max}}$. Since (7.3) is a linear equation, it does not care about the overall normalization of $\hat{\epsilon}_{\text{LO}}$, and so we initially take $\hat{\epsilon}_{\text{LO}}(\hat{z}) = e^{-\hat{z}^2/\pi}$ for $\hat{z} > \hat{z}_{\text{max}}$ and postpone normalizing $\hat{\epsilon}_{\text{LO}}$ until later.

Next, we choose a small increment $\Delta\hat{z} \ll 1$ and approximate (7.3) by

$$\hat{\epsilon}_{\text{LO}}(\hat{z}-\Delta z) \simeq \hat{\epsilon}_{\text{LO}}(\hat{z}) - \Delta z\int_0^1 dx\, x\left[\frac{d\hat{\Gamma}}{dx}\right]^{\text{LO}} \times\{x^{-1/2}\hat{\epsilon}_{\text{LO}}(x^{-1/2}\hat{z}) - \hat{\epsilon}_{\text{LO}}(\hat{z})\}. \tag{7.5}$$

Note that, for any value of $\hat{z}$, the arguments of the function $\hat{\epsilon}_{\text{LO}}$ on the right-hand side of (7.5) are never smaller than $\hat{z}$ itself. So, starting with $\hat{z} = \hat{z}_{\text{max}}$, we use (7.5) repeatedly, step by step, to calculate $\hat{\epsilon}_{\text{LO}}(\hat{z})$ for smaller and smaller values of $\hat{z}$, until we get to $\hat{z} = 0$. When we are done, we then normalize $\hat{\epsilon}_{\text{LO}}(\hat{z})$ so that

$$\int_0^\infty d\hat{z}\,\hat{\epsilon}_{\text{LO}}(\hat{z}) = 1. \tag{7.6}$$

A few more details about numerical implementation are given in appendix B 2.

Next, we substitute

$$\hat{\epsilon}(\hat{z}) \simeq \hat{\epsilon}_{\text{LO}}(\hat{z}) + \delta\hat{\epsilon}(\hat{z}) \tag{7.7}$$

into (7.2) and expand to first order in NLO quantities, giving

$$\frac{\partial\delta\hat{\epsilon}(\hat{z})}{\partial\hat{z}} = \int_0^1 dx\, x\left[\frac{d\hat{\Gamma}}{dx}\right]^{\text{LO}}\{x^{-1/2}\delta\hat{\epsilon}(x^{-1/2}\hat{z}) - \delta\hat{\epsilon}(\hat{z})\} + \int_0^1 dx\, x\left[\frac{d\hat{\Gamma}}{dx}\right]^{\text{NLO,fac}}_{\text{net}}\{x^{-1/2}\hat{\epsilon}_{\text{LO}}(x^{-1/2}\hat{z}) - \hat{\epsilon}_{\text{LO}}(\hat{z})\}. \tag{7.8}$$

If not for the last term, this would have the same form as the LO equation (7.3). The last term, however, acts as a driving term generated by the previously computed $\hat{\epsilon}_{\text{LO}}(\hat{z})$. To solve (7.8), we discretize it similar to (7.5) and start with $\delta\hat{\epsilon}(\hat{z}) = 0$ for $\hat{z} > \hat{z}_{\text{max}}$. Let $\delta\hat{\epsilon}_1(\hat{z})$ be the solution obtained through this procedure.

If $\delta\hat{\epsilon}_1(\hat{z})$ is a solution to (7.8), then so is

$$\delta\hat{\epsilon}(\hat{z}) = \delta\hat{\epsilon}_1(\hat{z}) + c\hat{\epsilon}_{\text{LO}}(\hat{z}) \tag{7.9}$$

for any constant c. The solution we need is one consistent with normalizing $\hat{\epsilon} = \hat{\epsilon}_{\text{LO}} + \delta\hat{\epsilon}$ so that $\int d\hat{z}\,\hat{\epsilon}(\hat{z}) = 1$ through first order. That normalization requires

$$\int_0^\infty d\hat{z}\,\delta\hat{\epsilon}(\hat{z}) = 0. \tag{7.10}$$

The properly normalized solution (7.9) can be obtained from any particular solution $\delta\hat{\epsilon}_1$ by

$$\delta\hat{\epsilon}(\hat{z}) = \delta\hat{\epsilon}_1(\hat{z}) - \hat{\epsilon}_{\text{LO}}(\hat{z})\int_0^\infty d\hat{z}\,\delta\hat{\epsilon}_1(\hat{z}), \tag{7.11}$$

provided we have normalized $\hat{\epsilon}_{\text{LO}}$ as in (7.6).

[29] Specifically, see Appendix B of Ref. [32].

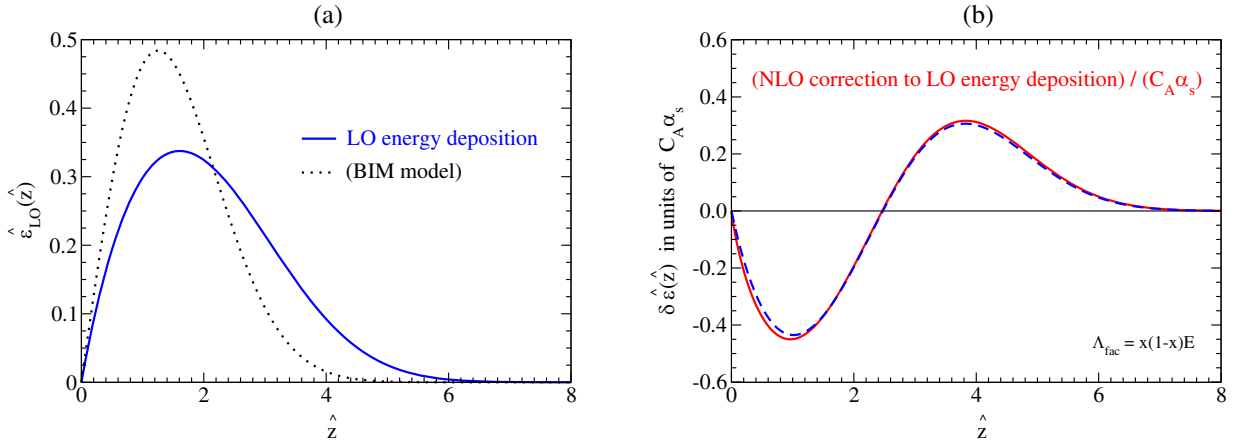

FIG. 12. (a) The solid curve shows the energy deposition distribution $\hat{\epsilon}_{\rm LO}(\hat{z})$ vs $\hat{z} \equiv z/\ell_0$, where the unit ℓ_0 is defined in (6.14). [For comparison, the dotted curve shows an analytic result (E6) derived from the BIM model.] (b) A similar plot of $\delta\hat{\epsilon}_{\rm LO}(\hat{z})/C_{\rm A}\alpha_{\rm s}$ for our canonical choice $\Lambda_{\rm fac} = x(1-x)E$ of factorization scale. For comparison, the dashed curve shows the first-order change (7.17) that would be induced in $\hat{\epsilon}_{\rm LO}(\hat{z})$ by rescaling the $\hat{z}$ axis in (a).

Finally, the expansion

$$S(Z) \simeq S_{\rm LO}(Z) + \delta S(Z) \tag{7.12}$$

of the shape function (1.1) to first order in $[d\Gamma/dx]^{\rm NLO,fac}_{\rm net}$ can be written in the form

$$S_{\rm LO}(Z) = \langle\hat{z}\rangle_{\rm LO}\hat{\epsilon}_{\rm LO}(Z\langle\hat{z}\rangle_{\rm LO}), \tag{7.13}$$

$$\delta S(Z) = \left[\langle\hat{z}\rangle_{\rm LO}\delta\hat{\epsilon}(\hat{\zeta}) + \delta\langle\hat{z}\rangle\frac{d}{d\hat{\zeta}}(\hat{\zeta}\hat{\epsilon}_{\rm LO}(\hat{\zeta}))\right]_{\hat{\zeta}=Z\langle\hat{z}\rangle_{\rm LO}}, \tag{7.14}$$

where $\langle\hat{z}\rangle_{\rm LO}$ is evaluated using $\hat{\epsilon}_{\rm LO}$, and $\delta\langle\hat{z}\rangle$ is

$$\delta\langle\hat{z}\rangle = \int_0^\infty d\hat{z}\,\hat{z}\delta\hat{\epsilon}(\hat{z}). \tag{7.15}$$

B. Results and checks

Figure 12 shows our numerical results for $\hat{\epsilon}_{\rm LO}(\hat{z})$ and $\delta\hat{\epsilon}(\hat{z})/C_{\rm A}\alpha_{\rm s}$. From the latter, we see that NLO corrections to the leading-order energy deposition distribution are large unless $C_{\rm A}\alpha_{\rm s}$ is indeed small. Similar to our earlier discussion of the Table II results for the moments of $\epsilon(z)$, this is not surprising; in Fig. 6, we saw that NLO corrections for the net rate $[d\Gamma/dx]_{\rm net}$ decreased the rate by $O(100\%) \times C_{\rm A}\alpha_{\rm s}$. A large decrease to the rate will mean a large change to how soon the shower stops, and so a large change to where the energy is deposited.

To understand the shape of $\delta\hat{\epsilon}(\hat{z})$ in Fig. 12(b), consider any change to $\hat{\epsilon}_{\rm LO}(\hat{z})$ that simply rescales the $\hat{z}$ axis,

$$\hat{\epsilon}_{\rm LO}(\hat{z}) \to \lambda\hat{\epsilon}_{\rm LO}(\lambda\hat{z}). \tag{7.16}$$

If we increase the stopping distance by choosing $\lambda = 1 - \xi$ and then formally expand to first order in ξ (just as we formally expand our overlap results to first order in $\alpha_{\rm s}$), then the change in $\hat{\epsilon}_{\rm LO}$ would be proportional to

$$-[\hat{\epsilon}_{\rm LO}(\hat{z}) + \hat{z}\hat{\epsilon}'_{\rm LO}(\hat{z})]. \tag{7.17}$$

The dashed line in Fig. 12(b) is a plot of (7.17) which, to excellent approximation, is proportional to the solid curve for $\delta\hat{\epsilon}(\hat{z})/C_{\rm A}\alpha_{\rm s}$. That is, the corrections that we see in Fig. 12(b) can mostly be absorbed into a change in the stopping distance and so into the value of $\hat{q}$.

Now turn to the shape function $S(Z) \simeq S_{\rm LO}(Z) + \delta S(Z)$, which is insensitive to constant changes that can be absorbed into $\hat{q}$. Figure 13 shows plots of $S_{\rm LO}(Z)$ and $\delta S(Z)$. Here, NLO corrections to $S_{\rm LO}(Z)$ are small even for $C_{\rm A}\alpha_{\rm s} = 1$, qualitatively consistent with our results for the moments of the shape function in Table III, but now with the clarification that the relatively large correction to the delicate fourth cumulant does not correspond to a significant effect on the shape distribution $S(Z)$. To emphasize this point, we reproduce in Fig. 14 the comparison presented in our summary paper [8] of $S_{\rm LO}(Z)$ vs $S_{\rm LO}(Z) + \delta S(Z)$ for $C_{\rm A}\alpha_{\rm s} = 1$.[30]

The shape functions shown in Fig. 13 were linearly extrapolated to the continuum limit $\Delta\hat{z} = 0$ from simulations at $(\Delta\hat{z}, \hat{z}_{\rm max}) = (0.0025, 20)$ and $(0.005,\ 20)$. To check that this is adequate, we compute moments from our numerical results for $S_{\rm LO}(Z)$ and $\delta S(Z)$ and compare them to our earlier moment calculations in Table III. Specifically,

[30]We have been careful to say $S_{\rm LO}(Z) + \delta S(Z)$ instead of simply $S(Z)$. That's because $S(Z)$ at this order is really $S^{\rm eff}_{\rm LO}(Z) + \delta S(Z)$. Section IV explained that $S_{\rm LO}$ and $S^{\rm eff}_{\rm LO}$ can be expected to differ already at $O(\sqrt{\alpha_{\rm s}})$, and we have not calculated $S^{\rm eff}_{\rm LO}$. However, the comparison of $S_{\rm LO}$ and $S_{\rm LO} + \delta S$ made in Fig. 14 is enough to investigate the relative importance of overlap effects δS.

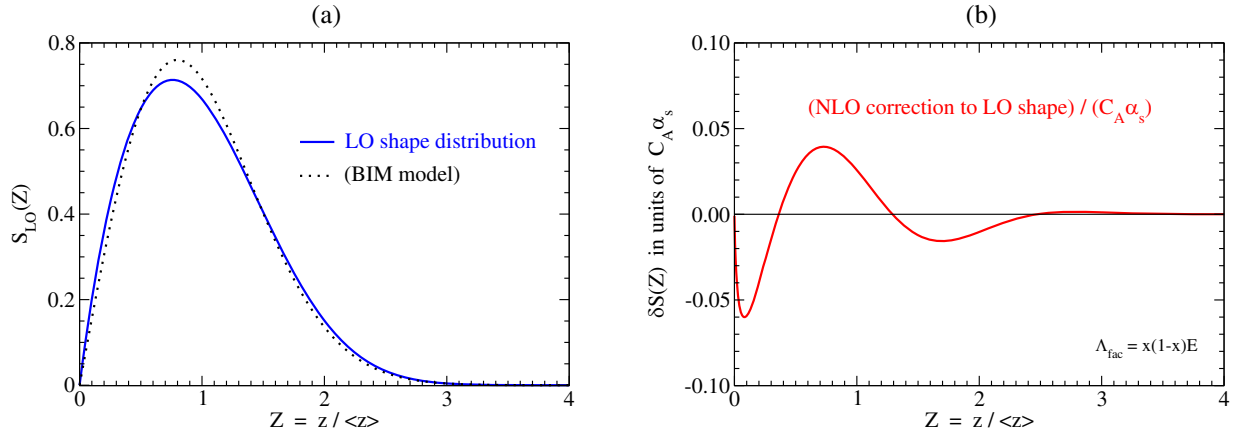

FIG. 13. (a) The solid curve shows $S_{\rm LO}(Z)$ vs $Z \equiv z/\langle z\rangle_{\rm LO}$. [For comparison, the dotted curve shows the analytic result (E8) from the BIM model.] (b) A plot of $\delta S(Z)/C_{\rm A}\alpha_{\rm s}$ for our canonical choice $\Lambda_{\rm fac} = x(1-x)E$ of factorization scale. Note the different scale of the vertical axis compared to (a).

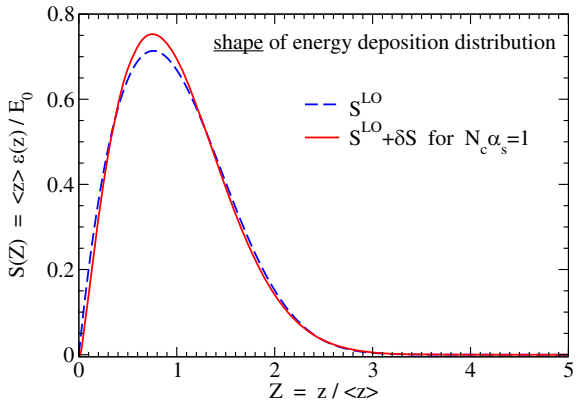

FIG. 14. Energy deposition shape with and without first-order overlapping formation time effects δS, for $C_{\rm A}\alpha_{\rm s} = 1$.

Fig. 15 shows the approach to the continuum limit of the relative size $\chi\alpha_{\rm s}$ of NLO corrections to the reduced moments and cumulants. As one can see from the figure, a linear extrapolation from our two smallest $\Delta\hat{z}$ values will do fairly well at reproducing our earlier (and more precise) moment results.[31] The precise numbers do not matter as the point of this exercise is simply to feel confident enough in the accuracy of Figs. 13 and 14 to support our qualitative conclusion that the NLO corrections to the shape function are small for $C_{\rm A}\alpha_{\rm s} \lesssim 1$.

1. An aside: BIM model for LO results

Our focus in this paper is on NLO corrections, which we have compared to the size of LO results. Like our NLO corrections, the LO energy deposition $\epsilon_{\rm LO}(z)$ and shape function $S_{\rm LO}(Z)$ have been computed numerically in Figs. 12(a) and 13(a). It is interesting to compare those numerical results to a model of LO shower development investigated by Blaizot, Iancu, and Mehtar-Tani (BIM) [30,31], which replaces the LO splitting rate (2.1) by something simpler that allows for analytic solutions. The BIM model of LO shower development gives the dotted curves in Figs. 12(a) and 13(a). (See Appendix E for details.) The BIM model result is notably different for the energy deposition $\epsilon_{\rm LO}(z)$ but is close to the exact LO result for the shape function $S_{\rm LO}(Z)$. Since our conclusion is that NLO effects for the shape function are small, the BIM model appears to give a reasonably good approximation to the shape $S(Z)$ of energy deposition (for the purely gluonic showers studied here).[32] That is, its more significant deviation in the case of $\epsilon(z)$ could be absorbed into the value of $\hat{q}$.

VIII. TIME EVOLUTION OF GLUON DISTRIBUTION

In this paper, we have focused on characteristics of the energy deposition distribution $\epsilon(z)$, for which the basic equation was (5.8). One might also be interested, more fundamentally, in the time evolution of the distribution of all shower gluon energies as a function of time. Though we will not make use of it in this paper, we present here the basic evolution equation as another example that all the necessary information about splitting rates is encoded in the net rate $[d\Gamma/dx]_{\rm net}$.

[31] See Appendix B 2 for a demonstration that errors associated with out choice of $\hat{z}_{\rm max}$ were negligible.

[32] If one compares the BIM model curve in Fig. 13(a) to the total LO + NLO curve in Fig. 14, then the BIM curve looks like it matches the total curve even better than it matches the LO curve. But this is accidental and represents a somewhat faulty comparison: The BIM curve in Fig. 13(a) is independent of the value of $C_{\rm A}\alpha_{\rm s}$, but the difference between the LO and LO + NLO curves in Fig. 14 is proportional to $C_{\rm A}\alpha_{\rm s}$, which was somewhat arbitrarily chosen to be $C_{\rm A}\alpha_{\rm s}(\mu) = 1$ for the purpose of Fig. 14.

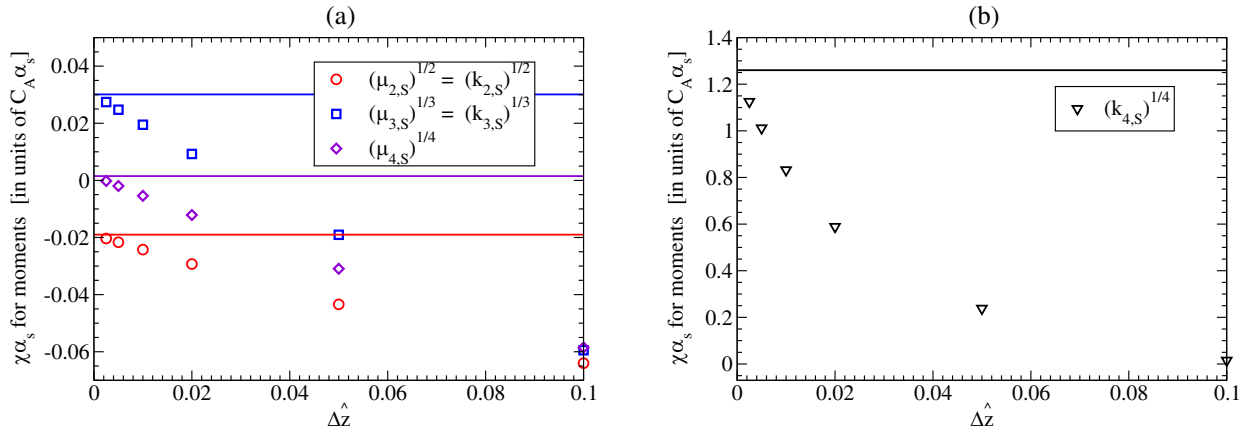

FIG. 15. The horizontal lines show the $\chi\alpha_s$ results of Table III for the relative size of NLO corrections to reduced moments and cumulants, as computed using the direct integration method of Sec. VI for $\Lambda_{\rm fac} = x(1-x)E$, i.e. $\kappa = 1$. The data points show, as a function of step size $\Delta\hat{z}$ for $\hat{z}_{\rm max} = 20$, the same moments computed instead from the $S_{\rm LO}(Z)$ and $\delta S(Z)$ functions found by the numerical methods of Sec. VII.

Reference [9] packaged the basic evolution equation as,[33,34]

$$\frac{\partial}{\partial t} n(\zeta, E_0, t) = -\Gamma(\zeta E_0) n(\zeta, E_0, t) + \int_\zeta^1 \frac{dx}{x} \left[\frac{d\Gamma}{dx}\left(\frac{\zeta E_0}{x}, x\right)\right]_{\rm net} n\left(\frac{\zeta}{x}, E_0, t\right), \tag{8.1}$$

where $n(\zeta, E_0, t)d\zeta$ represents the number of gluons with energy between ζE_0 and $(\zeta + d\zeta)E_0$ at time t. Our new observation about this equation is simply that (3.2) can be used to rewrite (8.1) completely in terms of $[d\Gamma/dx]_{\rm net}$,

$$\frac{\partial}{\partial t} n(\zeta, E_0, t) = \int_0^1 dx \left\{ \frac{\theta(x > \zeta)}{x} \times \left[\frac{d\Gamma}{dx}\left(\frac{\zeta E_0}{x}, x\right)\right]_{\rm net} n\left(\frac{\zeta}{x}, E_0, t\right) - x\left[\frac{d\Gamma}{dx}(\zeta E_0, x)\right]_{\rm net} n(\zeta, E_0, t)\right\}. \tag{8.2}$$

When discussing energy deposition, it is a little easier to describe the shower (following [30]) in terms of gluon energy density in ζ,

$$D(\zeta, E_0, t) \equiv \zeta E_0 n(\zeta, E_0, t), \tag{8.3}$$

instead of $n(\zeta, E_0, t)$. The corresponding version of (8.2) is

$$\frac{\partial}{\partial t} D(\zeta, E_0, t) = \int_0^1 dx \left\{ \theta(x > \zeta) \times \left[\frac{d\Gamma}{dx}\left(\frac{\zeta E_0}{x}, x\right)\right]_{\rm net} D\left(\frac{\zeta}{x}, E_0, t\right) - x\left[\frac{d\Gamma}{dx}(\zeta E_0, x)\right]_{\rm net} D(\zeta, E_0, t)\right\}. \tag{8.4}$$

As time progresses, $D(\zeta, E_0, t)$ develops a δ-function piece representing the amount of stopped energy,

$$D(\zeta, E_0, t) = E_{\rm stopped}(E_0, t)\delta(\zeta) + D_{\rm moving}(\zeta, E_0, t). \tag{8.5}$$

For a sanity check, we verify in Appendix F that the evolution equation (8.4) conserves total energy.

In applications where the relevant rates scale with energy exactly as $E^{-1/2}$, one may rescale variables as

[33] See Sec. 3.1.1 of Ref. [9], where our $n(\zeta, E_0, t)$ here is called $N(\zeta, E_0, t)$ there. For a sanity check of why $[d\Gamma/dz]_{\rm net}$ is appropriate in (8.1), see footnote 27 of Ref. [9].

[34] Our distribution $D(\zeta, E_0, t)$ is a $p_\perp$-integrated distribution. In principle, if one imagined a more general equation than (8.1) that fully handled overlap effects to NLO in $\alpha_s(\mu)$ for the evolution of an unintegrated distribution $\mathcal{D}(\zeta, \boldsymbol{p}_\perp, E_0, t)$, then our (8.1) should be equivalent to the $\boldsymbol{p}_\perp$ integral of that more general equation. We should also note that our (8.1) is a coarse-grained description that assumes one does not attempt to resolve time scales smaller than democratic formation times, which are of order democratic color decoherence times in the language used by authors who make antenna approximations. All effects associated with two overlapping formation times have instead already been integrated over time scales $\lesssim t_{\rm form}$ and absorbed into the formula for the effective rates $[d\Gamma/dx]_{\rm net}$ appearing in (8.1). So, for example, possible memory effects like the ones considered e.g. by Ref. [24] in antenna approximation do not appear explicitly in the structure of (8.1); they are instead implicitly accounted for (along with all other overlap effects not captured by an antenna approximation) by our rate formulas, in the situation described in Sec. I A. (See also footnote 4.)

$$t = E_0^{1/2}\tilde{t}, \qquad n(\zeta, E_0, t) = \tilde{n}(\zeta, \tilde{t}),$$
$$D(\zeta, E_0, t) = E_0 \tilde{D}(\zeta, \tilde{t}) \tag{8.6a}$$

$$\left[\frac{d\Gamma}{dx}(E, x)\right]_{\text{net}} = E^{-1/2}\left[\frac{d\tilde{\Gamma}}{dx}(x)\right]_{\text{net}}, \tag{8.6b}$$

to simplify (8.2) to

$$\frac{\partial}{\partial \tilde{t}}\tilde{n}(\zeta, \tilde{t}) = \frac{1}{\zeta^{1/2}}\int_0^1 dx \left[\frac{d\tilde{\Gamma}}{dx}\right]_{\text{net}} \times \left\{\frac{\theta(x > \zeta)}{x^{1/2}}\tilde{n}\left(\frac{\zeta}{x}, \tilde{t}\right) - x\tilde{n}(\zeta, \tilde{t})\right\} \tag{8.7}$$

or equivalently

$$\frac{\partial}{\partial \tilde{t}}\tilde{D}(\zeta, \tilde{t}) = \frac{1}{\zeta^{1/2}}\int_0^1 dx \left[\frac{d\tilde{\Gamma}}{dx}\right]_{\text{net}} \left\{\theta(x > \zeta)x^{1/2}\tilde{D}\left(\frac{\zeta}{x}, \tilde{t}\right) - x\tilde{D}(\zeta, \tilde{t})\right\}. \tag{8.8}$$

At leading order, where there are only $1 \to 2$ splitting processes, (8.8) is equivalent to an evolution equation used previously by Refs. [30,31] to study leading-order shower development in the BIM model.[35] Through the use of $[d\Gamma/dx]_{\text{net}}$, our (8.8) extends their equation to situations where there are more than just $1 \to 2$ splitting processes.

Note that $E^{-1/2}$ energy scaling is subtle at NLO, even when one chooses a factorization scale $\Lambda_{\text{fac}} \propto E$ such that $[d\Gamma/dx]_{\text{net}}^{\text{NLO,fac}}$ scales as $E^{-1/2}$. The subtlety is that $[d\Gamma/dx]_{\text{eff}}^{\text{LO}}$ then has $E^{-1/2}\ln^2 E$ instead of $E^{-1/2}$ dependence on energy. We have managed to ignore this difficulty in our analysis only because we have been specifically interested in the size of $\text{NLO}/\text{LO}_{\text{eff}}$ ratios, as discussed in Sec. IV.

One reason that we have not attempted to simulate (8.8) for this paper is that we expect it would be more numerically challenging to accurately reproduce the tiny NLO effects of Table III.

IX. WHY ARE NLO EFFECTS SO SMALL?

Why are our results for overlap effects on the shape of energy deposition so very small? The simplest characteristic of the shape function, for example, is its width $\sigma_S = \sigma/\ell_{\text{stop}}$, for which the relative size of NLO corrections listed in Table III was

$$[\chi\alpha_s]_{\sigma/\ell_{\text{stop}}}^{\text{energy}} = (-0.0191 + 0.0014\ln\kappa)C_A\alpha_s. \tag{9.1}$$

Seemingly, overlap effects which cannot be absorbed into $\hat{q}$ are almost negligible even for $C_A\alpha_s(\mu) = 1$ in large-N_c Yang-Mills theory. As noted in the summary paper [8], this conclusion is vastly different than an earlier analysis [32] of overlap effects in large-N_f QED for charge (rather than energy) deposition of a shower initiated by an electron. There, the result was

$$[\chi\alpha_{\text{EM}}]_{\sigma/\ell_{\text{stop}}}^{\text{charge}} = -0.87N_f\alpha_{\text{EM}}, \tag{9.2}$$

which would be an $O(100\%)$ effect for $N_f\alpha_{\text{EM}}(\mu) = 1$. When we set out performing the calculations in this paper, we were expecting gluon shower results somewhat similar in size to (9.2). We were very surprised by the tiny result (9.1).

One could wonder if there might be some miraculous reason why (9.1) should be exactly zero for a purely gluonic shower. Perhaps we were not careful enough with the precision of our numerics, or perhaps there was some tiny mistake in the rate formulas of Refs. [9–12]? But κ parametrizes our choice of factorization scale $\Lambda = \kappa x(1-x)$, and the κ dependence of (9.1) originates solely from the double and single IR logarithms subtracted by the definitions (3.13) and (3.14). The double logarithms have long been known [5–7] and are well-studied. The full single logarithms have been derived by two completely different methods [40,42] which give the same result. The steps that lead from there to the κ dependence (3.24) of the net rate, and then to the $\ln\kappa$ term in (9.1), are pretty straightforward.[36] Since one $O(1)$ value of κ is a good as another, we do not see how (9.1) could be a mistaken value for something that is actually exactly zero for all choices of κ.

Can we get any insight as to why (9.1) is so small compared to the analogous (9.2)? Though we do not have an explanation of why (9.1) is as very small as it is, it is possible to investigate some aspects of the suppression in more detail.

To study this, we will separate how the result (9.1) depends on $[d\Gamma/dx]_{\text{net}}^{\text{NLO,fac}}$ from how it depends on everything else. Equation (6.22) for (9.1) can be rewritten as

$$[\chi\alpha_s]_{\sigma/\ell_{\text{stop}}}^{\text{energy}} = \int_0^1 dx\, W(x)\left[\frac{d\Gamma}{dx}\right]_{\text{net}}^{\text{NLO,fac}} \tag{9.3a}$$

[35] See Eq. (4) of Ref. [30], where their (x, z) are our (ζ, x). Their $\mathcal{K}(x)$ (before they make the BIM model approximation of replacing $\mathcal{K}$ by $\mathcal{K}_0$) is our $[d\Gamma/dx]^{\text{LO}}$, up to a trivial overall normalization difference associated with their definition of rescaled time τ vs our $\tilde{t}$.

[36] It is worth noting that the x-independent terms of the κ dependence shown in (3.24) can be absorbed into a constant shift in $\hat{q}$ and so do not affect the shape distribution and so give no NLO corrections $\chi\alpha_s$ to moments of the shape distribution. The only term in (3.24) that does affect $\chi\alpha_s$ is the $\hat{s}(x)\ln\kappa$ term associated with IR single logs.

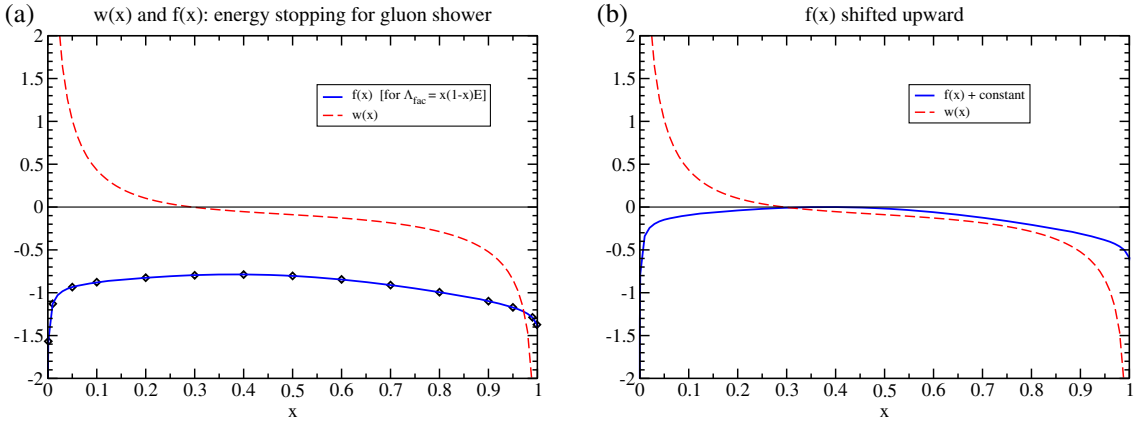

FIG. 16. (a) Plot of the NLO/LO net rate ratio $f(x)$ (solid curve) and the weight function $w(x)$ in the integral (9.4a) that gives (9.1). (b) The same, but $f(x)$ is shifted upward by a constant, as described in the text.

with weight function W defined by[37]

$$W(x') = \frac{x'(1-\sqrt{x'})^2}{2\mathrm{Avg}[x(1-\sqrt{x})^2]_{\mathrm{LO}}} - \frac{x'(1-x')}{2\mathrm{Avg}[x(1-x)]_{\mathrm{LO}}}. \quad (9.3b)$$

Now rewrite the above in terms of the NLO/LO rate ratio $f(x)$ defined by (3.18),

$$[\chi\alpha_{\mathrm{s}}]^{\mathrm{energy}}_{\sigma/\ell_{\mathrm{stop}}} = C_{\mathrm{A}}\alpha_{\mathrm{s}} \int_0^1 dx\, w(x) f(x), \quad (9.4a)$$

$$w(x') = \left[\frac{d\Gamma}{dx}(x')\right]^{\mathrm{LO}} \left\{ \frac{x'(1-\sqrt{x'})^2}{2\mathrm{Avg}[x(1-\sqrt{x})^2]_{\mathrm{LO}}} - \frac{x'(1-x')}{2\mathrm{Avg}[x(1-x)]_{\mathrm{LO}}} \right\}. \quad (9.4b)$$

Note that the definition (6.10a) of $\mathrm{Avg}[\cdots]_{\mathrm{LO}}$ means that

$$\int_0^1 dx'\, w(x') = 0. \quad (9.5)$$

This had to be because if $f(x)$ had been an x-independent constant, so that $[d\Gamma/dx]^{\mathrm{NLO,fac}}_{\mathrm{net}} \propto [d\Gamma/dx]^{\mathrm{LO}}$, then the NLO effects could be completely absorbed into a constant shift in $\hat{q}$, and the whole point of looking at shape characteristics such as σ_S is that the shape is insensitive to constant shifts in $\hat{q}$. So the integral (9.4a) must vanish for constant f.

Figure 16(a) shows a plot of $w(x)$ and $f(x)$. Because of (9.5), the w function has to be positive in some places and negative in others, but note how that manifests; it is positive on the left of the plot and negative on the right. It is not really antisymmetric in $x \to 1-x$, but qualitatively it is a crude distortion of something "antisymmetric." In contrast, $f(x)$ has the same sign on both sides of the plot; it is not really symmetric in $x \to 1-x$, but qualitatively it is a crude distortion of something symmetric. Note that the NLO $g \to gg$ contribution to $f(x)$ must be exactly symmetric because the daughter gluons are identical particles, but this symmetry is not respected by the $g \to ggg$ contribution.[38] These properties of $f(x)$ and $w(x)$ explain a partial cancellation when we compute the integral (9.4a) of their product $w(x)f(x)$.

We will make the last statement more concrete by plotting $w(x)f(x)$, but we find it more visually advantageous to first eliminate one piece that does not contribute to $\chi\alpha_{\mathrm{s}}$. Note that, because of (9.5), the integral (9.4a) for $\chi\alpha_{\mathrm{s}}$ will be unchanged if we replace $f(x)$ by $f(x)+c$, for any constant c. We choose to replace Fig. 16(a) by Fig. 16(b), where we have chosen c to make $f(x)+c$ small for the middle range of x values, while still maintaining that $f(x)+c$, like $f(x)$, has the same sign everywhere. Now we plot the product $w(x)[f(x)+c]$ as the solid curve in Fig. 17. The value of $\chi\alpha_{\mathrm{s}}$ is the area under that curve. One sees a positive contribution from the far right of the plot, partly canceled by a negative contribution from the far left, though it is hard to judge visually how precisely they cancel.

Now let us look at a similar analysis for the analogous, charge-stopping calculation for an electron-initiated shower in large-N_{f} QED. In the large N_{f} limit, it is possible to distinguish the original electron throughout the evolution of the shower, and the overall charge deposition of the shower is simply given by where the original electron finally stops

[37]Note that, in (9.3b), the variables x appearing in the $\mathrm{Avg}[\cdots]_{\mathrm{LO}}$'s are dummy variables associated with the definition (6.10a), unrelated to the integration variable x in (9.3a).

[38]It would not make sense to plot the NLO $g \to gg$ and $g \to ggg$ contributions separately because they have canceling power-law IR divergences [9], which are not handled by our factorization scheme (3.14). One might in principle imagine enhancing our factorization scheme to subtract power-law divergences for the separate contributions, but it does not seem worth the effort (and we do not currently have complete analytic results for all of the power-law divergences [9]).

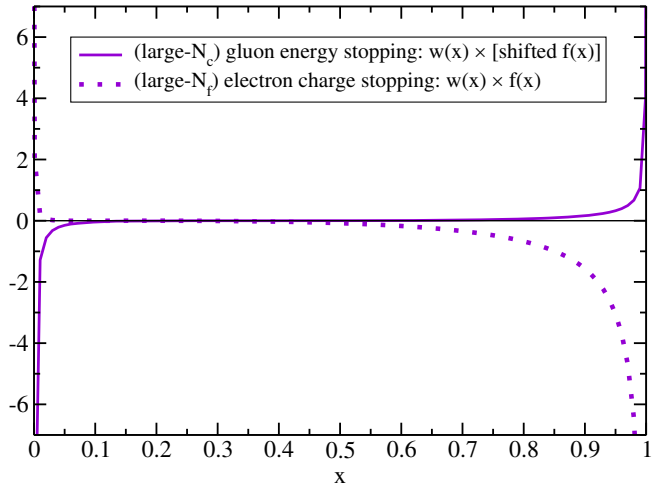

FIG. 17. The solid curve is the product of the $w(x)$ and shifted $f(x)$ functions of Fig. 16, and its integral gives (9.1). For comparison, the dotted curve shows a similar product for large-N_f QED (9.2).

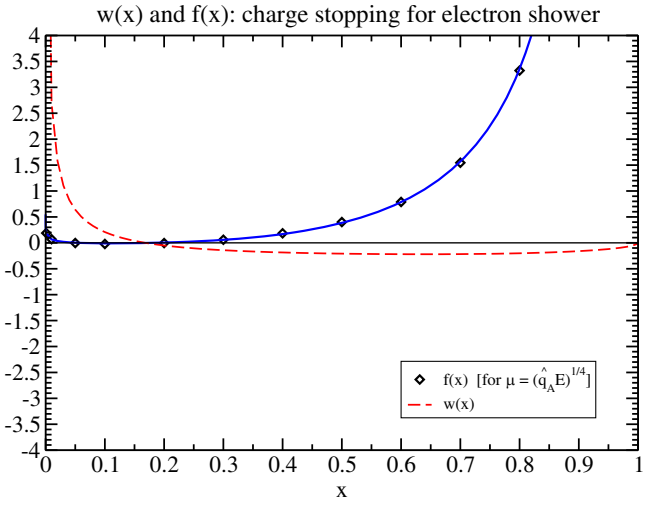

FIG. 18. Like Fig. 16(a), but here for charge stopping of electron showers in large-N_f QED.

and deposits its charge.[39] The relevant splitting rate for computing charge deposition is then the electron splitting rate $[d\Gamma/dx]_e$, where x represents the energy fraction of the original electron after the splitting compared to before the splitting. In Ref. [32], the formula analogous to (9.3) was (with minor adjustment)[40]

$$[\chi\alpha_{\rm EM}]^{\rm charge}_{\sigma/\ell_{\rm stop}} = \frac{\delta{\rm Avg}[(1-\sqrt{x})^2]}{2{\rm Avg}[(1-\sqrt{x})^2]_{\rm LO}} - \frac{\delta{\rm Avg}[(1-x)]}{2{\rm Avg}[(1-x)]_{\rm LO}}, \tag{9.6}$$

where here δAvg is computed using $[d\Gamma/dx]^{\rm NLO}_{e\to e}$ instead of $[d\Gamma/dx]^{\rm NLO,fac}_{\rm net}$. IR factorization is not necessary (there are no log IR divergences), and so there is no IR factorization scale $\Lambda_{\rm fac}$. Equation (9.6) can now be rewritten as

$$[\chi\alpha_{\rm EM}]^{\rm charge}_{\sigma/\ell_{\rm stop}} = \int_0^1 dx\, W_e(x) \left[\frac{d\Gamma}{dx}\right]^{\rm NLO}_{e\to e} \tag{9.7a}$$

with weight function

$$W_e(x') = \frac{(1-\sqrt{x'})^2}{2{\rm Avg}[(1-\sqrt{x})^2]_{\rm LO}} - \frac{(1-x')}{2{\rm Avg}[1-x]_{\rm LO}}. \tag{9.7b}$$

To put it in a form similar to (9.4),

$$[\chi\alpha_{\rm EM}]^{\rm charge}_{\sigma/\ell_{\rm stop}} = N_{\rm f}\alpha_{\rm EM}\int_0^1 dx\, w_e(x) f_e(x), \tag{9.8a}$$

$$w_e(x') = \left[\frac{d\Gamma}{dx}(x')\right]^{\rm LO}_{e\to e}\left\{\frac{(1-\sqrt{x'})^2}{2{\rm Avg}[(1-\sqrt{x})^2]_{\rm LO}} - \frac{(1-x')}{2{\rm Avg}[(1-x)]_{\rm LO}}\right\}, \tag{9.8b}$$

$$f_e(x) \equiv \frac{\left[\frac{d\Gamma}{dx}\right]^{\rm NLO}_{e\to e}}{N_{\rm f}\alpha_{\rm EM}\left[\frac{d\Gamma}{dx}\right]^{\rm LO}_{e\to e}}. \tag{9.8c}$$

Figure 18 shows plots of $w_e(x)$ and $f_e(x)$ analogous to the plots of $w(x)$ and $f(x)$ in Fig. 16.

There is no crude symmetry or antisymmetry here. Note in particular that even LO and NLO single splitting rates for $e\to e\gamma$ will not be symmetric in $x\to 1-x$ because the two daughters are not identical particles. [Unlike the discussion of Fig. 16, we will not shift $f_e(x)$ by a constant because it already, like Fig. 16(b), is almost as close as it can get to $f_e=0$ while having the same sign of $f_e(x)$ for all x.] The product of $w_e(x)$ and $f_e(x)$ is shown by the dotted curve in Fig. 17. One can see the qualitative difference with the gluonic case; the area under the dotted curve does not have any significant cancellation between positive and negative contributions. But also, the area associated with the right-hand side of the dotted curve is already bigger than that associated with the right-hand side of the solid curve.[41]

It is natural to wonder how much of the huge difference between the small vs large $\chi\alpha_s$'s of (9.1) and (9.2) are due to

[39] See the discussion in Sec. 2.2 of Ref. [32].

[40] Specifically, see Eq. (2.17) of Ref. [32]. The analysis of that paper later used a more complicated version, Eq. (2.26) of Ref. [32], which accounted for a piece of the rate that scaled with energy as $\beta_0 E^{-1/2}\ln E$, arising from a fixed choice of renormalization scale μ. One will get the simpler equation we have used by instead choosing $\mu\propto(\hat{q}rE)^{1/4}$ with constant r, similar to our (3.17). The difference with the fixed-μ result turns out to be small and does not significantly affect (9.2). [The change is less than 3% and does not depend on the choice of r.] We have not shown other reasonable choices, such as $\mu=(\hat{q}\kappa xE)^{1/4}$ analogous to our (3.16).

[41] We find numerically that (up to logarithms) both curves blow up as $(1-x)^{-1/2}$ as $x\to 1$, which is an integrable divergence.

having fermions in large-N_f QED (e.g. $e \to e\gamma$ and $\gamma \to e\bar{e}$ processes), and so how much different our QCD results might be if we included quarks in addition to gluons (e.g. $q \to qg$ and $g \to q\bar{q}$). Formally, quark processes are suppressed in the large-N_c limit if one takes N_c large while keeping N_f fixed, and so can be ignored for large-N_c gluon-initiated showers. However, since $N_c = 3$ and $N_f \geq 3$ [depending on the size of $\mu \sim (\hat{q}E)^{1/4}$] in QCD, a more relevant large-N_c limit would be to include quarks and treat N_f as also potentially large.

It is also natural to wonder whether, even for electron-initiated showers in large-N_f QED, there might be a significant difference between the size of overlap corrections for (i) the shape of the energy deposition distribution and (ii) the shape of the charge deposition distribution. And similarly for quark-initiated showers in QCD. We leave all of these questions for future study.

X. THEORIST ERROR

We should comment on the possibility of error in our calculation. There is, of course, theoretical error associated with the unknown size of yet-higher-order corrections and, in our case, the choice of factorization and renormalization scales. But one may be more concerned with what we instead refer to as theorist error. The calculation of overlapping splitting rates [9–15] was very long and very complicated. Though we and our previous collaborators have tried very hard to be meticulously careful, to independently check the details of all calculations, and to devise cross-checks, we cannot completely rule out the possibility of error. Ref. [9] lists a number of nontrivial sanity checks on our rate calculations,[42] though we later found one error in the calculation after the first publication of Ref. [9].[43] More recently, our best cross-check has been to show that the IR contribution to our very complicated, full expression for $[d\Gamma/dx]_{\rm net}$ gives the correct result for single (and not just double) IR logarithms. This was shown by (i) extracting [42] the single log coefficient (3.9) from the IR limit of our full rate calculation and comparing to (ii) a much simpler and completely independent derivation of the IR single logarithm [40], found by substituting the known single-log result [41] for soft radiative corrections to in-medium transverse momentum broadening into a BDMPS-Z-like calculation of the leading-order rate for a hard $g \to gg$ splitting.

In principle, the best way to have full confidence in our full result for $[d\Gamma/dx]_{\rm net}$ would be for an independent group to repeat the calculation, preferably using an independent method. A less arduous check might be to independently calculate $[\Delta d\Gamma/dxdy]_{g\to ggg}$ in the IR limit $y \to 0$ (for fixed x) and extract the nonlogarithm piece of that limit. Or to somehow independently compute $[d\Gamma/dx]_{\rm net}$ in the limits $x \to 0$ and/or $x \to 1$. But we are unsure how complicated such calculations might be.

All that said, we feel fairly confident in our final conclusion.

XI. CONCLUDING REMARKS

Our specific conclusion is that the effects of overlapping gluon splittings are numerically very small and inconsequential for the shape of the energy deposition of a purely-gluonic in-medium shower, at least with the simplifying assumptions used in our thought experiment. Put another way, the effects of overlapping formation times on the energy deposition distribution $\epsilon(z)$ itself are small provided one allows $\hat{q}$ to be an energy-dependent phenomenological jet quenching parameter for this purpose. The energy dependence of $\hat{q}_{\rm eff}(\omega)$ was investigated at leading-log order by the early work of Refs. [5–7], and expanded on in Refs. [43–45]. It would be interesting if those analyses could be extended to next-to-leading-log order (for which our very limited NLLO analysis of Sec. IV would be inadequate).

The results of this paper and its companion Letter [8] represent a first exploratory investigation into these topics. In particular, motivated by Sec. IX, it remains to be seen whether overlap corrections become more important when quarks are incorporated into our gluonic showers.

ACKNOWLEDGMENTS

The work of Arnold and Elgedawy was supported, in part, by the U.S. Department of Energy under Grant No. DE-SC0007974. We are deeply indebted to Han-Chih Chang and Tyler Gorda for their collaboration in the long chain of previous work that made our current results possible. We also thank Zifeng Liu who, several years ago, checked the argument for the asymptotic behavior (D18) of the energy-deposition distribution and also derived (unpublished) corrections to that behavior.

APPENDIX A: NLO RATES IN TERMS OF THE $\overline{\rm NLO}$ FORMULAS OF REF. [9]

The NLO rates used in this paper are given in Refs. [9,15] (and in particular Appendix A of each). But most of the rate formulas in those references are given for what they call $\overline{\rm NLO}$ rates. The purpose of this appendix is to be clear how the various NLO rates needed for this paper can be written in terms of the $\overline{\rm NLO}$ rate formulas given in Refs. [9,15].

The difference between NLO and $\overline{\rm NLO}$ is that Ref. [9] found it convenient to separate the renormalization scale dependence μ from the rest of the NLO $g \to gg$ rate, writing

[42]Specifically, see Sec. 5 of Ref. [9].
[43]See Appendix A of Ref. [42].

$$\left[\Delta\frac{d\Gamma}{dx}\right]^{\rm NLO}_{g\to gg} = \left[\Delta\frac{d\Gamma}{dx}\right]^{\overline{\rm NLO}}_{g\to gg} + \left[\frac{d\Gamma}{dx}\right]_{\rm ren\,log} \tag{A1}$$

with[44]

$$\left[\frac{d\Gamma}{dx}\right]_{\rm ren\,log} \equiv -\frac{\beta_0\alpha_{\rm s}}{2}\left[\frac{d\Gamma}{dx}\right]^{\rm LO}\left[\ln\left(\frac{\mu^2}{|\Omega_0|E}\right) + \ln\left(\frac{x(1-x)}{4}\right) + \gamma_E - \frac{\pi}{4}\right] \tag{A2}$$

and β_0 given by our (3.22). Above, Ω_0 is the complex frequency associated with the leading-order BDMPS-Z $g\to gg$ splitting rate (2.1), given by

$$\Omega_0 = \sqrt{\frac{-i\hat{q}_{\rm A}}{2E}\left(-1+\frac{1}{x}+\frac{1}{1-x}\right)} = \sqrt{\frac{-i(1-x+x^2)\hat{q}_{\rm A}}{2x(1-x)E}}, \tag{A3}$$

and $\gamma_{\rm E}$ is the Euler-Mascheroni constant. Note that the $\ln\mu$ dependence in (A2) matches (3.21). There is not necessarily anything significant about the x dependence and dimensionless constants in the rest of (A2)—they were just a combination that was convenient to algebraically separate from the $\overline{\rm NLO}$ rate in Ref. [9] and to integrate over y.

When written in terms of the $\overline{\rm NLO}$ rates of Refs. [9,15], our Eq. (2.3) is then[45]

$$\left[\Delta\frac{d\Gamma}{dx}\right]^{\rm NLO}_{g\to gg} = \left(\int_0^{1-x} dy\left[\Delta\frac{d\Gamma}{dxdy}\right]_{\rm virt\,I}\right) + (x\to 1-x) + \int_0^1 dy\left[\Delta\frac{d\Gamma}{dxdy}\right]_{\rm virt\,II} + \left[\frac{d\Gamma}{dx}\right]_{\rm ren\,log}, \tag{A4}$$

where $[\Delta d\Gamma/dxdy]_{\rm virt\,I}$ and $[\Delta d\Gamma/dxdy]_{\rm virt\,II}$ is the notation in those references for the $\overline{\rm NLO}$ versions of what we call $[\Delta d\Gamma/dxdy]^{\rm NLO}_{\rm class\,I}$ and $[\Delta d\Gamma/dxdy]^{\rm NLO}_{\rm class\,II}$ in this paper. Correspondingly, Eqs. (3.6), (3.7), and (3.14) of this paper can be rewritten, in terms of the rates presented in refs. [9,15], as[46]

$$\left[\frac{d\Gamma}{dx}\right]^{\rm NLO}_{\rm net} = \left[\frac{d\Gamma}{dx}\right]_{\rm ren\,log} + \left[\frac{d\Gamma}{dx}\right]^{\overline{\rm NLO}}_{\rm net} = \left[\frac{d\Gamma}{dx}\right]_{\rm ren\,log} + \int_0^{1/2} dy\left\{v(x,y)\theta\left(y<\frac{1-x}{2}\right) + v(1-x,y)\theta\left(y<\frac{x}{2}\right) + r(x,y)\theta\left(y<\frac{1-x}{2}\right)\right\}, \tag{A5}$$

$$v(x,y) \equiv \left(\left[\Delta\frac{d\Gamma}{dxdy}\right]_{\rm virt\,I} + \left[\Delta\frac{d\Gamma}{dxdy}\right]_{\rm virt\,II}\right) + (y\leftrightarrow 1-x-y), \tag{A6a}$$

$$r(x,y) \equiv \left[\Delta\frac{d\Gamma}{dxdy}\right]_{g\to ggg}, \tag{A6b}$$

and, most importantly,

$$\left[\frac{d\Gamma}{dx}\right]^{\rm NLO,fac}_{\rm net} \equiv \left[\frac{d\Gamma}{dx}\right]_{\rm ren\,log} + \int_0^{\infty} dy\left\{v(x,y)\theta\left(y<\frac{1-x}{2}\right) + v(1-x,y)\theta\left(y<\frac{x}{2}\right) + r(x,y)\theta\left(y<\frac{1-x}{2}\right) + \frac{C_{\rm A}\alpha_{\rm s}}{4\pi}\left[\frac{d\Gamma}{dx}\right]^{\rm LO}\frac{\ln y+\bar{s}(x)}{y}\theta(yE<\Lambda_{\rm fac})\right\}. \tag{A7}$$

Take care when using these formulas to note that the definitions of $[\Delta d\Gamma/dxdy]_{g\to ggg}$, $[\Delta d\Gamma/dxdy]_{\rm virt\,I}$, and $[\Delta d\Gamma/dxdy]_{\rm virt\,II}$ in Ref. [9] have been updated to include F diagrams in Ref. [15].[47]

APPENDIX B: NUMERICAL METHODS

1. Computation of $[d\Gamma/dx]^{\rm NLO,fac}_{\rm net}$

In (A7) for $[d\Gamma/dx]^{\rm NLO,fac}_{\rm net}$, there is a subtraction in the y integrand that removed the $y^{-1}\ln y$ and y^{-1} behavior of the integrand at small y which would otherwise have generated IR double- and single-logarithmic divergences. With that subtraction, the leftover behavior of the integrand at small y turns out to be of order $y^{-1/2}\ln y$, which is an integrable divergence. However, as a practical matter for numerical integration, it is more efficient to soften the integrable divergence by changing integration variable from y to

[44]Above, Eqs. (A1) and (A3) correspond to Eqs. (A.49) and (A.4) of Ref. [9]. Equation (A2) above is a slight rewriting of Eq. (A.50) of Ref. [9]. For that, we have used Eqs. (A.6) and (A.7) of Ref. [9], and we have also used the fact that $\Omega_0 = e^{-i\pi/4}|\Omega_0|$ to rewrite $\mathrm{Re}(i\Omega_0\ln(1/\Omega_0)) = \mathrm{Re}(i\Omega_0)[\ln(1/|\Omega_0|) - \frac{\pi}{4}]$.

[45]Equation (A4) above is just the combination of Eqs. (A.47)–(A.49) and (A.52) of Ref. [9] for the case of renormalized rates.

[46]The $\overline{\rm NLO}$ rate in (A5) above is Eq. (1.7) of Ref. [9]. $v(x,y)$ and $r(x,y)$ are defined as in Eq. (1.8) of Ref. [9].

[47]Specifically, see Eqs. (A.1), (A.18), and (A.19) of Ref. [15].

$u = y^{1/2}$, so that the behavior of the u integrand is merely $\ln u$ as $u \to 0$.

We use *Mathematica* [47] for the evaluations of the y integrand, including the necessary Δt integrations in the formulas for $[\Delta d\Gamma/dxdy]_{\text{virt I}}$, $[\Delta d\Gamma/dxdy]_{\text{virt II}}$, and $[\Delta d\Gamma/dxdy]_{g\to ggg}$ presented in Refs. [9,15]. Our unsophisticated attempts to use *Mathematica*'s built-in integrator to do the $u = y^{1/2}$ integrals were inefficient, however. Instead, we did the u integration by brute force using a simple midpoint Riemann sum covering the integration region $u = 0$ to $u_{\max} = [\max(x/2, (1-x)/2, \Lambda_{\text{fac}}/E)]^{1/2}$ where the integrand is nonzero. For sufficiently smooth functions, the error of a midpoint Riemann sum should scale as $O((\Delta u)^2)$, where Δu is the small step size. But there are two issues that spoil this rate of convergence: our integrand (i) has discontinuities at the thresholds for the various θ functions in (A7), and (ii) diverges as $\ln u$ as $u \to 0$. The simplest way to take care of issue (i) is to divide the integral up into the three regions where the integrand is continuous, and do each region separately with a midpoint Riemann sum.[48]

For the second issue, we numerically extract the coefficient c of the $c \ln u$ behavior as $u \to 0$, and then we correct the midpoint Riemann sum approximation to

$$\int_0^{u_{\max}} du\, f(u) = -\frac{\Delta u \ln 2}{2} c + \sum_{n=1}^{N} \Delta u f\left(\left(n - \frac{1}{2}\right)\Delta u\right), \tag{B1}$$

where $\Delta u = u_{\max}/N$. The factor of $\frac{1}{2}\Delta u \ln 2$ in the correction term comes from the identity

$$\lim_{N\to\infty}\left[\int_0^{N\Delta u} du\, \ln u - \sum_{n=1}^{N} \Delta u \ln\left(\left(n - \frac{1}{2}\right)\Delta u\right)\right] = -\frac{1}{2}\Delta u \ln 2. \tag{B2}$$

There are, no doubt, much more sophisticated integration methods that could have been used, but these were the simplest for us to quickly implement without diagnosing how to fine-tune the performance of general-purpose integrators; because our integration method is nonadaptive, however, one must monitor the numerical convergence with increasing N.

2. More details on numerical evaluation of $\hat{\epsilon}(\hat{z})$

In the backward-evolution equation (7.5) for $\hat{\epsilon}_{\text{LO}}(\hat{z})$, the integral

$$\int_0^1 dx\, x \left[\frac{d\hat{\Gamma}}{dx}\right]^{\text{LO}} \{x^{-1/2}\hat{\epsilon}_{\text{LO}}(x^{-1/2}\hat{z}) - \hat{\epsilon}_{\text{LO}}(\hat{z})\} \tag{B3}$$

has integrable singularities at the endpoints. Specifically, the integrand scales like $x^{-1/2}$ as $x \to 0$ and $(1-x)^{-1/2}$ as $x \to 1$. It is numerically more efficient to make a change of integration variable, similar to the $u = y^{1/2}$ earlier in this appendix, to reduce the singularity. Changing variables to $u = x^{1/2}$ in (B3) will help $x \to 0$ but will not do anything for $x \to 1$. A simple solution is to first split the integral up as

$$\int_0^1 dx \cdots = \int_0^{1/2} dx \cdots + \int_{1/2}^1 dx \cdots, \tag{B4}$$

and then change integration variable $x \to 1 - x$ in the last integral. Remembering that $[d\Gamma/dx]^{\text{LO}}$ is symmetric under exchange of its two daughters, (B3) then becomes

$$\int_0^{1/2} dx \left[\frac{d\hat{\Gamma}}{dx}\right]^{\text{LO}} (x\{x^{-1/2}\hat{\epsilon}_{\text{LO}}(x^{-1/2}\hat{z}) - \hat{\epsilon}_{\text{LO}}(\hat{z})\} + (1-x)\{(1-x)^{-1/2}\hat{\epsilon}_{\text{LO}}((1-x)^{-1/2}\hat{z}) - \hat{\epsilon}_{\text{LO}}(\hat{z})\}). \tag{B5}$$

Now the change of integration variable to $u = x^{1/2}$ will remove all $1/\sqrt{}$ divergences.

To do the integral (B3) with the discretized representation of $\hat{\epsilon}(\hat{\zeta})$ that we obtain for $\hat{z} \le \hat{\zeta} \le \hat{z}_{\max}$, we used *Mathematica* to interpolate the function and then integrated using that interpolation.

The integrals in (7.8) that determine $\delta\hat{\epsilon}(\hat{z})$ may be treated similarly, except that one must remember that $[d\Gamma/dx]_{\text{net}}$ is not symmetric under $x \to 1 - x$. So the driving term

$$\int_0^1 dx\, x \left[\frac{d\hat{\Gamma}}{dx}\right]_{\text{net}}^{\text{NLO,fac}} \{x^{-1/2}\hat{\epsilon}_{\text{LO}}(x^{-1/2}\hat{z}) - \hat{\epsilon}_{\text{LO}}(\hat{z})\} \tag{B6}$$

for that equation should be replaced by

$$\int_0^{1/2} dx \Bigg(x\left[\frac{d\hat{\Gamma}}{dx}(x)\right]_{\text{net}}^{\text{NLO,fac}} \{x^{-1/2}\hat{\epsilon}_{\text{LO}}(x^{-1/2}\hat{z}) - \hat{\epsilon}_{\text{LO}}(\hat{z})\} + (1-x)\left[\frac{d\hat{\Gamma}}{dx}(1-x)\right]_{\text{net}}^{\text{NLO,fac}} \times \{(1-x)^{-1/2}\hat{\epsilon}_{\text{LO}}((1-x)^{-1/2}\hat{z}) - \hat{\epsilon}_{\text{LO}}(\hat{z})\}\Bigg), \tag{B7}$$

followed by a change of variables to $u = x^{1/2}$.

In the main text, we demonstrated approach to the continuum limit in Fig. 15. Figure 19 shows our approach to the $\hat{z}_{\max} \to \infty$ limit for the smallest $\Delta\hat{z}$ value of Fig. 15. There is no noticeable difference between the results for $\hat{z}_{\max} = 10$ and $\hat{z}_{\max} = 20$, and so the value $\hat{z}_{\max} = 20$ used in Fig. 15 was plenty large enough.

[48] Alternatively, one can do a single integral over the total integration region and correct the midpoint rule in the steps where discontinuities occur, given that we know exactly where the points of discontinuity are.

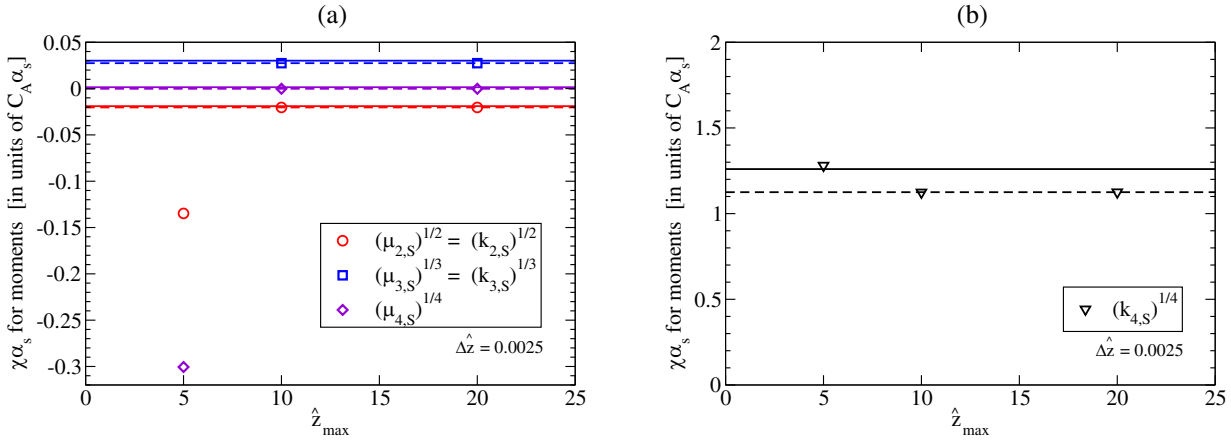

FIG. 19. Like Fig. 15 but here the data points show the dependence on $\hat{z}_{\max}$ for $\Delta\hat{z} = 0.0025$. The solid horizontal lines again show the results of Table III, and their difference with the $(\Delta\hat{z}, \hat{z}_{\max}) = (0.0025, 20)$ data points is the same as that in Fig. 15, due to the nonzero value of $\Delta\hat{z}$. We have drawn dashed horizontal lines corresponding to the $(\Delta\hat{z}, \hat{z}_{\max}) = (0.0025, 20)$ value to instead emphasize the relevant point for approximating $\hat{z}_{\max} \to \infty$; there is no significant difference between $\hat{z}_{\max} = 10$ and $\hat{z}_{\max} = 20$.

APPENDIX C: MORE ON Δb DEPENDENCE OF NLLO RESUMMATION

In this appendix, we argue that the resummation (4.18) is adequate to capture the Δb dependence of resummation at next-to-leading-log order (NLLO) but would fail at the next order (NNLLO). As in Sec. IV B, we will ignore the running of $\alpha_s(k_\perp)$, which was argued not to affect our conclusions in Sec. IV C.

1. Review of LLO resummation

We first review the leading-log order (LLO) resummation of LMW [41]. In our notation, we find it convenient to express the leading-log contribution to $\hat{q}_{\rm eff}$ from nth order in $\alpha_s(\mu)$ as

$$\delta^n\hat{q}_{\rm eff}(\Delta b) \approx \bar{\alpha}_s^n \hat{q}_{(0)} \int_{\tau_0}^{\infty}\frac{dt_1}{t_1}\int_{\hat{q}t_1}^{1/(\Delta b)^2}\frac{dk_{\perp 1}^2}{k_{\perp 1}^2}\int_{\tau_0}^{t_1}\frac{dt_2}{t_2} \times \int_{\hat{q}t_2}^{k_{\perp 1}^2}\frac{dk_{\perp 2}^2}{k_{\perp 2}^2}\cdots\int_{\tau_0}^{t_{n-1}}\frac{dt_n}{t_n}\int_{\hat{q}t_n}^{k_{\perp,n-1}^2}\frac{dk_{\perp n}^2}{k_{\perp n}^2}, \quad \text{(C1)}$$

where in this appendix we use the shorthand notation

$$\bar{\alpha}_s \equiv \frac{C_A\alpha_s}{\pi}. \quad \text{(C2)}$$

In our convention, $(k_{\perp 1}, t_1)$ are the transverse momentum and emission duration[49] of the first soft gluon, $(k_{\perp 2}, t_2)$ are those of an even softer gluon emission, and so forth, with $k_\perp$ ordering

$$\frac{1}{\Delta b} \gg k_{\perp 1} \gg k_{\perp 2} \gg \cdots. \quad \text{(C3)}$$

The first inequality in (C3) can be understood as following a pattern $(k_{\perp 0} \gg k_{\perp 1})$ similar to the others, because $1/\Delta b$ is the transverse momentum scale $(k_{\perp 0})$ corresponding to the lightlike Wilson loop of Fig. 9 from which the first gluon $(k_{\perp 1})$ is emitted. The other conditions for leading logs are that softer emissions take place within the duration of harder emissions, so that

$$t_1 \gg t_2 \gg t_3 \gg \cdots \gg \tau_0. \quad \text{(C4)}$$

The last inequality in (C4), implemented in the lower limits of all the time integrals, reflects the breakdown of the $\hat{q}$ approximation for emission times smaller than the mean free path τ_0, which was also a constraint in Fig. 11. The lower limits on the $k_\perp$ integrals correspond to the fact that the transverse momentum kicks $\Delta p_\perp \sim \sqrt{\hat{q}t}$ accumulated over the duration of an emission will disrupt the vacuum-like logarithms if $\Delta p_\perp$ is as large as the $k_\perp$ of that emission. Each double logarithm relies on nearly collinear emissions, and the kicks from the medium disturb collinearity.

Mathematically, in order to implement the conditions just described, the $k_\perp$ integrals in (C1) should be understood as requiring that each upper limit of integration be greater than the corresponding lower limit. That means in particular that the $k_{\perp 1}$ integration sets an upper limit

$$t_1 < \frac{1}{\hat{q}(\Delta b)^2} \quad \text{(C5)}$$

on the t_1 integration. We could have explicitly written that in (C1), but the motivation for the limits was easier to explain by initially writing the t_1 integral as unbounded.

In LMW's application, the relevant scale for Δb was $(\hat{q}L)^{-1/2}$, where L was the length of the medium traversed,

[49]The emission duration t_1 is what we called Δt in Fig. 11.

$$\Delta b \text{ here} \to \frac{1}{Q_s} \sim \frac{1}{\sqrt{\hat{q}L}} \text{ in LMW}. \tag{C6}$$

In our application, the scale analogous to L is, parametrically, the formation time for the underlying, hard splitting process. However, for the sake of the discussion of Sec. IV, we keep things here explicitly in terms of Δb.

There are many different ways to rewrite (C1), and we will provide several for the sake of reference when comparing to other papers. LMW use the variables[50]

$$\mathfrak{x} \sim \frac{\tau_0}{t} \tag{C7}$$

in place of our t's. After making this change of integration variable in (C1), one may change the order of integrations to write a formula equivalent to LMW's version,[51]

$$\delta^n \hat{q}_{\text{eff}}(\Delta b) \approx \bar{\alpha}_s^n \hat{q}_{(0)} \int_{\hat{q}\tau_0}^{1/(\Delta b)^2} \frac{dk_{\perp 1}^2}{k_{\perp 1}^2} \int_{\hat{q}\tau_0}^{k_{\perp 1}^2} \frac{dk_{\perp 2}^2}{k_{\perp 2}^2} \cdots \int_{\hat{q}\tau_0}^{k_{\perp,n-1}^2} \frac{dk_{\perp n}^2}{k_{\perp n}^2} \times \int_{\hat{q}\tau_0/k_{\perp n}^2}^{1} \frac{d\mathfrak{x}_n}{\mathfrak{x}_n} \cdots \int_{\hat{q}\tau_0/k_{\perp 2}^2}^{\mathfrak{x}_3} \frac{d\mathfrak{x}_2}{\mathfrak{x}_2} \int_{\hat{q}\tau_0/k_{\perp 1}^2}^{\mathfrak{x}_2} \frac{d\mathfrak{x}_1}{\mathfrak{x}_1}. \tag{C8}$$

Alternatively, to make contact with the variables (t, ω) used in Fig. 11, change integration variables in (C1) by using the parametric relation $t \sim \omega/k_\perp^2$ for the duration of vacuumlike gluon fluctuations,

$$\delta^n \hat{q}_{\text{eff}}(\Delta b) \approx \bar{\alpha}_s^n \hat{q}_{(0)} \int_{\tau_0}^{\infty} \frac{dt_1}{t_1} \int_{\hat{q}t_1^2}^{t_1/(\Delta b)^2} \frac{d\omega_1}{\omega_1} \int_{\tau_0}^{t_1} \frac{dt_2}{t_2} \times \int_{\hat{q}t_2^2}^{\omega_1 t_2/t_1} \frac{d\omega_2}{\omega_2} \cdots \int_{\tau_0}^{t_{n-1}} \frac{dt_n}{t_n} \int_{\hat{q}t_n^2}^{\omega_{n-1}t_n/t_{n-1}} \frac{d\omega_n}{\omega_n}, \tag{C9}$$

where the limits of the ω_1 integration again implicitly set the upper limit (C5) on t_1.

The analysis of Ref. [43] (which reviews the fixed coupling case as a warmup) uses the logarithmic variables

$$Y \equiv \ln\left(\frac{t}{\tau_0}\right), \qquad \rho \equiv \ln\left(\frac{k_\perp^2}{\hat{q}\tau_0}\right), \tag{C10}$$

in terms of which (C1) can be written

$$\delta^n \hat{q}_{\text{eff}} \approx \bar{\alpha}_s^n \hat{q}_{(0)} f_n\left(\ln\left(\frac{1}{\hat{q}\tau_0(\Delta b)^2}\right), \ln\left(\frac{1}{\hat{q}\tau_0(\Delta b)^2}\right)\right), \tag{C11a}$$

where (introducing our own notation "f_n")

$$f_n(Y,\rho) \equiv \int_0^Y dY_1 \int_{Y_1}^{\rho} d\rho_1 \int_0^{Y_1} dY_2 \int_{Y_2}^{\rho_1} d\rho_2 \cdots \times \int_0^{Y_{n-1}} dY_n \int_{Y_n}^{\rho_{n-1}} d\rho_n. \tag{C11b}$$

Equation (C11) tell us that the leading-log result at nth order is just $\bar{\alpha}_s^n \hat{q}_{(0)}$ times the hyper-volume of the integration region in (C11).

LMW's summation of all the leading-log $\delta^n \hat{q}_{\text{eff}}$ gives the formula (4.18) presented in the main text. Iancu and Triantafyllopoulos [43] give a little more detail, showing that

$$f_n(Y,\rho) = \frac{Y^n \rho^n}{(n!)^2} - \frac{Y^{n+1}\rho^{n-1}}{(n+1)!(n-1)!} \quad (n > 0) \tag{C12}$$

(which can be proven by induction). Summing all orders of α_s gives

$$1 + \sum_{n=1}^{\infty} \bar{\alpha}_s^n f_n(Y,\rho) = I_0(2\sqrt{\bar{\alpha}_s Y\rho}) - \frac{Y}{\rho} I_2(2\sqrt{\bar{\alpha}_s Y\rho}), \tag{C13}$$

and setting $Y = \rho = \ln(\frac{1}{\hat{q}\tau_0(\Delta b)^2})$ as in (C11a) then gives (4.18).

2. Δb dependence of logarithms at $O(\alpha_s)$

It will be useful to also review some of the qualitative aspects of double and single logs at $O(\alpha_s)$. The double-log approximation corresponds to the $n = 1$ case of (C1),

$$\delta\hat{q}_{\text{eff}}(\Delta b) \approx \bar{\alpha}_s \hat{q}_{(0)} \int_{\tau_0}^{1/\hat{q}(\Delta b)^2} \frac{dt_1}{t_1} \int_{\hat{q}t_1}^{1/(\Delta b)^2} \frac{dk_{\perp 1}^2}{k_{\perp 1}^2}, \tag{C14}$$

where we have used (C5). A picture of the integration region is shown in Fig. 20(a), which is equivalent to the integration region previously depicted in Fig. 11. LMW analyzed the subleading, single logarithms as well at this order. What will be important for our discussion are qualitative characterizations of the following parametric regions.

(i) Double logarithms are generated by integrating over the interior of the shaded region,

$$\tau_0 \ll t_1 \ll \frac{1}{\hat{q}(\Delta b)^2}, \quad \hat{q}t_1 \ll k_{\perp 1}^2 \ll \frac{1}{(\Delta b)^2}, \tag{C15}$$

[50]LMW represent (C7) with the symbol x. We use $\mathfrak{x}$ here to avoid confusion with our use of x elsewhere in this paper.

[51]Specifically, see Eq. (50) of Ref. [41], which only explicitly writes out the example $n = 2$, and make use of the translation (C6). Our $\delta^2\hat{q}_{\text{eff}}$ corresponds to their Eq. (50) divided by L, except that their numbering of the gluons is the reverse of ours, i.e. their $(k_{\perp 1}, \cdots k_{\perp n})$ are our $(k_{\perp n}, \ldots, k_{\perp 1})$ and their $(x_1, \ldots, x_n)$ are our $(\mathfrak{x}_n, \ldots, \mathfrak{x}_1)$. Their $Q_0^2 = \hat{q}\tau_0$.

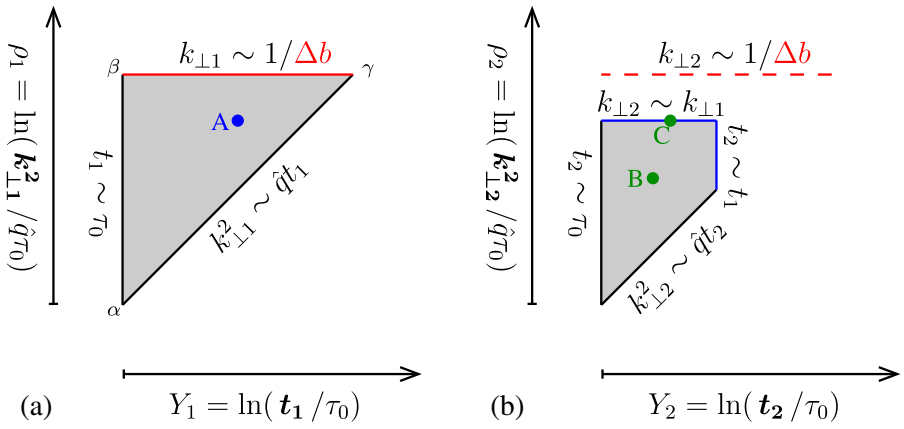

FIG. 20. (a) The double-log region of Fig. 11 in terms of the variables (Y, ρ) of (C10). (a + b) A depiction of the leading-log region at order $O(\alpha_s^2)$. In this figure, the extent of the (Y_2, ρ_2) region is drawn for the case where (Y_1, ρ_1) is at point "A."

such as the point labeled "A" in Fig. 20(a). The double log will be proportional to the area of the shaded region in the log-log coordinates of the figure.

(ii) Single logarithms arise from integrating along the edges, e.g. over

$$\tau_0 \ll t_1 \ll \frac{1}{\hat{q}(\Delta b)^2}, \qquad k_{\perp 1}^2 \sim \frac{1}{(\Delta b)^2} \tag{C16}$$

for the upper edge in Fig. 20(a), which is the edge most sensitive to the value of Δb. Because $k_{\perp 1}^2 \sim 1/(\Delta b)^2$ in (C16), the red line representing this edge should be thought of as having an $O(1)$ thickness in the log-log coordinates used in the figure. Similarly for the other edges. In the limit of large logarithms, the $O(1)$ thickness of the edges is parametrically small compared to the size of the shaded, double-log region. The point labeled "D" in Fig. 21(a) gives an example of how we'll graphically indicate points contributing to the single log.

(iii) No logarithms are generated by the corners, such as

$$t_1 \sim \frac{1}{\hat{q}(\Delta b)^2}, \qquad k_{\perp 1}^2 \sim \frac{1}{(\Delta b)^2}, \tag{C17}$$

which is labeled "γ" in the figure.

The single-log pieces can be thought of as the dominant contribution to the difference of (a) the full integral over all (ω_1, t_1) and (b) the double-log approximation (C14). It will be useful to give a name to the integral that gives this difference. We will call it

$$\bar{\alpha}_s \hat{q}_{(0)} \int \frac{dt_1}{t_1} \int \frac{dk_{\perp 1}^2}{k_{\perp 1}^2} F_{\rm sl}(t_1, k_{\perp 1}^2), \tag{C18}$$

where $F_{\rm sl}$ has support on the edges of the double log region and falls rapidly towards zero as (Y_1, ρ_1) moves away from those edges in Fig. 21(a). The subscript "sl" stands for

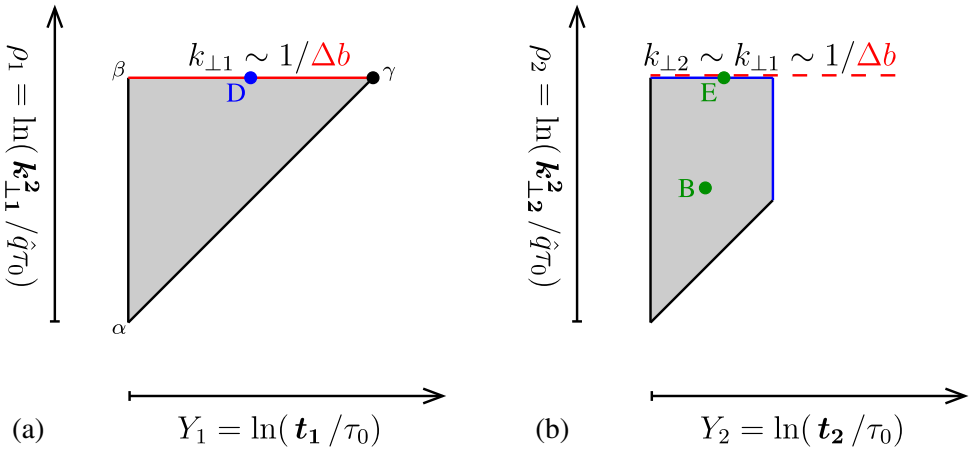

FIG. 21. Like Fig. 20, but here the extent of the (Y_2, ρ_2) region is drawn for the case where (Y_1, ρ_1) is at point "D."

"single log." Most details of $F_{\rm sl}$ will be unimportant. The important property of $F_{\rm sl}$ is that it will be uniform along each individual edge, by which we mean that integration of $F_{\rm sl}$ over the direction perpendicular to an edge gives (to good approximation in the large-log limit) the same result everywhere along that edge. The uniformity of each edge in this sense means that the contribution of each edge to (C18) will be proportional to a single logarithm, with a coefficient depending on the details of how $F_{\rm sl}$ behaves near that edge.

To give a concrete example of uniformity, consider the edge (C16) that is sensitive to the physics of $k_\perp \sim 1/\Delta b$. The (approximate) formula for $F_{\rm sl}$ along that edge may be extracted from LMW [41] in terms of the variables (t_1, ω_1),[52]

$$\begin{aligned} F_{\rm sl} &\simeq F_{\rm sl}^{\rm approx} \\ &= {\rm Re}\biggl\{\frac{1}{3}\biggl[\biggl(1+\frac{i\omega_1(\Delta b)^2}{2t_1}\biggr)e^{i\omega_1(\Delta b)^2/2t_1} \\ &\quad + 2i\frac{(1-e^{i\omega_1(\Delta b)^2/2t_1})}{\omega_1(\Delta b)^2/2t_1}\biggr] \\ &\quad - \theta\biggl(\frac{\omega_1(\Delta b)^2}{2t_1}<1\biggr)\biggr\}. \end{aligned} \tag{C19}$$

The detailed expression does not matter except to explicitly confirm the important point that this edge's $F_{\rm sl}$ is a function of only $\omega_1(\Delta b)^2/2t_1$. Since $t_1 \approx 2\omega_1/k_{\perp 1}^2$ in this region of vacuum-like emissions, the $F_{\rm sl}(t_1, k_{\perp 1}^2)$ of (C18) is actually a function of only $k_{\perp 1}^2(\Delta b)^2$ near this (red) edge of Fig. 21(a), and $k_{\perp 1}^2$ is the variable that parametrizes the direction perpendicular to that edge. This provides an example of how $F_{\rm sl}$ is "uniform" along an edge, which in this case means that $F_{\rm sl}^{\rm approx}(t_1, k_{\perp 1}^2) \simeq F_{\rm sl}^{\rm approx}((k_{\perp 1}\Delta b)^2)$ does not depend on t_1.

Because (C19) is localized near the edge, the limits of the $dk_{\perp 1}^2$ integral in (C18) that is perpendicular to the edge (C16) can be replaced (within the large-log approximation) by 0 to ∞. This gives

$$\begin{aligned} &\int_0^\infty \frac{dk_{\perp 1}^2}{k_{\perp 1}^2} F_{\rm sl}^{\rm approx}((k_{\perp 1}\Delta b)^2) \\ &\quad = \int_0^\infty \frac{du}{u} F_{\rm sl}^{\rm approx}(u) \\ &\quad = \text{an } O(1) \text{ constant independent of } \Delta b \end{aligned} \tag{C20}$$

for that edge.

Overall, the total result for double and single logs will have the form

$$\begin{aligned} \hat{q}_{\rm eff}(\Delta b) &= \hat{q}_{(0)} + \delta\hat{q}(\Delta b) \\ &\simeq \hat{q}_{(0)}\biggl\{1+\frac{\bar{\alpha}_{\rm s}}{2}\biggl[\ln^2\biggl(\frac{1}{\hat{q}\tau_0(\Delta b)^2}\biggr) \\ &\quad + \kappa\ln\biggl(\frac{1}{\hat{q}\tau_0(\Delta b)^2}\biggr)\biggr]\biggr\}, \end{aligned} \tag{C21}$$

where the single-log coefficient κ is some constant[53] that is independent of Δb. Equation (C21) refines (4.17) to now include the single log term. This large single logarithm does not generate any large Δb dependence when included in our earlier discussion of Sec. IV B. That is because we were only interested in $\Delta b \sim \mathcal{B}_0$ as in (4.16), and one may rewrite the single log term in (C21) as

$$\kappa\ln\biggl(\frac{1}{\hat{q}\tau_0(\Delta b)^2}\biggr) = \kappa\ln\biggl(\frac{1}{\hat{q}\tau_0\mathcal{B}_0^2}\biggr) - \kappa\ln\biggl(\frac{(\Delta b)^2}{\mathcal{B}_0^2}\biggr). \tag{C22}$$

On the right-hand side, the first term is a large logarithm but does not depend on Δb, whereas the second term depends on Δb but is not a large logarithm and so will not need to resummed.

3. Δb dependence at NLLO and NNLLO

Now move to the next order in $\alpha_{\rm s}$ by considering the $n = 2$ case of (C1). The corresponding leading-log region, which generates an $O(\alpha_{\rm s}^2\log^4)$ contribution to $\hat{q}_{\rm eff}$, corresponds to the combination of the shaded regions of Figs. 20(a) and 20(b). The leading log is generated by

[52]This comes from Eq. (32) of Ref. [41], where S is $-\frac{1}{4}\hat{q}_{\rm eff}x_\perp^2 L$ and where there is an implicit ${\rm Re}\{\cdots\}$ on the right-hand side. Our $\delta\hat{q}_{\rm eff}$ then corresponds to integrating the right-hand side of their (32) with integral

$$-\frac{4}{x_\perp^2 L}\int\frac{d\omega}{\omega}.$$

Comparing to the (ω, t) version

$$\bar{\alpha}_{\rm s}\hat{q}_{(0)}\int\frac{dt_1}{t_1}\int\frac{d\omega_1}{\omega_1}F_{\rm sl}$$

of our (C18) then determines $F_{\rm sl}$, except that we must subtract away the double log piece already included in the $n = 1$ version of (C9), where the edge we are focused on is the upper limit $t_1/(\Delta b)^2$ of the ω_1 integration there. That subtraction is implemented by the last term in our (C19). We have written the argument of the θ function to match the $k_{\perp 1}^2 \le 1/(\Delta b)^2$ condition in the (C1) version of the leading-log resummation.

[53]For details, see Eq. (45) of LMW [41], where $\underline{x}$ and l_0 are our Δb and τ_0. Divide both sides of that equation by L to get $\hat{q}_{\rm eff}$, and use the translation (C6) to replace the remaining occurrences of L by $1/\hat{q}(\Delta b)^2$. Note that this replaces their $\ln(8ml_0/\underline{x}^2\hat{q}L)$ by a Δb-independent constant of $O(1)$. The ml_0 and the integral in that formula arise from the boundary $t_1 \sim \tau_0$ in our Fig. 20(a) [what they call "boundary (c)"]. Since this boundary does not generate a logarithm with large dependence on the exact value of $\Delta b \sim \mathcal{B}_0$, we can ignore it in our analysis. We may also ignore the various complications in the analysis of this boundary, recently investigated by Ghiglieri and Weitz [48] for the case of a quark-gluon plasma.

points in the interior, such as the combined pair AB in the figure.

The combination AC contributes at NLLO, which is $O(\alpha_s^2 \log^3)$ for $n = 2$. This combination corresponds to

$$\frac{1}{\Delta b} \gg k_{\perp 1} \sim k_{\perp 2}. \tag{C23}$$

If we continue on to yet higher orders in α_s, the contributions at NLLO order that involves a pair like AC will have

$$\frac{1}{\Delta b} \gg k_{\perp 1} \sim k_{\perp 2} \gg k_{\perp 3} \gg \cdots. \tag{C24}$$

None of the points will be sensitive to the exact value of Δb, and so none of these contributions contribute to what we're interested in, which is the Δb dependence of resummed $\hat{q}_{\rm eff}$.

Now turn to the combination of Figs. 21(a) and 21(b), with $(t_1, k_{\perp 1}^2)$ along the edge $k_{\perp 1} \sim 1/\Delta b$. First, note that if $(t_1, k_{\perp 1}^2)$ were at the vertex γ, then we would lose both logs from the $(t_1, k_{\perp 1}^2)$ integration, and so this would be a NNLLO contribution instead of an NLLO one. So, at NLLO, we can replace the upper limit $1/\hat{q}(\Delta b)^2$ of (C5) on the t_1 integration by $1/\hat{q}\mathcal{B}_0^2$—a change which will only affect NNLLO.

So we should focus on combinations like DB, which correspond to NLLO contributions with

$$\frac{1}{\Delta b} \sim k_{\perp 1} \gg k_{\perp 2} \gg k_{\perp 3} \gg \cdots. \tag{C25}$$

None of $(t_2, \omega_2), (t_3, \omega_3), \ldots$ can be on an edge because having placed (t_1, ω_1) on an edge (e.g. point D in the figure) has already cost us a logarithm; having another point also on an edge would move us from NLLO to NNLLO. So we may use the leading-log approximation for all the (t_i, ω_i) integrals except for (t_1, ω_1). For the same reason, the $k_{\perp 2}$ integration in (C1) does not care about the exact value of $k_{\perp 1}$ at this order, only its order of magnitude, and so the upper limit $k_{\perp 1}^2$ of integration can be replaced by $1/\mathcal{B}_0$ since $k_{\perp 1} \sim 1/\Delta b \sim 1/\mathcal{B}_0$ in (C25). Altogether, NLLO contributions of type (C25) then contribute

$$\begin{aligned}
&\bar{\alpha}_s^n \hat{q}_{(0)} \int_{\tau_0}^{1/\hat{q}\mathcal{B}_0^2} \frac{dt_1}{t_1} \int_{k_{\perp 1} \sim 1/\Delta b} \frac{dk_{\perp 1}^2}{k_{\perp 1}^2} F_{\rm sl}(t_1, k_{\perp 1}^2) \int_{\tau_0}^{t_1} \frac{dt_2}{t_2} \\
&\quad \times \int_{\hat{q}t_2}^{1/\mathcal{B}_0} \frac{dk_{\perp 2}^2}{k_{\perp 2}^2} \cdots \int_{\tau_0}^{t_{n-1}} \frac{dt_n}{t_n} \int_{\hat{q}t_n}^{k_{\perp,n-1}^2} \frac{dk_{\perp n}^2}{k_{\perp n}^2} \\
&= \bar{\alpha}_s^n \hat{q}_{(0)} \int_{\tau_0}^{1/\hat{q}\mathcal{B}_0^2} \frac{dt_1}{t_1} \int_{k_{\perp 1} \sim 1/\Delta b} \frac{dk_{\perp 1}^2}{k_{\perp 1}^2} F_{\rm sl}(t_1, k_{\perp 1}^2) \\
&\quad \times f_{n-1}\left(\ln\left(\frac{t_1}{\tau_0}\right), \ln\left(\frac{1}{\hat{q}\tau_0 \mathcal{B}_0^2}\right) \right)
\end{aligned} \tag{C26}$$

to $\delta^n \hat{q}_{\rm eff}$ at NLLO. f_n is again defined by (C10) and (C11b). The $k_{\perp 1}^2$ integral in (C26) is the one presented in (C20) and so is independent of Δb (at this order in logs). Since there is no other Δb in (C26), we see that NLLO contributions from combinations like DB are independent of Δb.

For a combination like DE in Fig. 21, E would be sensitive to Δb since $1/\Delta b \sim k_{\perp 1} \sim k_{\perp 2}$. But this is an NNLLO contribution since both points are on edges.

We have now addressed the interesting cases. We conclude that NLLO does not generate any Δb dependence not already included in the LLO result (C1), which sums to the formula (4.18) used in the main text. Our analysis above suggests that additional Δb dependence will appear at NNLLO, but that is beyond the scope of what is needed for this paper.

4. A loose end: The prefactor of Eq. (4.20)

In the main text, we ignored a prefactor when discussing the Δb dependence of the leading-log resummation. The leading term in the large-argument expansion of I_1 in (4.18) actually gives

$$\begin{aligned}
\hat{q}_{\rm eff}(\Delta b) \approx \hat{q}_{(0)} &\left(\frac{1}{\hat{q}\tau_0 (\Delta b)^2} \right)^{2\sqrt{\bar{\alpha}_s}} \\
&\times \frac{1}{\sqrt{4\pi}} \left[\sqrt{\bar{\alpha}_s} \ln\left(\frac{1}{\hat{q}\tau_0 (\Delta b)^2} \right) \right]^{-3/2}
\end{aligned} \tag{C27}$$

instead of (4.20). Including the full prefactor then changes (4.21) and (4.22) to

$$\begin{aligned}
\hat{q}_{\rm eff}(\Delta b) \approx \hat{q}_{(0)} &\left(\frac{1}{\hat{q}\tau_0 \mathcal{B}_0^2} \right)^{2\sqrt{\alpha_s}} \left[1 - 2\sqrt{\bar{\alpha}_s} \ln\left(\frac{(\Delta b)^2}{\mathcal{B}_0^2} \right) \right] \\
&\times \frac{1}{\sqrt{4\pi}} \left[\sqrt{\bar{\alpha}_s} \ln\left(\frac{1}{\hat{q}\tau_0 \mathcal{B}_0^2} \right) \right]^{-3/2} \\
&\times \left[1 - \frac{3 \ln((\Delta b)^2/\mathcal{B}_0^2)}{2 \ln(1/\hat{q}\tau_0 \mathcal{B}_0^2)} \right]
\end{aligned} \tag{C28}$$

and

$$\hat{q}_{\rm eff}(\Delta b) = \hat{q}_{\rm eff}(\mathcal{B}_0) \left\{ 1 + O(\sqrt{\alpha_s}) + O\left(\frac{1}{\ln(1/\hat{q}\tau_0 \mathcal{B}_0^2)} \right) \right\}. \tag{C29}$$

Now remember that, when making the large-argument expansion of I_1 in (4.20), we were taking the large-logarithm limit where $\alpha_s \ln^2(1/\hat{q}\tau_0 (\Delta b)^2) \sim \alpha_s \ln^2(1/\hat{q}\tau_0 \mathcal{B}_0^2)$ is $\gg 1$. So the $O(1/\log)$ term in (C29) can be ignored compared to the $O(\sqrt{\alpha_s})$ term, leaving us with (4.22).

APPENDIX D: ASYMPTOTIC BEHAVIOR OF $\hat{\epsilon}_{\rm LO}(\hat{z})$

In this appendix, we will derive the asymptotic falloff of the energy stopping distribution $\epsilon_{\rm LO}(z)$ for large z. We follow a procedure similar to that used in Ref. [32] for the falloff of the leading-order charge distribution $\rho_{\rm LO}(z)$ at large z.[54] In that case, the conclusion was that

$$\rho_{\rm LO}(z) \sim e^{-\Gamma_{\rm LO}(E_0)z} \tag{D1}$$

for large z, where $\Gamma_{\rm LO}$ is the total leading-order rate for the relevant splitting process $e \to e\gamma$. In our case, however, the total rate for $g \to gg$ in $\hat{q}$ approximation is infinite because of the $x^{-3/2}$ [or symmetrically $(1-x)^{-3/2}$] IR divergence of Eq. (2.1) for $[d\Gamma/dx]^{\rm LO}$, and so (D1) suggests that the falloff of our $\epsilon_{\rm LO}(z)$ must be faster than simple exponential decay. We'll find that our large-z tail is approximately Gaussian.

Start from the leading-order energy deposition Eq. (7.3):

$$\frac{\partial\hat{\epsilon}_{\rm LO}(\hat{z})}{\partial\hat{z}} = \int_0^1 dx\, x\left[\frac{d\hat{\Gamma}}{dx}\right]^{\rm LO}\{x^{-1/2}\hat{\epsilon}_{\rm LO}(x^{-1/2}\hat{z}) - \hat{\epsilon}_{\rm LO}(\hat{z})\}. \tag{D2}$$

Note that the $x \to 0$ contribution to the integration converges because (i) $x[d\hat{\Gamma}/dx]^{\rm LO} \sim x^{-1/2}$ and (ii) $\epsilon_{\rm LO}(z')$ should fall to zero faster than, for example, $(z')^{-1/2}$ as $z' \to \infty$. The $x \to 1$ contribution to the integration converges because (i) $x[d\hat{\Gamma}/dx]^{\rm LO} \sim (1-x)^{-3/2}$ and (ii) there is a cancellation between the two terms inside the braces:

$$\{x^{-1/2}\hat{\epsilon}_{\rm LO}(x^{-1/2}\hat{z}) - \hat{\epsilon}_{\rm LO}(\hat{z})\} \sim 1 - x \quad \text{as } x \to 1. \tag{D3}$$

Now rewrite $\hat{\epsilon}_{\rm LO}(\hat{z})$ in the WKB-inspired form

$$\hat{\epsilon}_{\rm LO}(\hat{z}) \equiv e^{-\mathcal{W}(\hat{z})}, \tag{D4}$$

where, asymptotically, $\mathcal{W}(\hat{z})$ should be an increasing function of $\hat{z}$ so that $\epsilon_{\rm LO}(z) \to 0$ as $z \to \infty$. Plugging (D4) into the leading-order energy deposition Eq. (D2) gives

$$\mathcal{W}'(\hat{z}) = \int_0^1 dx\, x\left[\frac{d\hat{\Gamma}}{dx}\right]^{\rm LO}\{1 - x^{-1/2}e^{\mathcal{W}(\hat{z})-\mathcal{W}(x^{-1/2}\hat{z})}\}. \tag{D5}$$

Let us more carefully examine the cancellation (D3) as $x \to 1$, now in the language of (D5). For this limit, we define $\delta \equiv 1 - x \ll 1$, which gives

$$\mathcal{W}(\hat{z}) - \mathcal{W}(x^{-1/2}\hat{z}) \simeq -\frac{1}{2}\hat{z}\mathcal{W}'(\hat{z})\delta \tag{D6}$$

and so

$$\{1 - x^{-1/2}e^{\mathcal{W}(\hat{z})-\mathcal{W}(x^{-1/2}\hat{z})}\} \simeq 1 - (1-\delta)^{-1/2}e^{-\frac{1}{2}\hat{z}\mathcal{W}'(\hat{z})\delta}. \tag{D7}$$

$\hat{z}\mathcal{W}'(\hat{z})$ will be large for large $\hat{z}$. There are then two regions of small δ to consider. For x extremely close to 1, such that

$$\delta \ll \frac{1}{\hat{z}\mathcal{W}'(\hat{z})} \ll 1, \tag{D8}$$

(D7) gives

$$\{1 - x^{-1/2}e^{\mathcal{W}(\hat{z})-\mathcal{W}(x^{-1/2}\hat{z})}\} \simeq \frac{1}{2}[\hat{z}\mathcal{W}'(\hat{z}) - 1]\delta, \tag{D9}$$

which vanishes linearly as $\delta \to 0$ and describes the cancellation (D3). In contrast, in the other small-δ region

$$\frac{1}{\hat{z}\mathcal{W}'(\hat{z})} \ll \delta \ll 1, \tag{D10}$$

where x is close but not arbitrarily close to 1, the exponential term in (D7) will be suppressed, so that

$$\{1 - x^{-1/2}e^{\mathcal{W}(\hat{z})-\mathcal{W}(x^{-1/2}\hat{z})}\} \simeq 1. \tag{D11}$$

That means that the $\delta^{-3/2}$ divergence of $x[d\hat{\Gamma}/dx]^{\rm LO}$ will not be moderated in the integration region (D10), and so (when $\hat{z}$ is large) the integral in (D5) is dominated

$$\delta \sim \frac{1}{\hat{z}\mathcal{W}'(\hat{z})} \ll 1, \tag{D12}$$

which is the transition between the lower end of region (D10) and region (D8). We may therefore approximate the full integral (D5) by approximating $\delta \ll 1$ in the integrand, which corresponds to the approximation (D7). It is convenient to use that $\delta \ll 1$ approximation to also rewrite

$$(1-\delta)^{-1/2} \simeq e^{\delta/2}, \qquad x\left[\frac{d\hat{\Gamma}}{dx}\right]^{\rm LO} \simeq \frac{1}{\pi\delta^{3/2}}, \tag{D13}$$

and so (D5) becomes

$$\mathcal{W}'(\hat{z}) \simeq \int_0^\infty \frac{d\delta}{\pi\delta^{3/2}}\{1 - e^{-\frac{1}{2}[\hat{z}\mathcal{W}'(\hat{z})-1]\delta}\}. \tag{D14}$$

Note that we have replaced the upper limit of integration by ∞, which introduces negligible relative error in the large-$\hat{z}$ limit for the same reason that $\delta \ll 1$ dominated over $\delta \sim 1$. The integral gives

[54] Specifically, see Appendix B of Ref. [32].

$$\mathcal{W}'(\hat{z}) \simeq \sqrt{\frac{2}{\pi}[\hat{z}\mathcal{W}'(\hat{z}) - 1]}. \tag{D15}$$

Before solving (D15), we can simplify a bit by again remembering our expectation that $\hat{z}\mathcal{W}'(\hat{z}) \gg 1$ in the large $\hat{z}$ limit, so that (D15) becomes

$$\mathcal{W}'(\hat{z}) \simeq \sqrt{\frac{2}{\pi}\hat{z}\mathcal{W}'(\hat{z})}. \tag{D16}$$

Solving for $\mathcal{W}$ gives

$$\mathcal{W}(\hat{z}) \simeq \frac{\hat{z}^2}{\pi} \tag{D17}$$

at large $\hat{z}$, which is equivalent to the asymptotic behavior quoted in (7.4):

$$\hat{\epsilon}_{\rm LO}(\hat{z}) \sim e^{-\hat{z}^2/\pi}. \tag{D18}$$

There is a short-cut that we might have taken to determine (D18). Once we had completed enough of the argument to realize that the calculation of $\mathcal{W}(\hat{z})$ would be dominated by $\delta \ll 1$, we could have replaced $[d\Gamma/dx]^{\rm LO}$ by the BIM [30] model rate (E2), which agrees with $[d\Gamma/dx]^{\rm LO}$ in the limits $x \to 0$ and $x \to 1$. Then we could have extracted (D18) from the energy deposition distribution (E6) of the BIM model.

With some work, one could refine our leading large-$\hat{z}$ approximation to $\mathcal{W}$ to compute $O(\hat{z})$ corrections to the exponent in (D18) and even further to find power-law prefactors to the exponential.[55] However, we find in practice that (D18) by itself is adequate to get good numerical convergence of our results in the large-$\hat{z}_{\rm max}$ limit.

APPENDIX E: $\epsilon_{\rm LO}(\hat{z})$ IN THE BIM MODEL

In this appendix, we discuss, in our notation, the BIM model result for LO energy deposition [31].

Using the formula $P_{g\to gg}(x) = 2C_{\rm A}(1-x+x^2)^2/x(1-x)$ for the DGLAP splitting function, the LO splitting rate (2.1) can be rewritten as

$$\left[\frac{d\Gamma}{dx}\right]^{\rm LO} = \frac{C_{\rm A}\alpha_{\rm s}(1-x+x^2)^{5/2}}{\pi[x(1-x)]^{3/2}}\sqrt{\frac{\hat{q}_{\rm A}}{E}}. \tag{E1}$$

Blaizot, Iancu, and Mehtar-Tani (BIM) [30] realized that if one replaces the leading-order splitting rate (E1) by the simpler function

$$\left[\frac{d\Gamma}{dx}\right]_{\rm BIM} = \frac{C_{\rm A}\alpha_{\rm s}}{\pi[x(1-x)]^{3/2}}\sqrt{\frac{\hat{q}_{\rm A}}{E}}, \tag{E2}$$

then it is possible to solve leading-order shower development analytically. We will refer to this as the BIM model of shower development. The BIM rate (E2) is equal to the actual LO rate in the limit that one of the two daughters is soft, i.e. $x(1-x) \ll 1$. But for perfectly democratic splitting $x = 0.5$, the BIM rate overestimates the LO BDMPS-Z rate by a factor of $(4/3)^{5/2} \simeq 2$. In our notation, their analytic solution for the time development of the gluon density in x is

$$\hat{n}_{\rm BIM}(x,\hat{t}) = \frac{\hat{t}e^{-\hat{t}^2/\pi(1-x)}}{\pi[x(1-x)]^{3/2}} \quad \text{for } x > 0, \tag{E3}$$

with $\hat{t} \equiv t/\ell_0$, and ℓ_0 defined by (6.14).

In general, the energy which is still moving ($x > 0$) at time t is

$$E_{\rm moving}(t) = \int_{0^+}^1 dx\, xE_0 n(x, E_0, t). \tag{E4}$$

The moving energy decreases at the rate that energy is deposited into the medium, and so

$$\epsilon(z) = -\left.\frac{dE_{\rm moving}}{dt}\right|_{t=z} = -\left[\frac{d}{dt}\int_{0^+}^1 dx\, xE_0 n(x, E_0, t)\right]_{t=z}. \tag{E5}$$

Switching to dimensionless variables (7.1) and plugging in the BIM solution (E3) yields[56]

$$\hat{\epsilon}(\hat{z}) = -\frac{d}{d\hat{z}}e^{-\hat{z}^2/\pi} = \frac{2\hat{z}}{\pi}e^{-\hat{z}^2/\pi}. \tag{E6}$$

The corresponding stopping distance is

$$\hat{\ell}_{\rm stop}^{\rm BIM} = \langle\hat{z}\rangle_{\rm BIM} = \frac{\pi}{2}, \tag{E7}$$

and the shape function (1.1) is then

$$S_{\rm BIM}(Z) = \frac{\pi Z}{2}e^{-\pi Z^2/4}. \tag{E8}$$

The BIM stopping distance $\langle\hat{z}\rangle_{\rm BIM} \simeq 1.571$ is shorter than the LO stopping distance $\langle\hat{z}\rangle_{\rm LO} \simeq 2.1143$ of Table II because the BIM rate (E2) overestimates the splitting rate for democratic splittings. Other moments of the BIM energy stopping distribution are

$$\langle\hat{z}^n\rangle_{\rm BIM} = \pi^{n/2}\Gamma\left(1+\frac{n}{2}\right). \tag{E9}$$

[55] We do not expect these corrections to be the same as the BIM model result (E6).

[56] One way to do the x integral is to switch integration variable to $u \equiv \sqrt{x/(1-x)}$, which leads to a simple Gaussian integral in u. Our Eq. (E6) for $\hat{\epsilon}(\hat{z})$ is the same as Eq. (2.19) of Ref. [31] except for the choices of how we normalize our variable $\hat{z}$ and energy distribution $\hat{\epsilon}$.

APPENDIX F: ENERGY CONSERVATION FOR EQ. (8.4)

To see that the evolution equation (8.4) for $D(\zeta, E_0, t)$ conserves energy, integrate both sides of the equation over ζ and then switch the order of integration on the right-hand side to get

$$\frac{dE_{\text{total}}}{dt} = \int_0^1 dx \int_0^1 d\zeta \left\{ \theta(x > \zeta) \left[\frac{d\Gamma}{dx}\left(\frac{\zeta E_0}{x}, x\right)\right]_{\text{net}} D\left(\frac{\zeta}{x}, E_0, t\right) - x\left[\frac{d\Gamma}{dx}(\zeta E_0, x)\right]_{\text{net}} D(\zeta, E_0, t)\right\}. \tag{F1}$$

The ζ integral of the first term can be rewritten as

$$\int_0^x d\zeta \left[\frac{d\Gamma}{dx}\left(\frac{\zeta E_0}{x}, x\right)\right]_{\text{net}} D\left(\frac{\zeta}{x}, E_0, t\right) = \int_0^1 d\zeta' x \left[\frac{d\Gamma}{dx}(\zeta' E_0, x)\right]_{\text{net}} D(\zeta', E_0, t), \tag{F2}$$

where $\zeta' \equiv \zeta/x$. The first term of (F1) then cancels the second term, giving $dE_{\text{total}}/dt = 0$.

[1] L. D. Landau and I. Pomeranchuk, Limits of applicability of the theory of bremsstrahlung electrons and pair production at high-energies, Dokl. Akad. Nauk Ser. Fiz. **92**, 535 (1953).

[2] L. D. Landau and I. Pomeranchuk, Electron cascade process at very high energies, Dokl. Akad. Nauk Ser. Fiz. **92**, 735 (1953).

[3] A. B. Migdal, Bremsstrahlung and pair production in condensed media at high-energies, Phys. Rev. **103**, 1811 (1956).

[4] L. Landau, *The Collected Papers of L.D. Landau* (Pergamon Press, New York, 1965).

[5] J. P. Blaizot and Y. Mehtar-Tani, Renormalization of the jet-quenching parameter, Nucl. Phys. **A931**, 499 (2014).

[6] E. Iancu, The non-linear evolution of jet quenching, J. High Energy Phys. 10 (2014) 095.

[7] B. Wu, Radiative energy loss and radiative $p_\perp$-broadening of high-energy partons in QCD matter, J. High Energy Phys. 12 (2014) 081.

[8] P. Arnold, O. Elgedawy, and S. Iqbal, companion Letter, Are gluon showers inside a quark-gluon plasma strongly coupled? A theorist's test, Phys. Rev. Lett. **131**, 162302 (2023).

[9] P. Arnold, T. Gorda, and S. Iqbal, The LPM effect in sequential bremsstrahlung: Nearly complete results for QCD, J. High Energy Phys. 11 (2020) 053; 05 (2022) 114(E).

[10] P. Arnold and S. Iqbal, The LPM effect in sequential bremsstrahlung, J. High Energy Phys. 04 (2015) 070; 09 (2016) 072(E).

[11] P. Arnold, H. C. Chang, and S. Iqbal, The LPM effect in sequential bremsstrahlung 2: Factorization, J. High Energy Phys. 09 (2016) 078.

[12] P. Arnold, H. C. Chang, and S. Iqbal, The LPM effect in sequential bremsstrahlung: Dimensional regularization, J. High Energy Phys. 10 (**2016**) 100.

[13] P. Arnold, H. C. Chang, and S. Iqbal, The LPM effect in sequential bremsstrahlung: 4-gluon vertices, J. High Energy Phys. 10 (2016) 124.

[14] P. Arnold and S. Iqbal, In-medium loop corrections and longitudinally polarized gauge bosons in high-energy showers, J. High Energy Phys. 12 (2018) 120.

[15] P. Arnold, T. Gorda, and S. Iqbal, The LPM effect in sequential bremsstrahlung: Incorporation of instantaneous interactions for QCD, J. High Energy Phys. 11 (2022) 130.

[16] A. Kurkela and U. A. Wiedemann, Picturing perturbative parton cascades in QCD matter, Phys. Lett. B **740**, 172 (2015).

[17] Y. Mehtar-Tani and K. Tywoniuk, Sudakov suppression of jets in QCD media, Phys. Rev. D **98**, 051501 (2018); Y. Mehtar-Tani, D. Pablos, and K. Tywoniuk, Cone-Size Dependence of Jet Suppression in Heavy-Ion Collisions, Phys. Rev. Lett. **127**, 252301 (2021).

[18] P. Caucal, E. Iancu, A. H. Mueller, and G. Soyez, Vacuum-Like Jet Fragmentation in a Dense QCD Medium, Phys. Rev. Lett. **120**, 232001 (2018).

[19] B. G. Zakharov, Transverse spectra of radiation processes in-medium, JETP Lett. **70**, 176 (1999).

[20] U. A. Wiedemann and M. Gyulassy, Transverse momentum dependence of the Landau-Pomeranchuk-Migdal effect, Nucl. Phys. **B560**, 345 (1999); U. A. Wiedemann, Gluon radiation off hard quarks in a nuclear environment: Opacity expansion, Nucl. Phys. **B588**, 303 (2000).

[21] J. P. Blaizot, F. Dominguez, E. Iancu, and Y. Mehtar-Tani, Medium-induced gluon branching, J. High Energy Phys. 01 (2013) 143.

[22] L. Apolinário, N. Armesto, J. G. Milhano, and C. A. Salgado, Medium-induced gluon radiation and colour decoherence beyond the soft approximation, J. High Energy Phys. 02 (2015) 119.

[23] J. H. Isaksen and K. Tywoniuk, Precise description of medium-induced emissions, arXiv:2303.12119.

[24] J. Barata, F. Domínguez, C. A. Salgado, and V. Vila, A modified in-medium evolution equation with color coherence, J. High Energy Phys. 05 (2021) 148.

[25] J. Casalderrey-Solana, Y. Mehtar-Tani, C. A. Salgado, and K. Tywoniuk, New picture of jet quenching dictated by color coherence, Phys. Lett. B **725**, 357 (2013).

[26] Y. Mehtar-Tani, C. A. Salgado, and K. Tywoniuk, The radiation pattern of a QCD antenna in a dense medium, J. High Energy Phys. 10 (2012) 197.
[27] P. B. Arnold and C. Dogan, QCD splitting/joining functions at finite temperature in the deep LPM regime, Phys. Rev. D **78**, 065008 (2008).
[28] R. Baier, Y. L. Dokshitzer, A. H. Mueller, S. Peigne, and D. Schiff, Radiative energy loss and $p_\perp$-broadening of high energy partons in nuclei, Nucl. Phys. **B484**, 265 (1997).
[29] A. Peshier, QCD running coupling and collisional jet quenching, J. Phys. G **35**, 044028 (2008).
[30] J. P. Blaizot, E. Iancu, and Y. Mehtar-Tani, Medium-Induced QCD Cascade: Democratic Branching and Wave Turbulence, Phys. Rev. Lett. **111**, 052001 (2013).
[31] J. P. Blaizot and Y. Mehtar-Tani, Energy flow along the medium-induced parton cascade, Ann. Phys. (Amsterdam) **368**, 148 (2016).
[32] P. Arnold, S. Iqbal, and T. Rase, Strong- vs. weak-coupling pictures of jet quenching: A dry run using QED, J. High Energy Phys. 05 (2019) 004.
[33] R. Baier, Y. L. Dokshitzer, A. H. Mueller, S. Peigne, and D. Schiff, The Landau-Pomeranchuk-Migdal effect in QED, Nucl. Phys. **B478**, 577 (1996).
[34] R. Baier, Y. L. Dokshitzer, A. H. Mueller, S. Peigne, and D. Schiff, Radiative energy loss of high-energy quarks and gluons in a finite volume quark—gluon plasma, Nucl. Phys. **B483**, 291 (1997).
[35] B. G. Zakharov, Fully quantum treatment of the Landau-Pomeranchuk-Migdal effect in QED and QCD, Pis'ma Zh. Éksp. Teor. Fiz. **63**, 906 (1996) [JETP Lett. **63**, 952 (1996)].
[36] B. G. Zakharov, Radiative energy loss of high-energy quarks in finite size nuclear matter and quark-gluon plasma, Pis'ma Zh. Éksp. Teor. Fiz. **65**, 585 (1997) [JETP Lett. **65**, 615 (1997)].
[37] R. Baier, Y. L. Dokshitzer, A. H. Mueller, and D. Schiff, Medium induced radiative energy loss: Equivalence between the BDMPS and Zakharov formalisms, Nucl. Phys. **B531**, 403 (1998).
[38] B. G. Zakharov, Light cone path integral approach to the Landau-Pomeranchuk-Migdal effect, Yad. Fiz. **61**, 924 (1998) [Phys. At. Nucl. **61**, 838 (1998)].
[39] P. B. Arnold, Simple formula for high-energy gluon bremsstrahlung in a finite, expanding medium, Phys. Rev. D **79**, 065025 (2009).
[40] P. Arnold, Universality (beyond leading log) of soft radiative corrections to $\hat{q}$ in $p_\perp$ broadening and energy loss, J. High Energy Phys. 03 (**2022**) 134.
[41] T. Liou, A. H. Mueller, and B. Wu, Radiative $p_\perp$-broadening of high-energy quarks and gluons in QCD matter, Nucl. Phys. **A916**, 102 (2013).
[42] P. Arnold, T. Gorda, and S. Iqbal, The LPM effect in sequential bremsstrahlung: Analytic results for sub-leading (single) logarithms, J. High Energy Phys. 04 (2022) 085.
[43] E. Iancu and D. N. Triantafyllopoulos, Running coupling effects in the evolution of jet quenching, Phys. Rev. D **90**, 074002 (2014).
[44] P. Caucal and Y. Mehtar-Tani, Anomalous diffusion in QCD matter, Phys. Rev. D **106**, L051501 (2022).
[45] P. Caucal and Y. Mehtar-Tani, Universality aspects of quantum corrections to transverse momentum broadening in QCD media, J. High Energy Phys. 09 (2022) 023.
[46] P. B. Arnold, S. Cantrell, and W. Xiao, Stopping distance for high energy jets in weakly-coupled quark-gluon plasmas, Phys. Rev. D **81**, 045017 (2010).
[47] Wolfram Research, Inc., *Mathematica* (various versions), Champaign, IL (2018–2021).
[48] J. Ghiglieri and E. Weitz, Classical vs quantum corrections to jet broadening in a weakly-coupled quark-gluon plasma, J. High Energy Phys. 11 (2022) 068.